Stony Brook University

Expression and Functional Significance of MAGuKs on Cortical Interneurons

A Dissertation Presented

by

Gulcan Akgul

to

The Graduate School

in Partial Fulfillment of the

Requirements

for the Degree of

Doctor of Philsophy

in

Molecular and Cellular Biology

Stony Brook University

December 2012

Stony Brook University

The Graduate School

Gulcan Akgul

We, the dissertation committee for the above candidate for the
Doctor of Philosophy degree, hereby recommend
acceptance of this dissertation.

Lonnie P. Wollmuth - Dissertation Advisor
Professor, Department of Neurobiology and Behavior

Simon Halegoua – Chairperson of Defense
Professor, Department of Neurobiology and Behavior

Styliani-Anna E. Tsirka – Committee Member
Professor, Department of Neurobiology and Behavior

Mark E. Bowen – Committee Member
Assistant Professor. Department of Physiology and Biophysics

Arianna Maffei – Committee Member
Assistant Professor. Department of Neurobiology and Behavior

Z. Josh Huang - Committee Member
Professor, Cold Spring Harbor Laboratory

This dissertation is accepted by the Graduate School

Charles Taber
Interim Dean of the Graduate School

Abstract of the Dissertation

Expression and Functional Significance of MAGuKs on Cortical Interneuronsby

Gulcan Akgul

Doctor of Philosophy

in

Molecular and Cellular Biology

Stony Brook University

2012

GABAergic inhibitory interneurons, which constitute twenty percent of the entire neuron population, are crucial to the function of brain. They have several subgroups with distinct morphological, biochemical and most importantly physiological properties. Parvalbumin (PV) and Somatostatin (SOM) expressing inhibitory interneurons represent two major subgroups of interneurons in the cortex as well as most other brain regions. Their activity is driven by the excitatory input they receive from pyramidal neurons. SAP97 is a scaffolding protein at the postsynaptic density of the excitatory synapses. It has important functional roles in trafficking and clustering of various types of ion channels and therefore is involved in regulation of the electrical activity of neurons. Neither the expression nor the functional role of SAP97 in cortical interneurons have been addressed before. With in situ hybridization and single cell RT-PCR, we showed that the expression of SAP97 is restricted to a fraction of PV and SOM interneurons of both juvenile and adult mouse visual cortex and developmentally regulated. With

electrophysiology, we also found that there is a strong correlation with SAP97 expression and various membrane properties of PV interneurons. SAP97 expressing interneurons have less excitable membranes and fire faster action potentials. Moreover, they receive more frequent excitatory input. In agreement with that, when we overexpress SAP97 in PV interneurons that do not have endogenous SAP97, these interneurons showed electrophysiological properties that are similar to endogenous SAP97 expressing PV interneurons. Our results make important contributions to understanding the functional development of neurons, the regulation of their activity.

To

My lovely mother, Bayramşen, whose presence has given me the strength to keep going,

my devoted grandmother, Reşide and grandfather, İsmet

with my deepest love and compassion…

Sevgili annem Bayramşen, babaannem Reşide ve dedem İsmet'e ithafen...

Acknowledgments

I would like to give special thanks to my primary school teacher, Kasim Seker, who tried to answer my endless questions and not to kill my passion for knowledge with patience. Now when I look back, I can see that everything started back then.

I would like to extend my special thanks to my adviser, Dr. Lonnie Wollmuth who treated and trained me with great patience and respect over the years. Although we are very different from each other by any means, we found a balance and we have overcome many obstacles and troubles and we succeeded together.

I would also like to thank my committee members, Drs. Josh Huang, Simon Halegoua, Arianna Maffei, Stella Tsirka and Mark Bowen, who gave me very good advice during our meetings. Without them, I would easily get lost in the process.

The lovely, supporting members of Wollmuth Lab, especially Janet Allopenna and Dr. Catherine Salussolia for their friendship, Dr. Martin Prieto, Dr. Mike Prodromou, Dr. Jessica Helm, Dr. Alexandra Corrales-Eilers, Rashek Kazi, Dr. Iehab Talukder and Quan Alfred Gan deserve my gratitude.

I would like to extend my thanks to our neighbors, Dr. Gary Matthews, Dr. George Zanazzi and Diane Henry-Vanisko for their generous help and support as colleagues and friends over the years.

In addition to the names above, I would like to thank the students and the faculty of Neurobiology and Behavior Department and DLAR at SBU. It is impossible to write down all the names here, unfortunately. They were great help for me and such nice people.

Outside my professional world, I would like to thank all my room-mates and friends all around the world, e.g., Aysegul, Betul, Canan, Ebru, Elif T, Ender, Melike, MiJin, Naciye, Neriman, Nur, Sehnaz, Seyma, Volkan, Yasemin, Zulal… for their company, great help, support and encouragement.

Last but not least, I will give my endless thanks to my family; my father, Nurcan; my brother, Ismet; my sister, Ece; my aunt, Mukaddes; Gulay, Erdal, Mediha, Aynur, Emine, Sibel… for everything they have done in the last thirty years and for not letting me give up on anything anytime in my life.

Table of Contents

List of Figures/Illustrations

List of Tables

CHAPTER 1: GENERAL INTRODUCTION

Neocortex

The neocortex (cerebral cortex) is the brain region that performs complex, high-level information processing in mammals such as sensory perception and cognition. Most parts of the neocortex is divided into six horizontal layers (L1-L6; Fig. 1.1) with a differential composition of neuron types in each layer. The neocortex is also organized into functionally distinct vertical columns that are interconnected (Jones, 2000; Rakic, 2007). There are two major neuronal cell types in the neocortex: excitatory (glutamatergic) pyramidal neurons (70-80% of total neurons) and inhibitory (GABAergic) interneurons (20-30%). Pyramidal neurons send excitatory input within the cortex and to other brain regions to execute cortical functions whereas interneurons make connections within mostly local microcircuitry. Inhibitory interneurons provide regulatory mechanisms for pyramidal neuron activity and promote the complexity of neuronal computations. For instance, the spatiotemporal regulation of pyramidal neuron activity highly relies on the differential inputs they receive from interneuron subgroups (Freund and Katona, 2007; Palmer et al., 2012). Besides the presence of the numerous subgroups of interneurons in the cortex, the number and types of interneurons within the cortical layers and columns vary and contribute to the complexity and specialization of the neocortex and neocortical circuitry.

Interneurons are fundamental to brain functions

Ramon y Cajal, the famous Spanish Nobel Laureate who initiated systematic neuroanatomy, described interneurons as the “butterflies of the soul” (Ramón y Cajal S. Textura del sistema nervioso del hombre y vertebrados. Vol. 2. Moya; Madrid, Spain: 1899). His Golgi stainings on the brain tissues of different organisms showed that these small neurons had different morphologies and were more numerous in the brains of complex organisms. These ideas formed

the basis for the argument made by Cajal that interneurons have important roles in the regulation of complex brain functions. Although interneuron activity is critical in all brain regions, my studies focused on neocortical interneurons.

Precision of brain functions and computational complexity of neuronal circuits are regulated with numerous classes of neurons and the interplay of excitatory and inhibitory activity among these neurons. Of these classes inhibitory (GABAergic) interneurons represent a significant minority of neurons in the brain (15-30 %) (Fishell and Rudy, 2011) and play a crucial role in maintaining homeostasis and regulating neuronal circuits (Turrigiano, 2008; Wenner, 2011). These interneurons control hyperexcitability of the brain (Bekenstein and Lothman, 1993). They modulate the incoming input to and output response from pyramidal neurons (Freund and Katona, 2007; Palmer et al., 2012). Additionally, at the network level, both feedforward and feedback inhibition reduce the number of simultaneously active principal cells in various brain regions including cortex, hippocampus and amygdala (Callaway, 2004; Lawrence and McBain, 2003; Szinyei et al., 2000) and exert gain control over these cells (Buzsaki et. al., 2007). Further, inhibitory interneurons form an electrically coupled network (Fukuda and Kosaka, 2000) and control spike timing of hippocampal (Gelman and Marin, 2010) and cortical (Buzsaki and Draguhn, 2004) excitatory neurons creating oscillatory activity in different brain regions. Consequently, disruption of GABAergic function has been implicated in numerous neurodevelopmental disorders such as epilepsy, mental retardation, autism, and schizophrenia (Bozzi et al., 2012; Marin, 2012). For example, disinhibition of excitatory neurons can leave the oscillatory activity of networks uncontrolled leading to epilepsy (Bozzi et al., 2012; Dichter and Ayala, 1987). The defective inhibiton that arises from the decrease in glutamate receptor (Belforte et al., 2010; Korotkova et al., 2010) or GAD67 expression (Hashimoto et al.,

2003) in particular interneuron subgroups as well as the decrease in the overall number of interneurons in the prefrontal cortex (Benes et al., 1991) contribute to the pathophysiology of schizophrenia.

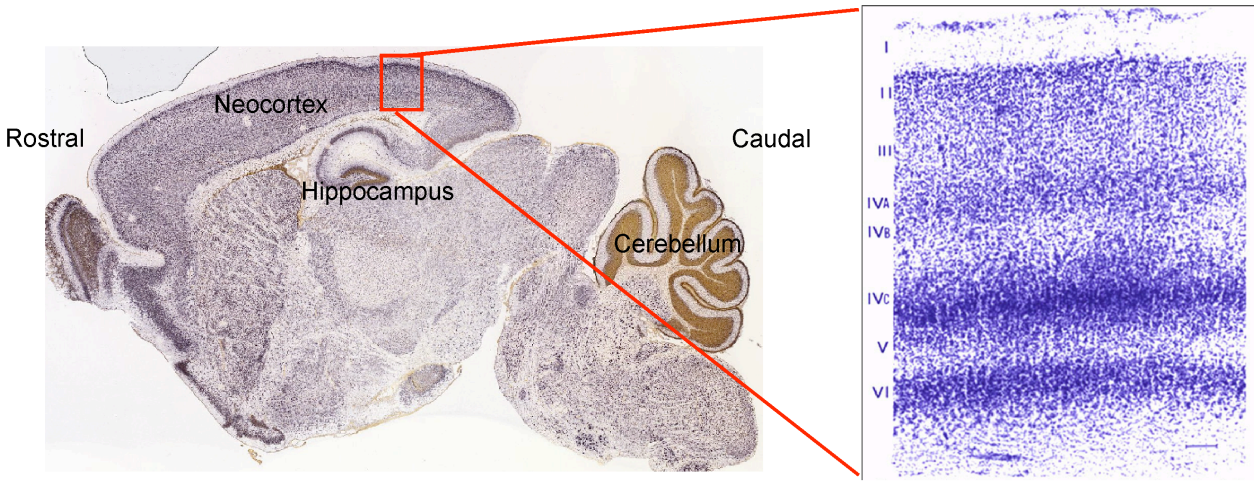

Figure 1.1. Layered structure of the mouse neocortex.
A sagittal section of the mouse brain showing different brain regions including cortex. Anatomical directions are labeled as Rostral (toward the front) and Caudal (toward the back). Some important brain regions are also labeled: Neocortex, Hippocampus and Cerebellum. The red rectangle is highlighting a part of the visual cortex. The high magnified image on the right delineating the six layers of the visual cortex: L1-L6. Layer 1 contains very few cell bodies and in each layer the soma size and cell number vary giving the differential staining characteristics to the tissue.

Interneuron Diversity and Subgroups

GABAergic interneurons exhibit anatomical and physiological diversity and contribute to the complexity of brain functions. They are prominently found in brain regions associated with cognitive functions. Therefore, defining the function of each type is essential to understand cellular basis of brain functions.

Based on biochemical, anatomical, and physiological properties, a variety interneuron subgroups has been pronounced (Fishell and Rudy, 2011; Markram et al., 2004). Although many of the particular properties are correlated with some others, for example anatomical basket cells having fast-spiking firing pattern, this type of correlation is not present in all classifications (Ascoli et al., 2008; Markram et al., 2004). I will review some of the major classification properties of different subgroups (Table 1.1).

Table 1.1. Subgroups of cortical interneurons

Molecular Marker	Morphology	Dendritic Anatomy	Firing Pattern	Targeting	Origin
PV	Basket, Multipolar, Chandelier	Aspiny	Fast-spiking	Perisomatic AIS	MGE
SOM	Martinotti, bitufted, bipolar	Spiny	Low threshold spiking Accommodating, Adapting	Distal tuft dendrites	MGE
CR	Bitufted		Irregular-spiking		CGE
CCK			Burst-spiking Regular-spiking		CGE
VIP	Bipolar, bitufted, small basket		Burst-spiking Irregular-spiking		CGE

PV: Parvalbumin, SOM: Somatostatin, CR: Calretinin, CCK: Cholecystokinin, VIP: Vasoactive Intestinal Protein. Cortical interneurons emerge from two regions in embryonic brain: MGE, Medial ganglionic eminence; CGE, Caudal ganglionic eminence. (Fishell and Rudy, 2011; Markram et al., 2004).

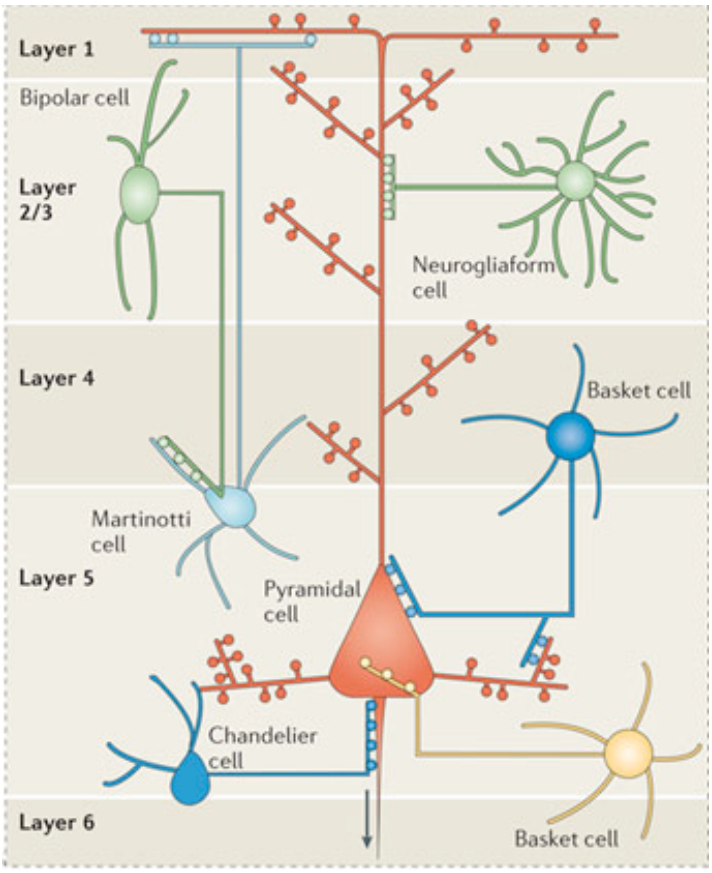

Figure 1.2. Different classes of cortical interneuron are distinguished on the basis of their morphology, neurochemical content, intrinsic electrophysiological properties and pattern of connectivity.
In the mouse neocortex, for example, basket cells constitute a relatively heterogeneous population of interneurons that are parvalbumin expressing and fast spiking and primarily target the soma and basal dendrites of pyramidal cells, whereas chandelier cells synapse on the axon initial segment. Other classes of interneurons, such as Martinotti cells that are somatostatin expressing primarily contact the dendrites of pyramidal cells, whereas some types of interneuron, including bipolar cells, are specialized in targeting other interneurons. Adapted from (Marin, 2012).

Biochemical (Molecular Markers) Classification

One way to classify GABAergic interneurons into smaller, more homogenous groups is to differentiate them with molecular markers. The most common molecular markers used to classify GABAergic interneurons have been calcium-binding molecules (e.g., parvalbumin, calbindin and calretinin; Figs. 1.3 & 1.4) and neuropeptides (e.g., cholecystokinin, neuropeptide Y, somatostatin, vasoactive intestinal polypeptide; Figs. 1.3 & 1.4) (Gonchar et al., 2007; Kubota and Kawaguchi, 1994). Parvalbumin (PV) and somatostatin (SOM) expressing interneurons represent the two major interneuron subgroups in the cortex (Gonchar et al., 2007). Molecular marker expression overlaps with anatomical and physiological properties to some extent. For instance, parvalbumin (PV) expressing basket cells and Chandelier Cells are fast-spiking (DeFelipe, 1993; DeFelipe et al., 1989; Kawaguchi, 1995). Still, it is hard to use a single molecular marker for a certain subgroup and draw reliable and exclusive conclusions about the anatomy and the physiology of that subgroup. Ultimately, the presence of several markers is required to confidently identify any one of these subgroups, along with some other properties.

Recently, developmental studies in the interneuron field characterized new molecular markers for the interneuron precursors making it possible to track interneuron populations over development (Fishell and Rudy, 2011). A significant advantage of the discovery of molecular markers is that they allowed to create transgenic animal lines to label, track and manipulate particular interneuron subgroups to study their function, and connectivity (Taniguchi et al., 2011). These transgenic lines opened new venues of research. Along with recombinant viral vectors (Betley and Sternson, 2011; Papale et al., 2009), they make it possible to monitor the development and circuit integration (Batista-Brito and Fishell, 2009; Taniguchi et al., 2011; Tricoire et al., 2010) and to modify gene expression of specific interneurons (Papale et al., 2009).

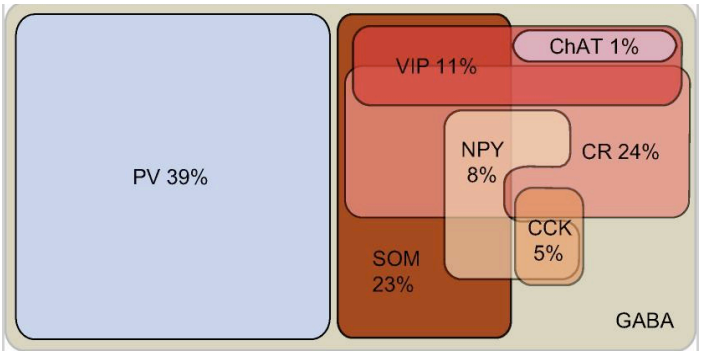

Figure 1.3. Distribution of biochemically defined interneuron subgroups in the cortex.
PV stands for parvalbumin expressing, fast-spiking basket and Chandelier cells that constitute 39 % of all interneuron population in mouse visual cortex. SOM, somatostatin expressing, adapting non-fast-spiking interneurons. Many of them are Martinotti cells. It is not a homogenous group. CR, calretinin; VIP, vasoactive intestinal protein; ChAT, choline acetyltransferase; NPY, neuropeptide protein Y; CCK, cholecystokinin. Adapted from (Gonchar et al., 2007).

Morphological Classification

Cellular and dendritic morphology of interneurons are another parameter used to differentiate interneuron subgroups. It is a traditional method heavily used by scientists before the molecular markers were identified and used. Some of the defined morphology for the soma and the dendritic branching of interneurons are basket cells (further divided into smaller groups), bipolar cells, Chandelier cells, Martinotti cells and bitufted cells (Table 1.1; Fig. 1.2). Basket cells, for example, are defined by the basket-like appearance around the pyramidal neuron that is innervated by several basket cells. Bipolar cells, on the other hand, are directly recognized with their ovoid shaped soma and dendritic branching originated at two poles of their soma. The morphological properties of the interneurons might correlate with some other properties to a certain level. For example, basket cells have defined fast spiking firing pattern (Cauli et al., 1997) that make them an electrophysiologically separate subgroup as well.

Electrophysiological Classification

Electrophysiological properties of the interneurons are one of the most important parameters used to define an interneuron subgroup since it ultimately gives functional information. Originally, all inhibitory interneurons were described as fast spiking (FS) (Fig. 1.5B) (Connors and Gutnick, 1990; Jonas et al., 1994) but eventually other firing patterns were also discovered (Ascoli et al., 2008; Gibson et al., 1999). For example, regular-spiking pattern resembling the firing pattern of pyramidal neurons (Fig. 1.5A) is exhibited by some of Martinotti cells (Kawaguchi and Kubota, 1996). Other subgroups can have firing patterns such as irregular-spiking, stuttering, and accommodating (Ascoli et al., 2008; Gupta et al., 2000; Markram et al., 2004).

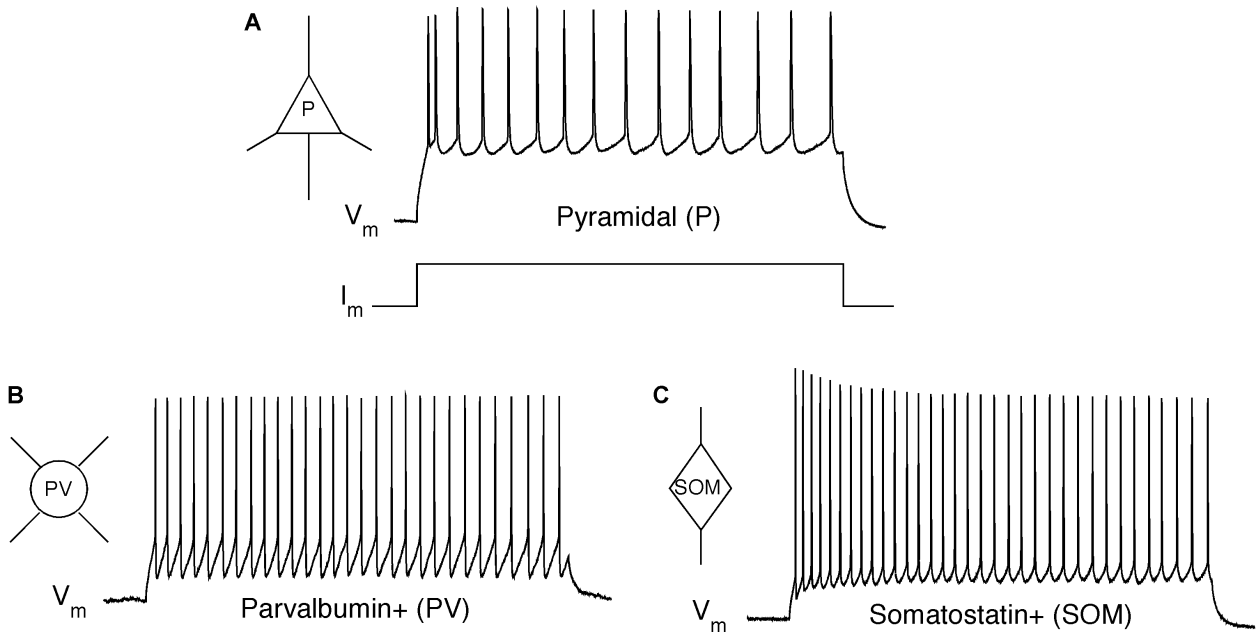

Figure 1.5. Firing patterns of different neuron types.
A) Pyramidal neurons have adapting, regular spiking firing pattern in response to injected current. B) In comparison to the firing pattern of pyramidal neurons, multipolar PV interneurons have nonadapting, nonaccommodating fast spiking firing pattern. C) Bitufted, SOM interneurons have adapting, accommodating firing pattern distinguished from both pyramidal neurons and PV interneurons. P, Pyramidal; PV, Parvalbumin; SOM, Somatostatin; Vm, membrane potential; Im, membrane current.

Synaptic Targeting

For a functional classification of interneurons, the sites where they synapse on the target neuron are as important as their electrophysiological properties. While some subgroups (CR and VIP) preferentially synapse on other interneurons (Caputi et al., 2009; Gonchar and Burkhalter, 1999) and thus regulate the activity of different GABAergic subgroups, most interneurons target local pyramidal neurons.

Different subcellular domains of pyramidal neurons have different functional roles and need independent modulation (Spruston, 2008). Spatiotemporal division of labor is managed with different subgroups of inhibitory interneurons that are specialized to innervate different domains of pyramidal neurons, either perisomatic or dendritic domains. The perisomatic domain and axon initial segment are responsible for the summation of postsynaptic potentials arriving from all dendritic branches (Bender and Trussell, 2012). Because axon initial segment is responsible for action potential generation, interneurons synapsing on the perisomatic domains or axon initial segments control output from pyramidal neurons. They can synchronize pyramidal cell populations creating oscillatory activity (Cobb et al., 1995). Chandelier Cells are PV positive inhibitory interneurons that target axon initial segment (Peters and Harriman, 1990; Peters et al., 1990) and basket cells target perisomatic domains and proximal dendrites of the pyramidal neurons (Di Cristo et al., 2004). Each basket cell can make ~2000 synaptic connections in the local microcircuits gaining a powerful control over network activity.

On the other hand, dendritic inhibition has a small effect on action potential generation (Williams and Stuart, 2003). The main reason for that is the distance of the site of synaptic inhibition and site of action potential generation. The inhibitory synaptic inputs have negative effect only on the local excitatory postsynaptic potentials (EPSPs) elicited within the same time

window of potential change. Additionally, the number of dendritic inhibitory synapses is much lower relative to the number of perisomatic inhibitory synapses. Interneurons targeting specific dendritic regions (Fig. 1.2) can selectively gate excitatory input from different sources, thereby changing their relative contributions to the output of the cell. Excitatory input can even trigger Ca^{2+} dependent action potentials at the dendrites (Schiller et al., 1997). Inhibitory synaptic inputs that are added to the spatial summation can regulate dendritic spikes. Somatostatin expressing, dendritic targeting interneurons (Fig. 1.2) (Gonchar et al., 2002) for example, substantially increases the threshold level of excitation needed to trigger local Ca^{2+} spikes in the layer 5 pyramidal neurons of the cortex (Murayama et al., 2009).

Interneurons in Networks/Microcircuits

The input-output properties of the interneurons are functionally important in regard to their role in neural networks. Processing sensory information relies on the interaction between different brain regions at the gross anatomical level, on the complexity of cortical circuits and on the diversity and specificity of each neuron. The properties of different neuronal subgroups (e.g., Kerlin et al., 2010; Runyan et al., 2010) have different roles in the structure and activity of cortical networks.

One of the roles of the interneurons in networks is to prevent runaway excitation and as a result maintain homeostasis in brain. This idea of interneuron function explains their involvement in epilepsy (DeFelipe, 1999). The excitation/inhibition balance is maintained by feedforward and feedback loops (Figs. 1.6) between excitatory and inhibitory neurons. If interneurons receive their driving excitatory input from non-target pyramidal neurons (feedforward excitation), they mediate feedforward inhibition (Fig. 1.6A). Fast-spiking interneurons in the cortex that are innervated by thalamocortical afferents form a feedforward

inhibitory pathway (e.g., Porter et al., 2001). Conversely, if the driving source of input to an interneuron is the local target pyramidal neurons, they provide feedback inhibition in return (Fig. 1.6B). These reciprocal connections allow a more dynamic excitation-inhibiton balance within neural networks.

Inhibitory interneurons also play important roles in generating oscillatory activity in the brain. Oscillations are synchronized rhythmic activity of neuronal populations within a region or between brain regions. Oscillatory activity of neuronal networks is thought to be fundamental of brain processing since certain oscillations correlate with certain normal /abnormal (schizophrenia, autism etc.) behavioral and cognitive states (Buzsaki and Draguhn, 2004; Jonas et al., 2004; Sohal, 2012). Oscillatory activity of neuronal populations can be maintained if not generated by inhibitory networks. Although the exact mechanisms of oscillations are not understood yet, it is evident that interneuron activity is critical. For example, interneurons synchronize pyramidal neurons by controlling their spike timing and create oscillatory activity at gamma frequencies (Whittington et al., 1995) and the same type of oscillations can be initiated with synchronization of interneuron networks and disrupted with opposite manipulation of the system (Cardin et al., 2009; Sohal et al., 2009). With high firing rates (Up to 200 Hz for PV cells) and chemical and electrical connections (Galarreta and Hestrin, 1999; Gibson et al., 1999) between each other, inhibitory interneuron networks (especially PV interneurons) are the key elements of the oscillations in proposed models. However, the diversity of interneurons is a big obstacle for explaining their precise role in rhythmic activity.

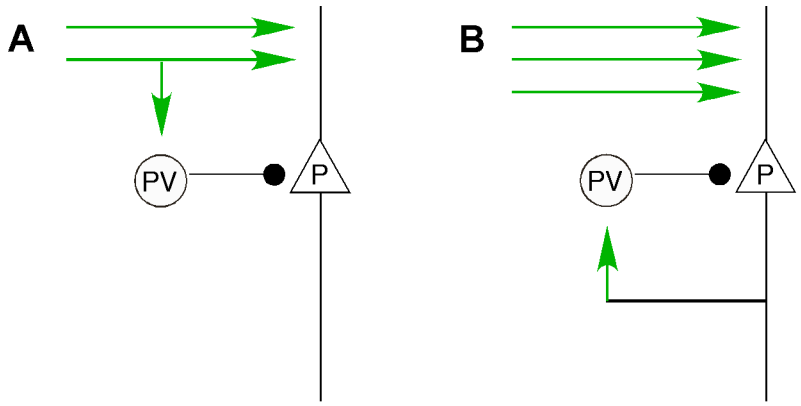

Figure 1.6. Feedforwad and feedback inhibitory circuits.
A) Fast spiking PV interneurons mediating feedforward inhibition (Black point) upon receiving excitatory input (Green arrows) from nontarget principal neurons. B) The interneuron mediating feedback inhibition (Black point) to the principal neuron sends feedback excitatory input (Green arrow) on it.

Glutamatergic Synapses on Interneurons

Since interneurons are essential for normal brain function and maintaining physiological homeostasis, their activation should be precisely regulated and modulated. They receive both excitatory and inhibitory input through glutamatergic and GABAergic synaptic activity. Although glutamatergic synaptic input is the driving force for their activity, the nature and regulation of this type of input onto inhibitory interneurons is poorly understood. Here, I will investigate the molecular mechanisms that regulate glutamatergic synaptic transmission onto cortical PV and SOM interneurons.

Glutamate is the major excitatory neurotransmitter in the central nervous system (CNS). Its excitatory effect is created upon binding of glutamate to the ionotropic glutamate receptors that leads to ion influx and membrane depolarization. Ionotropic glutamate receptors are divided into three subtypes: alpha-amino-3-hydroxyl-5-methyl-4-isoxazole-propionate (AMPA) receptors, N-Methyl-D-Aspartate (NMDA) receptors and Kainate (KA) receptors. Each subtype is constituted with different subunits that give the particular receptor its different biophysical properties. AMPA receptors can be formed as homomers or heteromers and create the fast component of the excitatory postsynaptic potential/current (EPSP/EPSC) (Fig. 1.7). AMPARs are cation selective allowing Na^+ and K^+ influx but only GluA2-lacking AMPARs can let Ca^{2+} influx (Hume et al., 1991; Traynelis et al., 2010). NMDARs on the other hand, are obligate heteromers with GluN1 subunit being the common subunit in all. Additionally they have GluN2A, B, C and D subunits. They create the slow component of the EPSCs (Fig. 1.7). They mediate Ca^{2+} influx regardless of their subunit composition (MacDermott et al., 1986; Traynelis et al., 2010) and therefore, are responsible for cellular excitotoxicity under stress and in several

disease states (Fan and Raymond, 2007). Ca^{2+} permeability of GluRs is also critical for long-term synaptic plasticity (Hunt and Castillo, 2012; Kessels and Malinow, 2009).

The molecular composition and regulation of the glutamatergic synapses that drive interneuron activity is extremely important and exhibit distinct structural and electrophysiological characteristics in comparison to their counterparts onto the pyramidal neurons. For example, inhibitory interneurons, unlike pyramidal neurons, have mostly Ca^{2+}-permeable AMPARs (CP-AMPARs) (Geiger et al., 1995; Wang and Gao, 2010); the predominant subunits expressed in fast spiking interneurons in the cortex are GluA1 and GluA4. On the other hand, interneuron activity is less sensitive to NMDAR antagonists than pyramidal neurons suggesting the expression and the function of these receptors in the interneurons are very limited (Angulo et al., 1999; Goldberg et al., 2003a). The lower NMDAR activity might be compensated with increased CP-AMPARs in these cells. Additionally, in comparison to pyramidal neurons, GluN2C and GluN2D subunits are more abundant in cortical and hippocampal interneurons (Monyer et al., 1994; Standaert et al., 1996).

The differential GluR subunit composition at the synapses onto interneurons has several functional consequences. First of all, the abundance of GluA1/4 containing AMPARs and the low level of NMDAR expression and activity in the interneurons result in very fast large synaptic currents allowing the recruitment of the interneurons within narrow time windows.

In diseases such as schizophrenia, NMDAR hypofunction is strongly correlated with the decreased inhibitory activity and the emergence of the symptoms (Rotaru et al., 2011). Furthermore, the loss of NMDARs in fast spiking PV interneurons have negative effects on normal cognitive behaviors of the mice: it disrupts gamma oscillations and working memory

(Carlen et al., 2011). The mechanisms that regulate differential GluR expression at the glutamatergic synapses onto different types of neurons are critical to the normal and abnormal brain function and should be addressed.

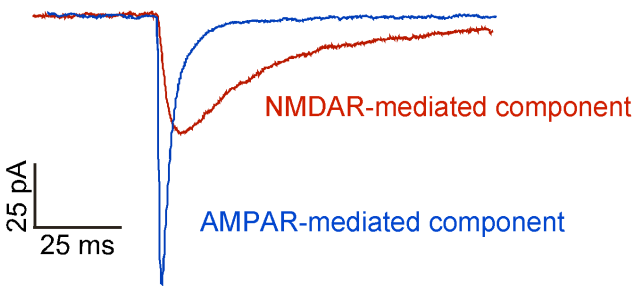

Figure 1.7. Examples of AMPAR-mediated and NMDAR-mediated excitatory postsynaptic currents (EPSC).
At synapses, AMPARs mediate the fast component of the EPSC (highlighted in blue) whereas NMDARs mediate the slow component (highlighted in red) due to ion influx, which result in membrane depolarization.

Postsynaptic Density

In the cortex as well as in other brain regions, there are two morphologically identified types of synapses: symmetric and asymmetric synapses (Fig. 1.8). Symmetric synapses constitute 5-25% of the entire synaptic pools and are mostly inhibitory (GABAergic). Asymmetric synapses account for 75-95% of all cortical synapses and are excitatory (glutamatergic) synapses. Their asymmetry arises because of the electron dense post-synaptic density (PSD) enriched with membrane and cytoplasmic proteins (DeFelipe et al., 2002).

The PSD contains more than 400 different types of proteins (Sheng and Hoogenraad, 2007) including the receptors and cell adhesion molecules at the membrane and the cytoplasmic proteins that form macromolecular complexes (Fig 1.9). The size and the molecular composition of the PSD vary from cell type to cell type or from brain region to brain region. PSDs are around 360 nm of diameter and 4 nm of thickness on average (Sheng and Hoogenraad, 2007). The protein content of the PSD is subject to regulation upon synaptic activity (Bats et al., 2007; Schmid et al., 2008; Zheng et al., 2010); molecules come in and out of the PSD and through trafficking, lateral diffusion and endocytosis (Hirling, 2009), controlling the protein dynamics of the PSD. For example, AMPARs can be trafficked to the membrane upon increased synaptic activity (Choquet, 2010). Proteasomal degradation is another mechanism that regulates protein content of the PSD due to changes in synaptic activity (Bingol and Schuman, 2005).

The PSD has structural and functional importance to the formation of the glutamatergic synapses and their activity. First, the PSD serves as the structural site for glutamate receptors to be localized apposed to the presynaptic release site (Sheng and Hoogenraad, 2007). Additionally, presynaptic and postsynaptic sites are physically stabilized with interacting cell adhesion

molecules positioned face to face at both sites (Nam and Chen, 2005; Song et al., 1999) (Fig. w). Another role of the PSD is to form a molecular mesh that mediates synaptic signaling. These signaling pathways couple synaptic activity to gene expression and protein trafficking (Hou et al., 2011; Rial Verde et al., 2006).

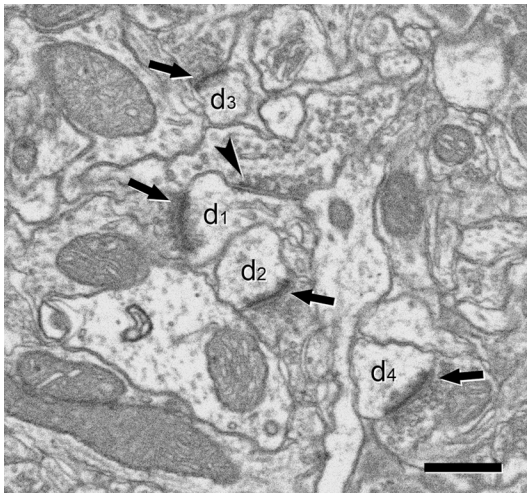

Figure 1.8. Ultrastructural appearance of asymmetric and symmetric synapses.
Four asymmetric synapses (arrows) and one symmetric synapse (arrowhead) can be identified on four dendritic spines (d_1 to d_4). Asymmetric synapses show a thick post-synaptic density. The symmetric synapse has a thin post-synaptic density, very similar to the pre-synaptic density, and it is located on the neck of a dendritic spine (d_1). Scale bar, 500 nm (Merchan-Perez et al., 2009).

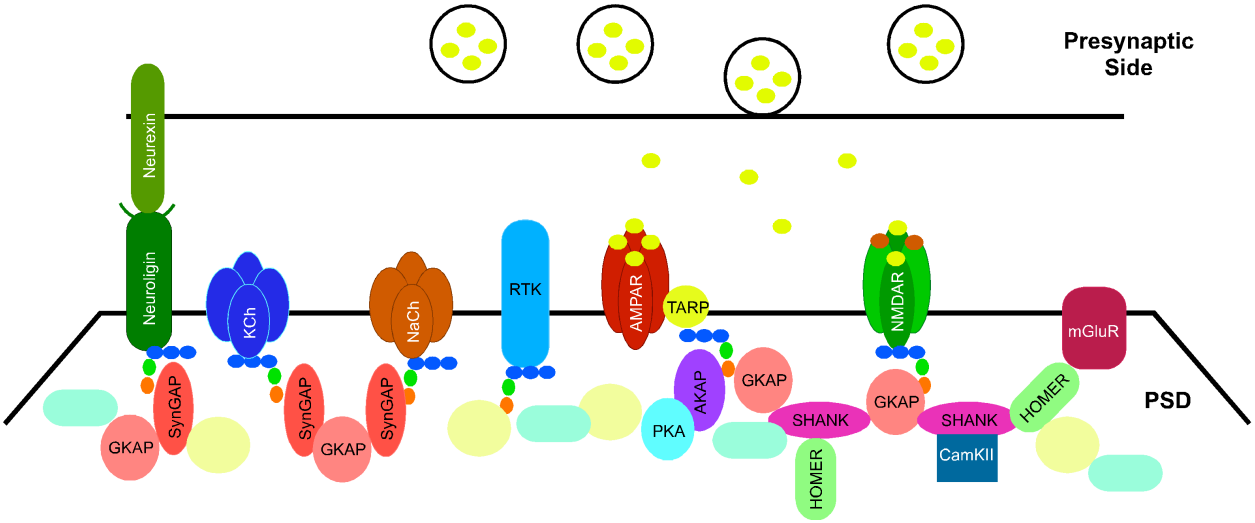

Figure 1.9. Molecular composition of the postsynaptic density (PSD).
Glutamate filled vesicles are at the presynaptic site ready to be released. Core scaffold proteins of the PSD - PSD-95 (bead-like, modular structures in blue, green and ornage), GKAP, Shank, and Homer - interact with each other and postsynaptic membrane proteins (Cell adhesion molecules, K channels, Na Channels, Glutamate receptors) and signaling molecules (SynGAP, CaMKII, PKA). AMPAR, AMPA receptor; CaMKII, calcium/calmodulin-dependent protein kinase II; mGluR, metabotropic glutamate receptor; NMDAR, NMDA receptor; SynGAP, synaptic Ras-GTPase-activating protein; TARP, transmembrane AMPA receptor regulatory protein. Adapted from (Sheng and Hoogenraad, 2007).

MAGUKs

Membrane associate guanylate kinases (MAGUKs) are scaffolding proteins at the PSD and the central organizers of glutamatergic synapses. The family has four main members in the CNS: PSD-95, PSD-93, SAP102 and SAP97. All show a common modular arrangement (Fig. 1.10): three PSD-95/Discs-Large/ZO-1 (PDZ), one SRC Homology 3 (SH3) and one Guanylate kinase (GUK) domains all of which provide harbors for interactions with other proteins in the cytoplasm as well as the cell membrane (Fig. 1.9) (Kim and Sheng, 2004). In pyramidal neuron, MAGUKs regulate the trafficking and clustering of the receptors at the postsynaptic membrane (Elias and Nicoll, 2007). They can also modulate biophysical properties of the GluR subunits. Furthermore, they control downstream signals of receptor activation. Consequently, they have a role synaptic transmission and restructuring the PSD (Futai et al., 2007; Kuriu et al., 2006; Regalado et al., 2006). In addition to their normal biology, MAGUKs have also been studied in the context of several neurobiological diseases such as Alzheimer's, stroke and Huntington's, and have been proposed as the possible pharmacological targets in disease treatment (Gardoni, 2008; Gardoni et al., 2009).

Figure 1.10. The modular structure of membrane associated guanylate kinases (MAGUKs). Four members of the family share the same domain organization: 3 PSD-95/Discs-Large/ZO-1 (PDZ), 1 SRC Homology 3 (SH3) and 1 Guanylate kinase (GUK) domain. All these domains are protein-protein interaction sites; GUK domain has no kinase activity.

PSD-95

PSD-95 is the most abundant MAGUK in brain and is used as an excitatory postsynaptic marker. Like the other members of the family, it is involved in trafficking, anchoring and clustering of GluRs and other ion channels (e.g., Kv1.1-1.4) (Elias and Nicoll, 2007; Tiffany et al., 2000). PSD-95 binds directly to NMDAR subunits NR1/NR2A (Kornau et al., 1995; Sans et al., 2003). In contrast, PSD-95 and AMPAR subunit interactions require AMPAR auxiliary subunits known as transmembrane AMPAR regulatory proteins (TARPs), which have PDZ-binding motifs (Schnell et al., 2002). In parallel to these observations, in disease states (e.g., Parkinson's), PSD-95/GluR assemblies are disturbed (Gardoni et al., 2009; Picconi et al., 2004). In addition to its role in basic synaptic transmission, PSD-95 has an affect on regulation of short-term synaptic plasticity by mediating presynaptic-postsynaptic communication (Futai et al., 2007).

PSD-93

Although there is functional redundancy among the MAGUK members in regard to their role in glutamatergic synaptic transmission, they can also show different expression patterns and functions (Elias et al., 2006; Elias and Nicoll, 2007; Kim and Sheng, 2004). For example, PSD-93 expression is more prominent in cerebellar Purkinje cells than the other MAGUKs (Brenman et al., 1996) suggesting it can have cell-type specific roles. MAGUKs show differential subcellular localization as well. For example, PSD-95 and PSD-93 were shown in different synapses on the same pyramidal neurons (Elias et al., 2006) suggesting synapse specific roles for particular MAGUKs. Moreover, in mouse hippocampus, PSD-93 has opposite affect on long-term synaptic plasticity in comparison to PSD-95 (Carlisle et al., 2008) suggesting that these two MAGUKs are involved in different signaling pathways in neurons.

SAP102

SAP102 shows a similar expression profile in brain with the time-course of synaptogensis. The protein level peaks early in development (P15-16) and then goes down (Muller et al., 1996; Standley et al., 2000). It has a role in receptor trafficking in immature synapses. The expression of SAP102 itself at the synaptic sites is also regulated and dependent bidirectionally on activity (Sun and Turrigiano, 2011).

SAP97

SAP97 is the most distinct member of the MAGUK family. It has a broader expression pattern and is seen in other tissue types (e.g., epithelial tissue) (Yamanaka and Ohno, 2008) and as a result SAP97 knock-out mice do not survive after birth (Caruana and Bernstein, 2001). However, cultured neurons from these embryos exhibit normal synaptic transmission (Klocker et al., 2002). In neurons, in addition to the dendrites, the axons are also immunopositive for SAP97 (Muller et al., 1995). Similar to PSD-95, SAP97 mediates transsynaptic communication (Regalado et al., 2006). Its involvement in GluR trafficking has been proposed early in biogenesis (Leonard et al., 1998). However, the role of SAP97 in AMPAR or NMDAR trafficking and clustering in glutamatergic synaptic transmission has not been clarified completely (Elias et al., 2006; Elias and Nicoll, 2007; Regalado et al., 2006). Unlike the other MAGUKs, it directly binds to AMPARs (GluA1 subunit) (Cai et al., 2002; Leonard et al., 1998). In addition to GluR subunits, SAP97 interacts with a variety of membrane proteins including Kv, Kir and Na channels (Kim and Sheng, 1996; Petitprez et al., 2011; Tiffany et al., 2000) (Leonoudakis et al., 2001; Vikstrom et al., 2009) and regulates anchoring and clustering of several types of Kv and Na channels in heterologous expression systems (Tiffany et al., 2000) and cardiac myocytes (Abi-Char et al., 2008; Stiffler et al., 2007) and therefore, controls cardiac excitability. In addition to that, SAP97

might be involved in the emergence of the symptoms and the progression of several neurobiological diseases. For example, in Alzheimer's Disease, SAP97/GluR1 interaction is disrupted (Wakabayashi et al., 1999).

All members of the MAGUK family are widely expressed in various types of neurons in the brain and exhibit important functional roles in pyramidal neurons in particular. Nevertheless, the function of these proteins in the inhibitory interneurons is not known.

CHAPTER 2: EXPRESSION PATTERN OF MAMBRANE-ASSOCIATED GUANYLATE KINASES IN INTERNEURONS OF THE VISUAL CORTEX

ABSTRACT

GABAergic interneurons are key elements regulating the activity of local circuits, and abnormal inhibitory circuits are implicated in certain psychiatric and neurodevelopmental diseases. The glutamatergic input that interneurons receive is a key determinant of their activity, yet its molecular structure and development, which are often distinct from those of glutamatergic input to pyramidal cells, are poorly defined. The membrane-associated guanylate kinase (MAGUK) homologs PSD-95/SAP90, PSD-93/chapsyn110, SAP97, and SAP102 are central organizers of the postsynaptic density at excitatory synapses on pyramidal neurons. We therefore studied the cell-type-specific and developmental expression of MAGUKs in the nonoverlapping parvalbumin (PV)- and somatostatin (SOM)-positive interneurons in the visual cortex. These interneuron subtypes account for the vast majority of interneurons in the cortex and have different functional properties and postsynaptic structures, being either axodendritic (PV+) or axospinous (SOM+). To study cell-type-specific MAGUK expression, we used DIG-labeled riboprobes against each MAGUK along with antibodies against either PV or SOM and examined tissue from juvenile (P15) and adult mice. Both PV+ and SOM+ interneurons express mRNA for PSD-95, PSD-93, and SAP102 in P15 and adult tissue. In contrast, these interneuron subtypes express SAP97 at P15, but for adult visual cortex we found that most PV+ and SOM+ interneurons show low or no expression of SAP97. Given the importance of SAP97 in regulating AMPA receptor GluA1 subunit and NMDA receptor subunits at glutamatergic synapses, these results suggest a developmental shift in glutamate receptor subunit composition and regulation of

glutamatergic synapses on PV+ and SOM+ interneurons.

INTRODUCTION

In the cortex, a variety of biochemically, morphologically, and functionally distinct subgroups of GABAergic interneurons regulate the activity of local microcircuits (Markram et al., 2004; Silberberg et al., 2005). The excitatory glutamatergic input onto cortical interneurons is a key determinant of their function and can be altered with activity (Hennou et al., 2002; Kullmann and Lamsa, 2007) and development (Hennou et al., 2002). In addition, abnormal inhibitory (GABAergic) circuits are implicated in certain psychiatric and neurodevelopmental diseases, such as schizophrenia and autism (Di Cristo, 2007; Lisman et al., 2008). Schizophrenia, for example, may reflect in part a decreased glutamatergic innervation and NMDAR expression on GABAergic interneurons in the prefrontal cortex (Lisman et al., 2008). Still, despite their important role in regulating GABAergic activity, the molecular structure, development, and dynamics of glutamatergic synapses on interneurons are poorly defined. Although glutamatergic synapses on interneurons may share key features and mechanisms with pyramidal neurons, GABAergic interneuron subgroups often express distinct glutamate receptor subunits (e.g., only Ca^{2+}-permeable AMPAR subunits and the NMDAR GluN2C subunit (Angulo et al., 1997; Geiger et al., 1995; Martina et al., 2003; Moga et al., 2002), can lack spines (Goldberg et al., 2003a; Goldberg and Yuste, 2005; Kawaguchi and Kubota, 1993), and can show distinct features of synaptic plasticity (Kullmann and Lamsa, 2007; Nissen et al., 2010).

Membrane-associated guanylate kinases (MAGUKs) are scaffolding proteins and central organizers of glutamatergic synapses. The MAGUK family has four members that can be expressed in the postsynaptic density (PSD) of excitatory synapses: PSD-95, PSD-93, SAP97, and SAP102 (Funke et al., 2005; Sheng and Hoogenraad, 2007). These proteins share high sequence similarity as well as similar domain structure: three PDZ domains followed by an SH3

and a GK domain (Funke et al., 2005; Sheng and Hoogenraad, 2007). In general, these PSD proteins have been implicated in trafficking, clustering, and regulating GluRs (Elias and Nicoll, 2007; Newpher and Ehlers, 2008; Robertson et al., 2009), as intracellular adaptor proteins (Funke et al., 2005), and as elements in brain dysfunction (Gardoni, 2008). They interact with different GluR subunits (Kim and Sheng, 2004; Leonard et al., 1998), GluR-interacting proteins (see, e.g., Bats et al., 2007; Chen et al., 2000), and cytoplasmic proteins (Sheng and Hoogenraad, 2007). Accordingly, they have different functions at specific synapses (Elias et al., 2008; Regalado et al., 2006). In addition, EM studies suggest preferential localization of MAGUK members in different excitatory synapses and subsynaptic compartments (synaptic vs. extrasynaptic; Aoki et al., 2001). All members of the MAGUK family are expressed in the mouse and rat brain, including the cortex (Kim and Sheng, 1996; Allen Brain Atlas; http://mouse.brain-map.org/). However, they show strong developmental and brainregion- and cell-type-specific expression patterns (Aoki et al., 2001; Fukaya et al., 1999; Fukaya and Watanabe, 2000). In addition, although their cell-type-specific expression can be defined in certain brain regions with well-defined structure (e.g., cerebellum; http://mouse.brain-map.org/; Brenman et al., 1996; Chetkovich et al., 2002b; Muller et al., 1995), this is not possible in the cortex, where pyramidal neurons and a variety of interneuron subgroups are mixed together.

In the cortex, the two most prominent interneuron subgroups are parvalbumin (PV)- and somatostatin (SOM)-positive. These nonoverlapping interneuron subgroups of the cortex differ not only in terms of biochemical markers but also in morphology, membrane properties, synaptic targeting, and subcellular architecture (Burkhalter, 2008; Markram et al., 2004). PV+ interneurons are mainly multipolar basket cells that are fast-spiking and that target exclusively perisomatic domains of pyramidal neurons, having a strong influence on action potential

generation (Freund, 2003; Freund and Katona, 2007). On the other hand, SOM+ interneurons are bitufted Martinotti cells that are regular- spiking and that target mainly more distal dendrites, influencing primarily synaptic integration (Markram et al., 2004; Thomson and Bannister, 2003). Notably, glutamatergic synapses on PV+ interneurons are axodendritic (aspiny), whereas on SOM+ interneurons they are axospinous (spiny; Goldberg and Yuste, 2005; Kawaguchi and Kubota, 1993). In addition, although the identity of GluR subtypes is not well-defined on these cells, they both express Ca2+-permeable AMPARs (Geiger et al., 1995; Moga et al., 2002).

Given the importance of MAGUKs in organizing and regulating pyramidal-to-pyramidal synapses (Montgomery et al., 2004; Sheng and Hoogenraad, 2007), we defined their cell-type-specific expression profiles in PV+ And SOM+ interneurons as a function of developmental age. To do so, we used a combination of in situ hybridization and immunohistochemistry to characterize the mRNA expression pattern of MAGUKs in these interneurons in the visual cortex. Surprisingly, we find that the four MAGUKs show a comparable expression pattern in the two interneuron subgroups. However, SAP97 was developmentally regulated, with a subset of both PV+ and SOM+ interneurons showing greatly decreased expression in adult. The identity of these interneuron subsets and the functional consequences of SAP97 absence in adults remain unknown.

MATERIALS AND METHODS

Animals

Maintenance of all animal and the surgical procedures used were approved by the institutional animal care and usage committee at Stony Brook University and were in line with the guidelines established by the National Institutes of Health.

Tissue preparation

Fifteen (juvenile)- or fifty-six (adult)-day-old mice were deeply anesthetized with intraperitoneal administration of ketamine (0.12 cc/100 g) and xylazine (0.05 cc/100 g) and then perfused transcardially with 0.1 M phosphate buffer (PB) and fixed with 4% paraformaldehyde. Brains were dissected out and postfixed in the same fixative for 3 hours at room temperature. A postfixed brain was left in 30% sucrose solution for dehydration at 4^0C and was then cut longitudinally into two hemispheres. A hemisphere was then immersed in Shandon M-1 embedding matrix (Thermo Scientific, Rockford, IL) and cryosectioned at -20^0C (Leica LM1850; Leica Microsystems, Bannockburn, IL) at 20 lm thick. Sections were kept in cryobuffer (27% glycerol, 27%ethylene glycerol) at -20^0C. All solutions were DEPC-treated and autoclaved to avoid RNA degradation by RNases.

Antibodies

The following primary antibodies were used: rabbit polyclonal anti-PV (Abcam, Cambridge, MA) and rat monoclonal anti-SOM (Chemicon, Temecula, CA; Table 1). As secondaries, we used fluorescent Alexa 488-conjugated anti-rabbit and anti-rat IgG (Molecular Probes, Eugene, OR) or alkaline phosphatase-conjugated anti-DIG (anti-DIG-AP; Roche Applied Science, Indianapolis, IN) and hydrogen peroxide-conjugated anti-DIG (anti-DIG-POD; Roche Applied

Science). Table 2.1 summarizes the source, properties, and dilution of the antibodies used in the present study. Rabbit anti-PV recognizes a single band on a Western blot of rat cerebellar tissue extract and also labels a subset of GABAergic interneurons in mouse cortical tissue (manufacturer's data sheet). Immunolabeling is consistent with previous studies (Supp. Info. Figs. 3, 5). Rat anti-SOM recognizes a single ~17-kDa band of the molecular weight marker on the Western blot of mouse brain tissue extract. Although the published data on the brain tissue proposes a dominant 15-kDa band for somatostatin (Morel et al., 1983), higher molecular weight bands were observed in human and fish tissue (Shields, 1980; Levy et al., 1993). Immunolabeling is consistent with previous results (Supp. Info. Figs. 4, 5).

In situ hybridization

Probes

Antisense riboprobes for each gene were transcribed with T7 RNA polymerase (Roche Applied Science) in the presence of digoxigenin-11-UTP (Roche Applied Science). Digoxigenin-labeled RNA probes were purified with Centri-Sep spin columns (Princeton Separations, Adelphia, NJ). Resulting probes were tested for RNA integrity and size by electrophoresis (1% agarose gel). For quantification, serial dilutions of the probes as well as the DIG-labeled control RNA were UV-linked onto the nylon membranes.

Alkaline phophatase-conjugated anti-DIG fragments (Roche Applied Science) were used to detect digoxigenin incorporated into the probes. Digoxigenin-antibody complexes were further incubated with NBT/BCIP substrate, and color change was monitored. Estimations of probe concentrations were made based on the control RNA signals on the membrane. Riboprobes for each MAGUK (PSD-95, PSD-93, SAP97, and SAP102) were designed based on the analysis of their cDNA sequence alignments. Both a and b isoforms of PSD-95 and SAP97 (Chetkovich et

al., 2002b; Schluter et al., 2006; Waites et al., 2009) are targeted with their respective riboprobes. The following PCR primers were used for the probe synthesis:

PSD-95 forward: ATGCTCCCCCAGACATCACAA;

PSD-95 reverse: CCAAGG ATGATGATGGGACGA;

PSD-93 forward: GCTGCACAGAAAGATGGGAGG;

PSD-93 reverse: GGAGCCTTTGTGAAGGACCAC;

SAP97 forward: TCGGGTCTTGGTTTCAGC;

SAP97 reverse: GGCGGACCTGCTGATCTA;

SAP102 forward: GACGTCCATCAACGGTAC;

SAP102 reverse: CAGCTTGTACTCTCTGCC.

Specificity controls

Specificity of the riboprobes was further tested with dot blot analysis. Serial dilutions (0.001-10 ng) of full length mRNA of each MAGUK were UV-linked to a nylon membrane and hybridized with DIG-labeled riboprobes under the same conditions as in the in situ hybridization on the tissues. Each antisense riboprobe hybridized, in a concentration-dependent manner (based on increasing intensity), with its complementary MAGUK transcript. Hybridizations with nontarget MAGUKs either were not detected or occurred only at high concentrations of the transcript (10 ng; Supp. Info. Fig. 1). In addition, our riboprobes recapitulate layer- and cell-type-specific expression in the cerebellum (Supp. Info. Fig. 2).

Hybridization

Before hybridization, tissue sections were washed with phosphate-buffered saline (PBS), placed on precleaned slides, and air dried. Sections were then digested with predigested proteinase-K

(20 μg/ml) for 7 minutes and then postfixed with cold 4% paraformaldehyde for 10 minutes at room temperature. Postfixed tissue sections were acetylated for 10 minutes and washed in 1X Tris/glycine (pH 7.0) for 30 minutes at room temperature. Washes between each application were performed with 1X PBS. Sections were then prehybridized for 2 hours at 65^0C in a hybridization solution (50% formamide, 4X SSC, 5X Denhardt's solution, yeast RNA, salmon sperm DNA, dextran sulfate) without probe and hybridized with 500 ng DIG-labeled probe in the same hybridization solution overnight at 65^0C in a humidified chamber. Sense probes, a probe targeting Xenopus laevis heterogeneous nuclear ribonucleoprotein A/B (hnrpab) gene, and a hybridization reaction without any probe were used as controls. Posthybridization treatments included washes in 50% formamide/2X SSC at 65^0C and RNaseA digestion (Sigma-Aldrich, St. Louis, MO) at 37^0C. Successful hybridizations were detected with anti-DIG fragments. Tissue was blocked for 30 minutes in blocking solution (100 mM Tris-Cl, pH 7.5, 150 mM NaCl, 0.5% Triton X-100, 2% normal sheep serum). Tissue sections were then incubated with a polyclonal antibody against digoxigenin conjugated to either alkaline phosphatase (1:1,000) or hydrogen peroxide (1:100).

For chromogenic detection, sections were incubated in color-detection buffer (100 mM Tris-Cl, pH 9.5, 100 mM NaCl) containing NBT/BCIP. After color development, sections were left to dry overnight and mounted with Permount (Fisher Scientific, Pittsburgh, PA). For fluorescent detection, sections were incubated with fluorescent detection buffer (100 mM Tris-Cl, pH 8.0, 100 mM NaCl, 10 mM MgCl2) containing either an alkaline phosphatase substrate, HNPP/Fast Red TR Mix (Roche Applied Science), or a hydrogen peroxide substrate, CY3-tyramide signal amplification (TSA-CY3; PerkinElmer, Wellesley, MA). The sections were then

mounted with Vectashield mounting medium (Vector Laboratories, Burlingame, CA). Images were taken and analyzed with a Zeiss LSM 510 confocal microscope.

Combined in situ hybridization and immunohistochemistry

In the experiments in which we used both in situ hybridization and immunohistochemistry, the second technique was integrated into the in situ hybridization protocol at the secondary antibody (anti-DIG fragments) incubation step. Anti-PV and anti-SOM antibodies were included in the antibody mix for overnight incubation. After the washes, in situ hybridization signal was developed with either HNPP/Fast Red TR kit or TSA-indirect amplification kit, and the tissues were incubated with fluorescent secondary antibodies to develop immunohistochemistry signal. The sections were then mounted and imaged as noted previously.

Quantification of cell-type-specific expression

Identification of PV+ and SOM+ cells was done by means of design-based (assumption-free, unbiased) stereology (Peterson, 1999). Mouse brains from at least three different animals were used for each condition. Sections were collected using systematic-random sampling. The 20-µm slices were collected in six parallel sets, each set consisting of 10-14 sections, with each section separated by 120 µm. Among the six sets, four were randomly assigned to a particular MAGUK, and the remaining two sets were used for control experiments or discarded. Analysis of signal intensities for in situ hybridization and immunohistochemistry was done with the Profile Analysis component of LSM 510 software. For each section, only the central focal plane, avoiding the edges of the section, was used for sampling. Stage movements were made by hand to move between nonoverlapping sample fields. For each section, the background intensity was determined on a region where there were no obvious neuronal soma. Each PV+ and SOM+ interneuron (intensity at least 50% greater than background) with a well-defined nucleus was

scored for MAGUK expression. Lines were drawn through the cell using at least three different angles (see Fig. 3). When peaks for the MAGUK signal for at least one of these lines were 50% more than the background and paralleled the PV+ and SOM+ distribution, they were scored positive. In certain instances, it was impossible to score a cell as MAGUK-positive or -negative because of adjacent cells or the overall positioning of the PV+ or SOM+ soma. These cases were recorded as ambiguous.

RESULTS

By using a combination of in situ hybridization and immunohistochemistry, we characterized the cell-type specific mRNA expression of four MAGUKs (PSD-95, PSD-93, SAP97, SAP102) in PV+ and SOM+ interneurons in mouse brain, focusing on the visual cortex. We selected layers 2/3 and layer 5 to be representative of the cortex and monitored age dependence by measuring expression in both juvenile (P15) and adult mouse brains. We chose P15 as the earliest developmental point because synaptogenesis begins around this time (Miller, 1986), and PV gene expression is turned on in the cortex after P14 (see, e.g., Gonchar et al., 2007).

PV+ and SOM+ interneurons in the visual cortex of juvenile (P15) and adult mice express PSD-95 mRNA

Figures 2.1 and 2.2 show confocal images of tissue sections, encompassing the visual cortex, from juvenile (P15; Fig. 2.1) and adult (Fig. 2.2) mouse brains labeled with either PV (Figs. 2.1A1-C3, 2.2A1-B3) or SOM (Figs. 2.1D1-F3, 2.2C1-D3) antibody (green) and hybridized with DIG-labeled PSD-95 riboprobes (red). Figure 2.1A1-A3, D1-D3 shows images of the visual cortex of a mouse brain at low magnification (10X), with the approximate boundaries of the layers demarcated in Figure 2.1A3, D3. PV+ interneurons, which represent about ~40% of cortical GABA+ interneurons, and SOM+ interneurons (~30%) are dispersed throughout the entire visual cortex (Fig. 1A1, D1; Gonchar et al., 2007; Markram et al., 2004). Magnified images of cells in layers 2/3 and layer 5 for P15 mouse tissue are shown in Figure 2.1B1-B3, E1-E3 and Figure 2.1C1-C3, F1-F3, respectively. Consistent with previous reports (Gonchar et al., 2007), PV staining is observed both in the cytoplasm and in the nucleus (Fig. 2.1B1, C1). In contrast to PV, SOM staining is restricted to the cytoplasm (Fig. 2.1E1, F1), as is the signal for PSD-95 (Fig. 2.1B2, C2, E2, F2). Figure 2.1B3,C3 shows merged images of the PV and PSD-95

signals with our approach to define overlap between them (shown in Fig. 2.3). Figure 3A3 shows a merged image (same as Fig. 2.1B3) of the analyzed cell (for additional details see Materials and Methods). As shown in Figure 2.3B1-B3, the peak PV signal (green) was used to define the borders of the PV+ cell (dashed lines), and then the peak MAGUK signal was used, taking into account surrounding cells, to define whether the cell was positive or negative for the MAGUK. In this instance, the PSD-95 signal (red) is clearly located within the PV+ borders. Among the 32 cells in layers 2/3 and the 28 cells in layer 5 that were positive for PV, almost all scored positive for PSD-95 mRNA in P15 mouse visual cortex (Table 2.2).

In adult mice, a similar expression pattern of PSD-95 was also observed in PV+ interneurons (Fig. 2.2A1-B3, Table 2.2). Similarly, as shown in the merged images (Fig. 2.1E3, F3), PSD-95 mRNA colocalizes with the SOM signal, a point further illustrated in the colocalization analysis (Fig. 2.3C1-D3). Indeed, almost all identified SOM+ interneurons in layers 2/3 (74 total) and layer 5 (114 total) in P15 mice scored positive for PSD-95 (Table 2.2). SOM+ Interneurons in adult animals also express PSD-95 mRNA (Fig. 2.2C1, D3, Table 2.2). In summary, the nonoverlapping PV+ and SOM+ interneuron populations in the cortex both express PSD-95 mRNA at minimum from P15 to adult.

PV+ and SOM+ interneurons in the visual cortex of juvenile (P15) and adult mice express PSD-93 mRNA

Figure 2.4 shows cell-type-specific PSD-93 mRNA expression for PV+ (Fig. 2.4A1-B3) and SOM+ (Fig. 2.4C1-D3) interneurons in layers 2/3 of P15 (Fig. 2.4A1-A3, C1-C3) and adult (Fig. 2.4B1-B3, D1-D3) mouse visual cortex. PSD-93 shows wide cellular expression in both P15 (Fig. 2.4A2, C2) and adult (Fig. 2.4B2, D2) tissue. The merged images show that PSD-93 mRNA colocalizes with PV in P15 (Fig. 2.4A3) and adult (Fig. 2.4B3) tissue (colocalization

analysis not shown). Over 90% of PV+ cells in both P15 and adult tissue scored positive for PSD-93 mRNA (Table 2.2). PV+ interneurons in layer 5 showed a similar strong colocalization (data not shown; Table 2.2). For P15 and adult SOM+ interneurons, PSD-93 mRNA is also expressed in layers 2/3 (Fig. 2.4C1-D3) and layer 5 (data not shown; Table 2.2). Therefore, like PSD-95, both PV+ and SOM+ Interneurons express PSD-93 mRNA at P15 and adult.

PV+ and SOM+ interneurons in the visual cortex of juvenile (P15) and adult mice express SAP102 mRNA

Figure 2.5 shows cell-type-specific SAP102 mRNA expression for PV+ (Fig. 2.5A1-B3) and SOM+ (Fig. 2.5C1-D3) interneurons in layers 2/3 of P15 (Fig. 2.5A1-A3, C1-C3) and adult (Fig. 2.5B1-B3, D1-D3) mouse visual cortex. In contrast to other MAGUKs, SAP102 in situ hybridization gave punctate staining probably because of the different signal detection technique used (TSA-CY3; see Material and Methods), which provides increased sensitivity (Breininger and Baskin, 2000). Nevertheless, as shown in the merged images, these punctate signals showed a clear overlap with PV in P15 (Fig. 2.5A3) and adult (Fig. 2.5B3) tissue (colocalization analysis not shown). Over 85% of PV+ cells in both P15 and adult tissue scored positive for SAP102 mRNA (Table 2.2). PV+ interneurons in layer 5 showed a similar strong colocalization (data not shown; Table 2.2). For P15 and adult, SAP102 mRNA is also colocalized with SOM in layers 2/3 (Fig. 2.5C1-D3) and layer 5 (data not shown; Table 2.2). Therefore, both PV+ and SOM+ interneurons express SAP102 mRNA at P15 and adult.

SAP97 mRNA shows a developmental expression pattern in both PV+ and SOM+ interneurons in the visual cortex

Figure 2.6 shows cell-type-specific SAP97 mRNA expression for PV+ (Fig. 2.6A1-B3) and SOM+ (Fig. 2.6C1-E3) interneurons in layers 2/3 of P15 (Fig. 2.6A1-A3, C1-C3) and adult (Fig. 2.6B1-B3, D1-E3) visual cortex. In P15 tissue, the merged images show that SAP97 mRNA colocalizes with PV and SOM (Fig. 2.6A3, C3), a result also found in layer 5 (data not shown). Indeed, over 85% of cells positive for PV or SOM in layers 2/3 and layer 5 in P15 tissue scored positive for SAP97 mRNA (Table 2.2). In adult tissue, on the other hand, most PV+ and SOM+ interneurons scored negative for SAP97. For PV (Fig. 2.6B1-B3), the triangles point to a representative PV+ cell that was scored negative for SAP97, whereas the arrowhead indicates a PV+ cell that scored positive. This point is illustrated more specifically in Figure 2.7, which shows the quantitative analysis for the PV+ cells that are either negative [Fig. 2.7A1-A3, B; note the absence of a higher intensity halo/ring around the nucleus especially in regions remote from the two adjacent cells and that no SAP97 signal (red) was above baseline in association with the PV signal as illustrated in Fig. 2.7B] or positive (Fig. 2.7C1-C3, D; note the halo/ring around the nucleus that is greater than the background and is associated with the PV signal as illustrated in Fig. 2.7D) for SAP97. Expression of SAP97 in SOM+ cells in adult tissue (Fig. 2.6D1-D3) was also restricted. Figure 2.6D1-D3 indicates a SOM+ cell that is negative for SAP97 hybridization (triangle; for quantification analysis see Fig. 2.7E1-E3, F), and Figure 2.6E1-E3 indicates a SOM+ cell that is positive for SAP97 hybridization (arrowhead; see Fig. 2.7G1-G3, H). In adult tissue, over 60% of PV+ or SOM+ interneurons in layers 2/3 and layer 5 scored negative for SAP97 mRNA (Table 2.2). The developmental regulation of SAP97 mRNA expression in mouse visual cortex also occurs in layer 5, with Figure 2.8 illustrating examples of PV+ and SOM+

Interneurons with low and high SAP97 expression levels. Figure 2.8A1, A3 shows PV+ cells scored negative (triangle) and positive (arrow) for SAP97. The colocalization analysis of PV and SAP97 signals is represented in Figure 2.8D1-D3, E, F1-F3, G (note the absence of halo/ring for SAP97 signal around the nucleus of the neuron in Fig. 2.8D1-D3). Figure 2.8B1-B3 shows an example of SOM+ interneurons in layer 5 that scored negative for SAP97 and Figure 2.8C1-C3 shows SOM+ interneurons that scored positive for SAP97.

DISCUSSION

By using combined in situ hybridization and immunohistochemistry, we demonstrate for the first time the celltype-specific expression of MAGUKs in cortical interneurons, specifically, those positive for PV or SOM. Surprisingly, although the glutamatergic synapses on PV+ and SOM+ interneurons show distinct morphological and functional properties (see the introductory paragraphs), they express all four MAGUKs comparably, with a subset of both subgroups showing a reduced expression of SAP97 in adult animal. Although the four MAGUKs are structurally similar, our riboprobes were highly specific (see Materials and Methods) and did not show any obvious cross-reactivity (Supp. Info. Fig. 2.1). In addition, the MAGUKs do show cell-type-specific expression in the brain (see the introductory paragraphs), and our riboprobes confirm these ideas in the cerebellum (Supp. Info. Fig. 2; Brenman et al., 1996; Muller et al., 1995). Thus, the expression patterns of the various MAGUKs in PV+ and SOM+ interneurons are specific, although their functional significance, their specific subcellular distributions, and the developmental role of changes in SAP97 expression remain unknown. Finally, although our experiments were done on the visual cortex, our results are applicable more widely to all PV+ and SOM+ interneurons in the cerebral cortex.

Interneuron subgroups in the visual cortex

In the mouse visual cortex, various subgroups of GABAergic interneurons have been characterized on the basis of the combinations of biochemical markers that they express, such as PV, SOM, calretinin (CR), neuropeptide-Y (NPY), vasoactive intestinal polypeptide (VIP), and cholecystokinin (CCK), among others (Burkhalter, 2008; Markram et al., 2004). These subgroups often show different physiological and anatomical properties. We studied PV+ (fast-spiking) and SOM+ (regular-spiking) interneurons because they constitute a majority (~65%) of

the interneurons in the cortex (Gonchar et al., 2007). In addition, they present an interesting structural contrast in their glutamatergic synapses: PV+ interneurons are aspiny, whereas SOM+ interneurons form spiny synapses (Goldberg and Yuste, 2005; Kawaguchi and Kubota, 1993). In our study, we screened MAGUK mRNA expression at P15, the age when eye-opening occurs with initiation of activity dependent plasticity, and PV+ and SOM+ interneurons are still relatively immature, as well as in adult tissue.

MAGUK expression in PV+ and SOM+ interneurons

We used riboprobes to detect MAGUK mRNA in mouse brain tissue. The advantage of in situ hybridization is that mRNA is found mostly in the cell soma and is easy to colocalize with cellular markers (i.e., PV and SOM). However, although in situ hybridization indicates gene expression, it does not indicate protein expression or the distribution of proteins at a synapse. Our experiments show that both PV+ and SOM+ Interneurons express PSD-95 (Figs. 2.1-2.3, Table 2.2), PSD-93 (Fig. 2.4, Table 2.2), and SAP102 (Fig. 2.5, Table 2.2) mRNA at all ages tested (P15 and adult). Indeed, in almost all instances, the MAGUK signal colocalized with the interneuron marker >90% of the time. SAP97, on the other hand, is strongly expressed in both interneuron subgroups at P15 (Figs. 2.6, 2.7, Table 2.2), but its expression drops to an undetectable level in more than half (approximately 60%) of the interneurons in adult animals (Figs. 2.6, 2.7, Table 2.2). Either the interneurons do not express the mRNA at all or its expression is too low to be detected with the tools that we used.

Interneuron groups that are defined with certain biochemical markers can often be divided into further subgroups based on coexpression with another biochemical marker (Burkhalter, 2008; Gonchar et al., 2007; Markram et al., 2004). For example, SOM+ interneurons partially overlap with CR+ interneurons (Gonchar et al., 2007). SAP97 expression

in adult animals may be restricted to such a subgroup of PV+ and SOM+ interneurons. However, because PV+ and SOM+ interneurons do not overlap (Gonchar et al., 2007; Supp. Info. Fig. 5) and no known biochemical marker is common to both subgroups, it is presently not clear what this additional marker might be. Nevertheless, given the key role of SAP97 in regulating AMPA and NMDA receptors at glutamatergic synapses (see below), it will be critical to define the functional significance of these distinct classes of PV+ and SOM+ interneurons in adult.

Functional significance of MAGUKs at glutamatergic synapses on interneurons

A major group of interacting partners of MAGUKs are GluRs. MAGUKs bind directly to NMDA receptor subunits (Gardoni, 2008; Kim and Sheng, 2004) and associate with AMPA receptors typically via TARPs (Chen et al., 2000). The exception of course is SAP97, the only MAGUK that can bind directly to AMPA receptors, specifically, GluA1 (Leonard et al., 1998; Sans et al., 2001). Overexpression of SAP97 increases the number of GluA1-containing AMPA receptors at synaptic sites on pyramidal neurons as a result of enhanced trafficking and clustering of the receptors (Rumbaugh et al., 2003; Waites et al., 2009). Additionally, SAP97 is involved in the sorting and trafficking of NMDA receptors to glutamatergic synapses on pyramidal neurons (Jeyifous et al., 2009). The expression of GluR subtypes and subunits at glutamatergic synapses on interneurons is often different from that on pyramidal neurons (see, e.g., Geiger et al., 1995; Martina et al., 2003; Moga et al., 2002). For example, NMDA receptor expression in PV+ and SOM+ interneurons of rat hippocampus is lower than in pyramidal neurons (Nyiri et al., 2003), and the GluN2C index is higher (Martina et al., 2003). In addition, they often express Ca^{2+}-permeable AMPA receptor subunit combinations (GluA1, -A3, and/or -A4; Angulo et al., 1997; Geiger et al., 1995; Moga et al., 2002). Nevertheless, subunit-specific expression patterns of GluRs in interneurons are not well defined. The subunitspecific expression of the receptors might

be correlating with the expression of MAGUKs in the interneurons and could possibly be related to changes in interneuron excitation during the critical period of visual cortex plasticity (Maffei and Turrigiano, 2008) Nevertheless, additional experiments will be needed to define this relationship.

Dysfunction of GABAergic interneurons is implicated in neurodevelopmental and psychiatric disorders (Di Cristo, 2007; Lisman et al., 2008). In addition, decreased NMDAR expression level is prominent in psychiatric diseases such as schizophrenia and bipolar disorder (Kristiansen et al., 2007; Lisman et al., 2008). In parallel, abnormal MAGUK expression levels are observed in various brain regions in these psychiatric diseases (see, e.g., Kristiansen et al., 2007). Low expression and activity of NMDARs and GABAergic interneurons might be the result of dysfunction of MAGUKs at the glutamatergic synapses onto these interneurons. Understanding glutamate receptor trafficking and synaptic activity in GABAergic interneurons will be essential to comprehending the regulation of interneuron activity and the role in disease development.

In conclusion, our study demonstrates the interneuronal expression pattern of MAGUKs at the mRNA level in mouse visual cortex of juvenile (P15) and adult animals. Although we showed a broad mRNA expression of MAGUKs in PV+ and SOM+ interneurons, the synaptic localization of their protein expression, the interaction of MAGUKs with specific GluRs at interneuron synapses, and the potential contribution of MAGUKs to the structure and function of aspiny and spiny glutamatergic synapses on interneurons remain unknown.

TABLES AND FIGURES

Table 2.1. Antibodies used in the present study.

Antigen	Immunogen	Antibody information	Dilution used
Parvalbumin (rabbit anti-PV)	Purified rat skeletal muscle parvalbumin	Abcam (Cambridge, MA), rabbit polyclonal, ab11427	1:1000
Somatostatin (rat anti-SOM)	Synthetic 1-14 cyclic somatostatin conjugated to bovine thyroglobulin using carbodiimide	Chemicon (Temecula, CA), rat monoclonal, MAB354	1:200

Table 2.2. Colocalization of MAGUKs in PV+ and SOM+ interneurons in the mouse visual cortex.

		P15		Adult	
		#	%	#	%
Layers 2/3	PSD-95	32 (32)	100	66 (66)	100
	PSD-93	59 (62)	95	104 (110)	95
PV+	SAP97	53 (54)	98	38 (97)	39
	SAP102	91 (93)	98	147 (161)	91
Layers 5	PSD-95	28 (29)	97	90 (95)	95
	PSD-93	69 (71)	97	109 (121)	90
PV+	SAP97	46 (54)	85	29 (74)	39
	SAP102	85 (88)	97	117 (135)	87
Layers 2/3	PSD-95	74 (74)	100	83 (88)	94
	PSD-93	101 (108)	94	45 (51)	88
SOM+	SAP97	48 (51)	94	35 (107)	33
	SAP102	91 (93)	98	147 (161)	91
Layers 5	PSD-95	114 (117)	97	38 (38)	100
	PSD-93	87 (90)	97	34 (42)	81
SOM+	SAP97	24 (25)	96	22 (65)	34
	SAP102	86 (87)	99	63 (64)	98

refers to the number of cells that were PV+ or SOM+ and positive for the particular MAGUK. Total number of cells screened for each condition is indicated in parentheses. A minimum of three different animals were measured for each condition.

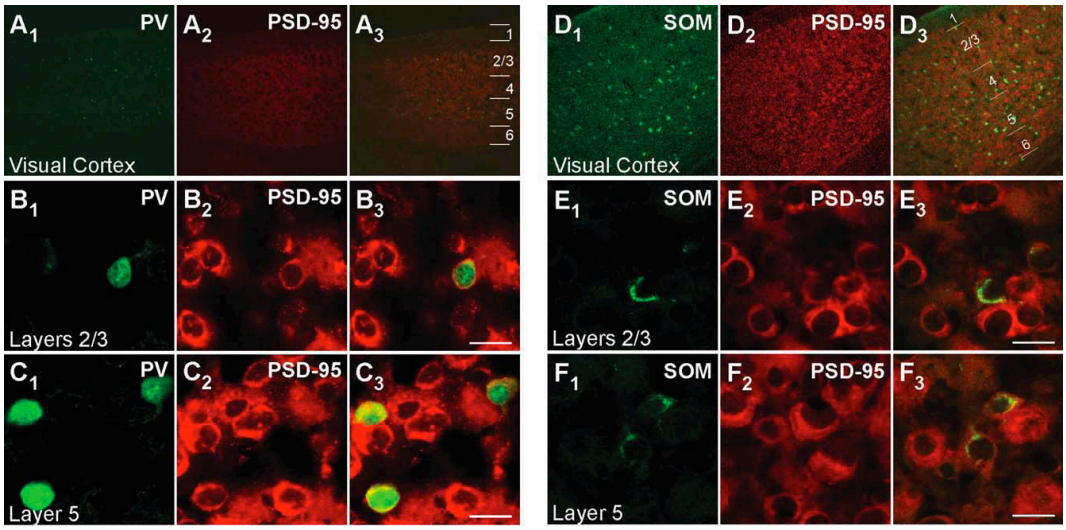

Figure 2.1. PSD-95 mRNA expression in PV+ and SOM+ interneurons in juvenile (P15) mouse visual cortex.

Confocal images of combined in situ hybridization and immunohistochemistry for PSD-95 and either PV or SOM in the mouse visual cortex. Tissue sections were obtained from juvenile (P15) mouse visual cortex. In the left columns, sections were labeled with rabbit anti-PV (green; A1, B1, C1) or rat anti-SOM (green; D1, E1, F1). In the middle columns (A2, B2, C2, D2, E2, F2), the same sections were hybridized with DIG-labeled PSD-95 riboprobe (red). Our riboprobe detected both spliced isoforms (a and b) of PSD-95. The right columns (A3, B3, C3, D3, E3, F3) show merged images. The visual cortex is shown at low magnification (10X; A1–A3, D1–D3), with approximate boundaries between layers demarcated in A3, D3. Other images are at 63X, highlighting layers 2/3 (B1–B3, E1–E3) or layer 5 (C1–C3, F1–F3) to show cell-type-specific expression of PSD-95. Scale bars = 20 μm.

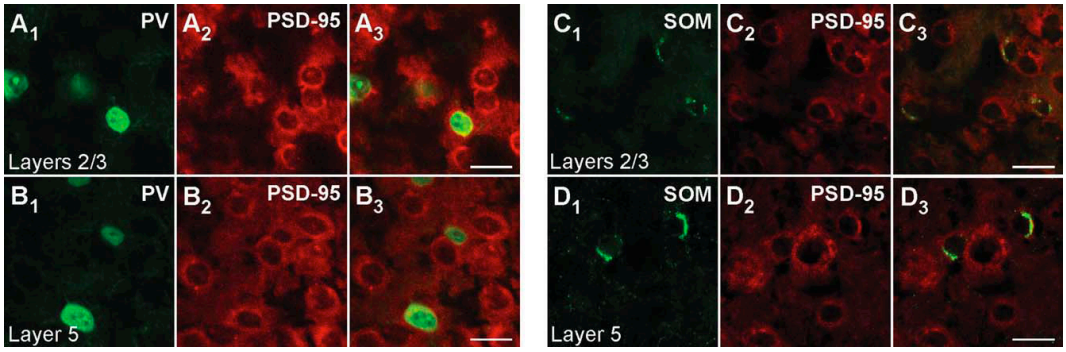

Figure 2.2. PSD-95 mRNA in PV+ and SOM+ interneurons in adult mouse visual cortex. Confocal images of combined in situ hybridization and immunohistochemistry for PSD-95 and either PV or SOM in the mouse visual cortex. Tissue sections were obtained from adult mouse visual cortex. In the left columns, sections were labeled with rabbit anti-PV (green; A, B1) or rat anti-SOM (green; C1, D1). In the middle columns (A2, B2, C2, D2), the same sections were hybridized with DIG-labeled PSD-95 riboprobe (red). The right columns (A3, B3, C3, D3) show merged images. The images are at 63X, highlighting layers 2/3 (A1–A3, C1–C3) or layer 5 (B1–B3, D1–D3). Scale bars = 20 μm.

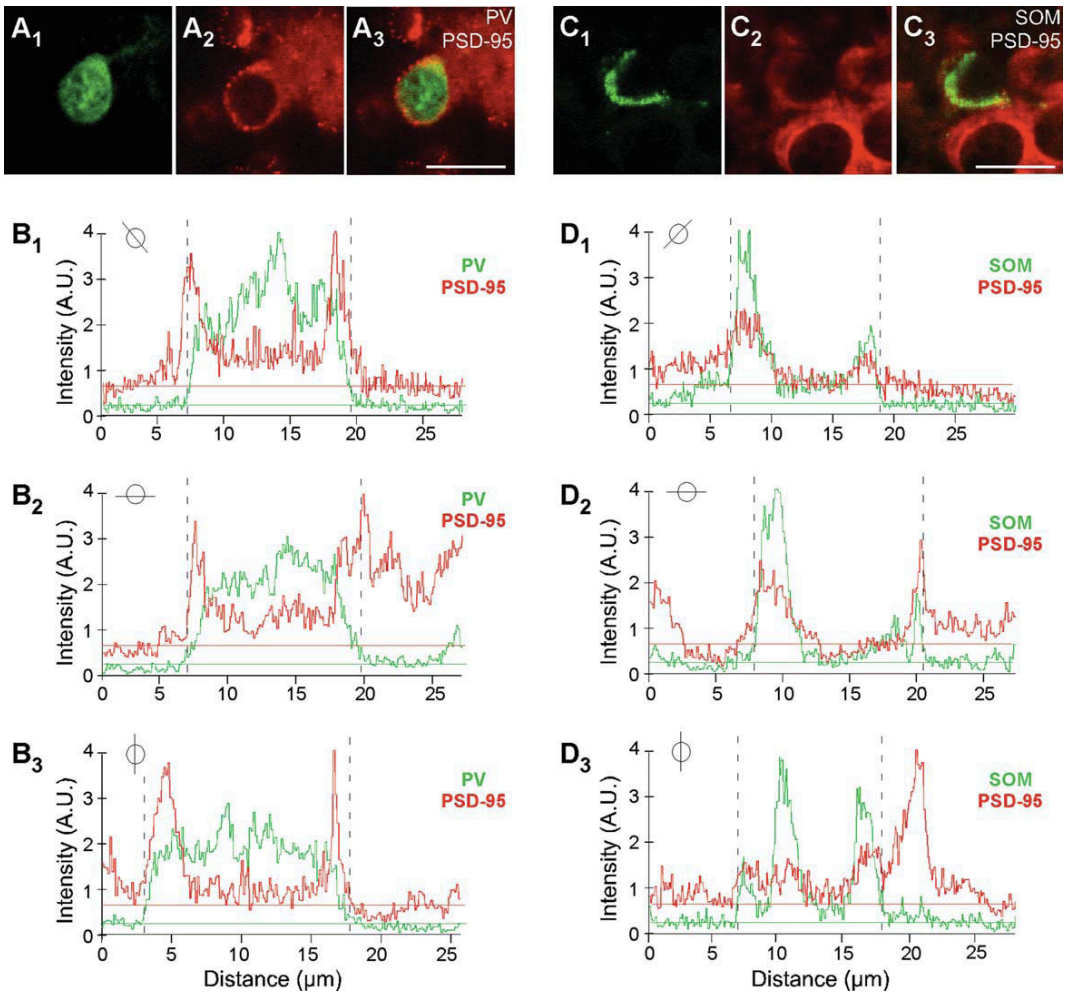

Figure 2.3. Colocalization analysis of PSD-95 and PV or SOM.
A1–A3: Confocal images of a juvenile (P15) mouse brain section labeled with rabbit anti-PV (green) and hybridized with DIG-labeled PSD-95 riboprobe (red; enlarged version of Fig. 2.1B1–B3). Note the halo/ring around the apparent nucleus. B1–B3: Plots of the signal intensities of PV (green) and PSD-95 (red) for a line that cuts through the immunopositive (PV+) cell for the images in (A1–A3; the specific line through the cell is indicated in the small circle inset). The horizontal lines show the average baseline signal intensity for PV (green) and PSD-95 (red; see Materials and Methods). The region where PV signal is greater than the baseline (dashed lines on graphs) is identified as a PV+ interneuron. Note that the peak PSD-95 signal matches and overlaps with the PV signal, except for the nucleus, where PV is present but PSD-95 is not. C1–C3: Confocal images of a juvenile (P15) mouse brain section labeled with rat anti-SOM (green) and hybridized with DIG-labeled PSD-95 riboprobe (red; enlarged version of Fig. 2.1E1–E3). D1–D3: Plots of the signal intensities of SOM (green) and PSD-95 (red) for a line that cuts through the immunopositive (SOM+) cell for the image in (C1–C3; see small circle inset). Note that the SOM signal is not uniformly present around the soma. A.U., arbitrary units. Scale bars = 20 µm.

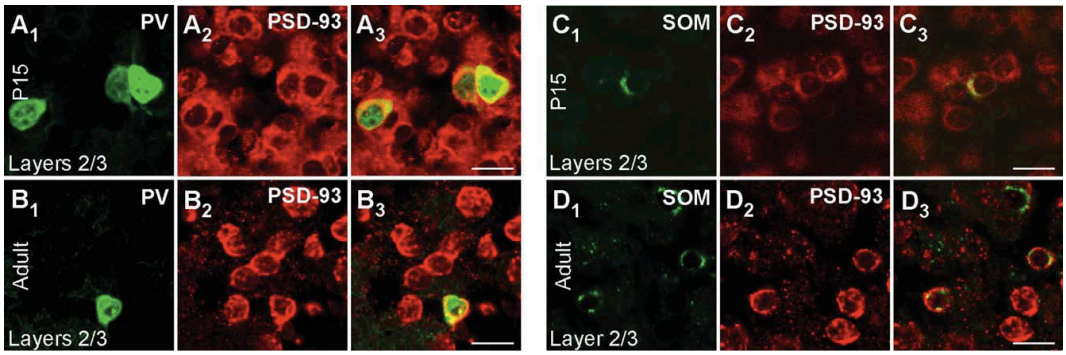

Figure 2.4. PSD-93 mRNA expression in PV+ and SOM+ interneurons in the mouse visual cortex.

Confocal images of combined in situ hybridization and immunohistochemistry for PSD-93 and PV or SOM in the mouse visual cortex. Tissue sections were obtained from juvenile (P15; A1–A3, C1–C3) or adult (B1–B3, D1–D3) mouse visual cortex. In the left columns, sections were labeled with either rabbit anti-PV (A1, B1) or rat anti-SOM (C1, D1; green). In the middle columns (A2, B2, C2, D2), the same sections were hybridized with DIG-labeled PSD-93 riboprobe (red). The right columns (A3, B3, C3, D3) show merged images. Images are at 63X. Scale bars = 20 μm.

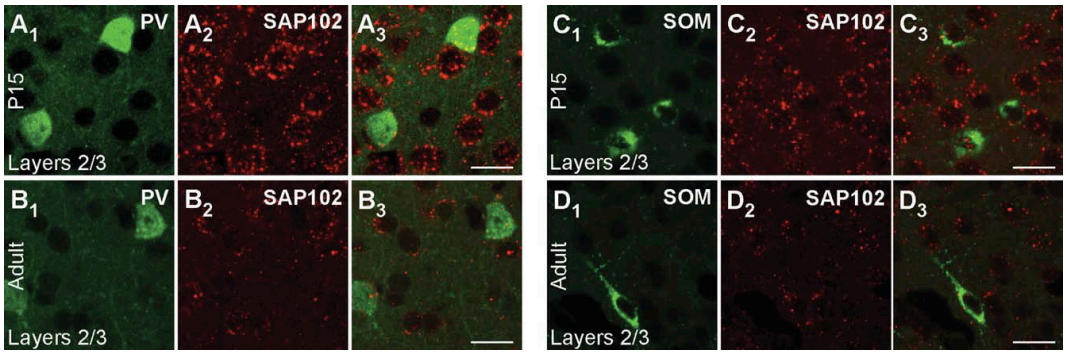

Figure 2.5. SAP102 mRNA expression in PV+ and SOM+ interneurons in the mouse visual cortex.

Confocal images of combined in situ hybridization and immunohistochemistry for SAP102 and PV or SOM in the mouse visual cortex. Tissue sections were obtained from juvenile (P15; A1–A3, C1–C3) or adult (B1–B3, D1–D3) mouse visual cortex. In the left columns, sections were labeled with either rabbit anti-PV (A1, B1) or rat anti-SOM (C1, D1; green). In the middle columns (A2, B2, C2, D2), the same sections were hybridized with DIG-labeled SAP102 riboprobe (red). The right columns (A3, B3, C3, D3) show merged images. Images are at 63X. Scale bars = 20 μm.

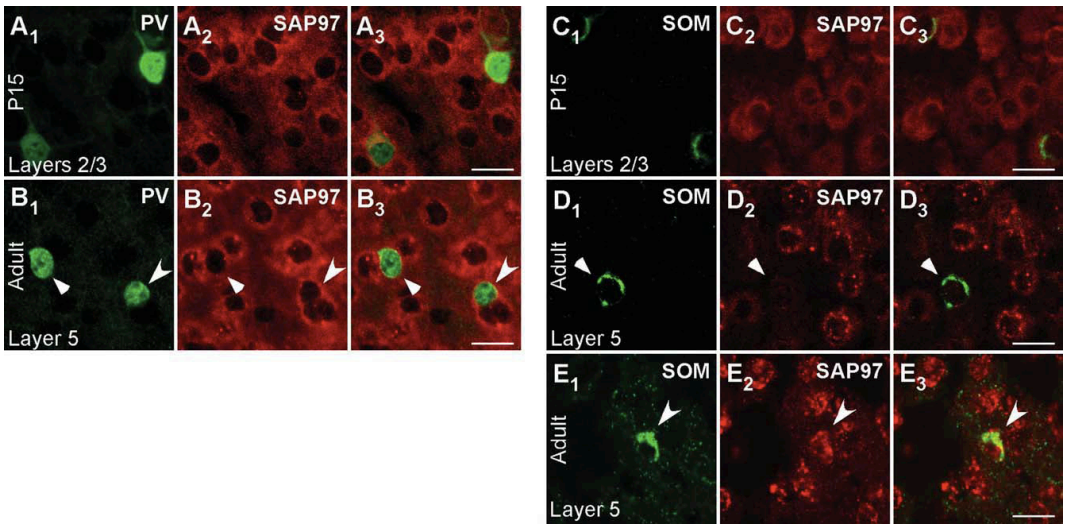

Figure 2.6. Developmentally regulated expression of SAP97 mRNA in PV+ and SOM+ interneurons in layers 2/3 of the mouse visual cortex.

Confocal images of combined in situ hybridization and immunohistochemistry for SAP97 and PV or SOM in the mouse visual cortex. Tissue sections were obtained from juvenile (P15; A1–A3, C1–C3) or adult (B1–B3, D1–E3) mouse visual cortex. In the left columns, sections were labeled with either rabbit anti-PV (A1, B1) or rat anti-SOM (C1, D1, E1; green). In the middle columns (A2, B2, C2, D2, E2), the same sections were hybridized with DIG-labeled SAP97 riboprobe (red). Our riboprobe detected both spliced isoforms (a and b) of SAP97. The right columns (A3, B3, C3, D3, E3) show merged images. Images are at 63X. For adult tissue images (B1–B3, D1–E3), triangles point to PV+ and SOM+ interneurons that are negative, and arrowheads point to interneurons that are positive for SAP97 mRNA. Scale bars = 20 μm.

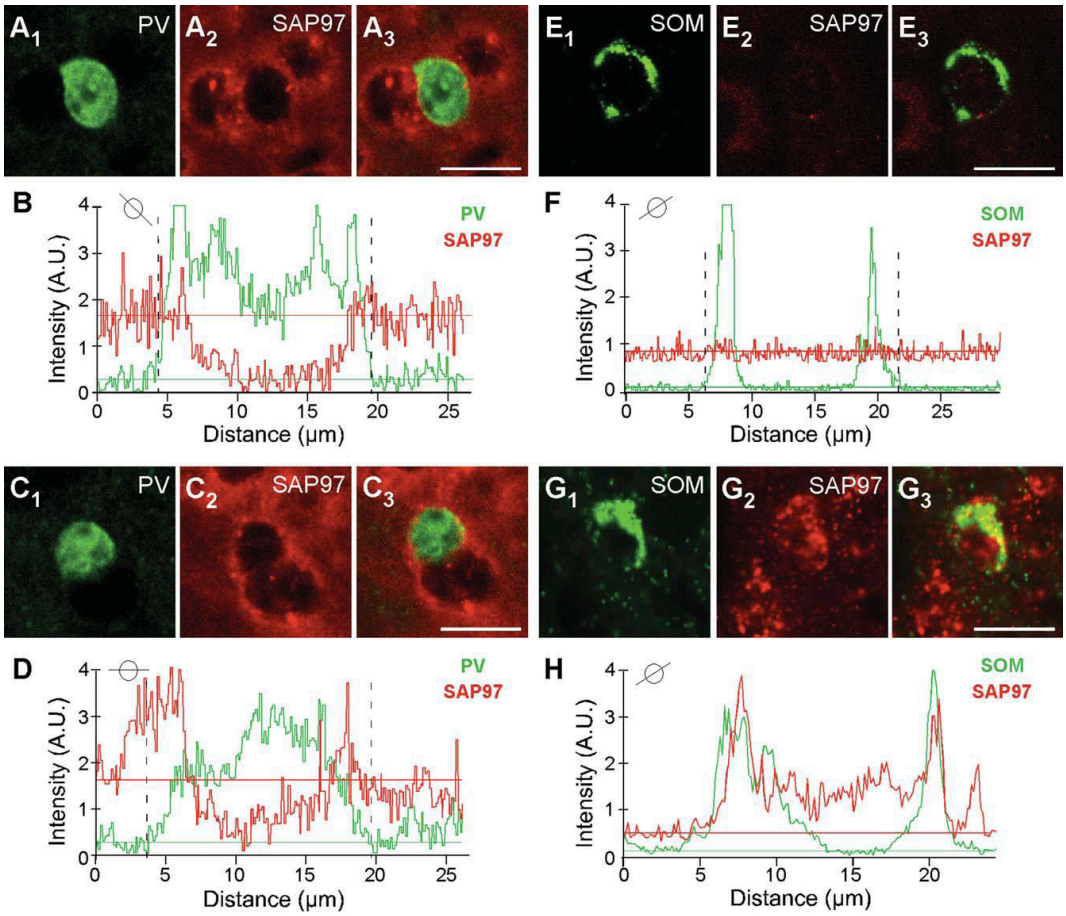

Figure 2.7. Colocalization analysis of SAP97 and PV or SOM.
A1–A3, C1–C3: Confocal images of an adult mouse brain section labeled with rabbit anti-PV (green) and hybridized with DIG-labeled SAP97 riboprobe (red; enlarged version of Fig. 2.6B1–B3). B, D: Plots of the signal intensities of PV (green) and SAP97 (red; B, low expressing; D, high expressing) for a line that cuts through each of the immunopositive (PV+) cells (see small circle insets). The analysis is identical to that in Figure 2.3. In B, a peak SAP97 signal relative to its baseline is difficult to identify, and the PV+ cell was scored negative. Note that, in this instance, we avoided drawing analysis lines that went through the adjacent non-PV+ cells. In D, although there are background complications, a peak SAP97 signal could be associated with the PV signal. E1–E3, G1–G3: Confocal images of an adult mouse brain section labeled with rat anti-SOM (green) and hybridized with DIG-labeled SAP97 riboprobe (red; enlarged version of Fig. 2.6D1–D3, E1–E3). F, H: Plots of the signal intensities of SOM (green) and SAP97 (red; F, low expressing; H, high expressing) for a line that cuts through each of the immunopositive cells (see small circle insets). A peak SAP97 signal was not present, and the SOM+ cell was scored negative. In H, the peak SAP97 signal matches and overlaps with the SOM signal. A.U., arbitrary units. Scale bars = 20 μm.

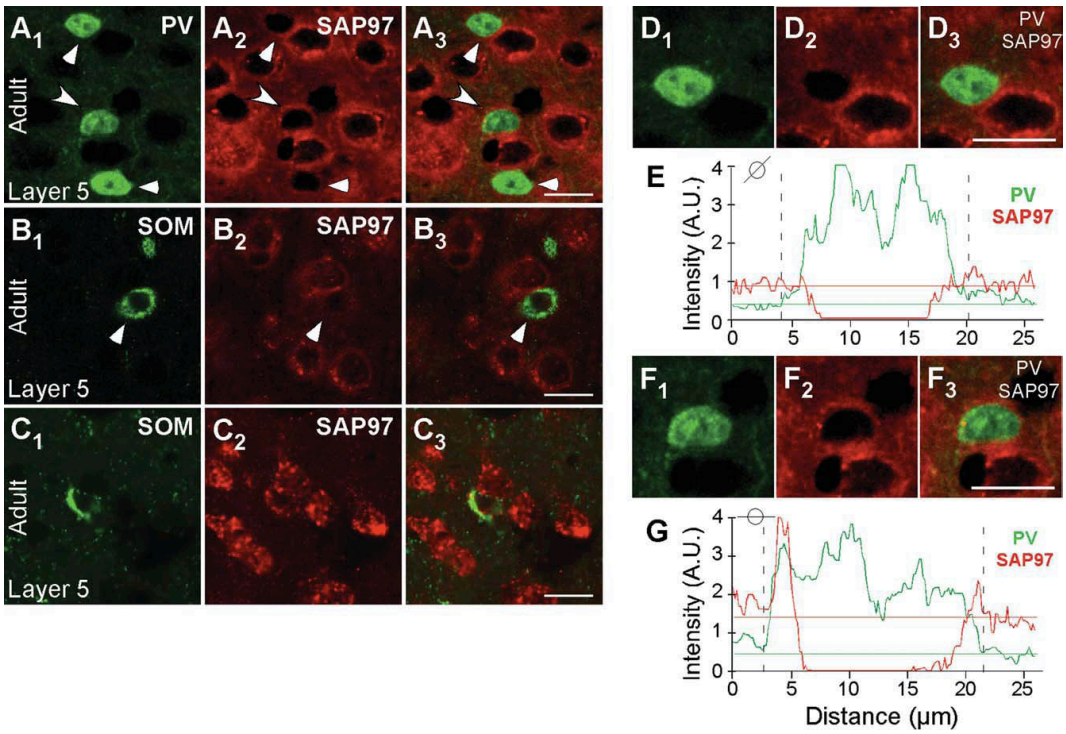

Figure 2.8. Developmentally regulated expression of SAP97 mRNA in PV+ and SOM+ interneurons in layers 5 of the mouse visual cortex.

Confocal images of combined in situ hybridization and immunohistochemistry for SAP97 and PV or SOM in the mouse visual cortex. Tissue sections were obtained from adult mouse visual cortex. In the left column, sections were labeled with either rabbit anti-PV (A1) or rat anti-SOM (B1, C1; green). In the middle column (A2, B2, C2), the same sections were hybridized with DIG-labeled SAP97 riboprobe (red). The right column (A3, B3, C3) shows merged images. Images are at 63X. Triangles point to PV+ and SOM+ interneurons that are negative, and arrowheads point to interneurons that are positive for SAP97 mRNA. D1–G: Enlarged versions of the two cells (D1–D3, F1–F3) in A1–A3 and the plots of the signal intensities of PV (green) and SAP97 (red; E, low expressing; G, high expressing) for a line that cuts through each of the immunopositive (PV+) cells (see small circle insets). In G, the peak SAP97 signal is associated with the PV signal. A.U., arbitrary units. Scale bars = 20 μm.

SUPPLEMENTAL INFORMATION

Expression Pattern of MAGUKs in Interneurons of the Visual Cortex

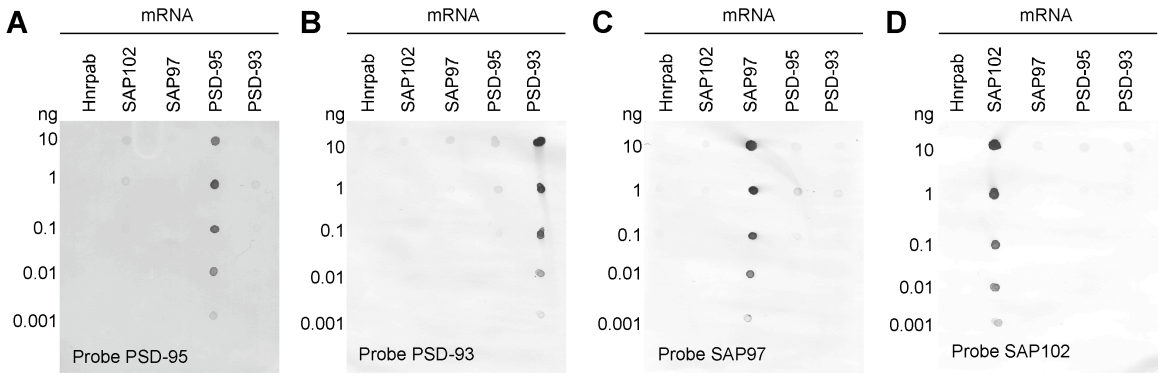

Supplemental Figure 2.1. The MAGUK riboprobes show high specificity for their corresponding mRNA.
Nylon membranes (Ambion, Austin, TX) (A-D) were dot-blotted with gradients (0.001-10 ng) of MAGUK and Hnrpab (as a negative control) mRNAs. Membranes were hybridized with either DIG-labeled PSD-95 (A), PSD-93 (B), SAP97 (C) or SAP102 (D) riboprobes. Anti-DIG-AP fragments (1:1000) and NBT/BCIP (Roche Applied Science, Indianapolis, IN) were used to develop hybridization signal. Dark spots on each membrane show successful hybridizations between the probe and the mRNA. Note that the intensity of the spots changes in a concentration dependent manner with the spots largely restricted to a riboprobe and its corresponding mRNA. Full length MAGUK and *X. laevis* Hnrpab mRNAs were transcribed *in vitro* with mMESSAGE mMACHINE™ Kit (Ambion, Austin, TX). RNA concentrations were determined with SmartSpec™ 3000 Spectrophotometer (Bio-Rad, Hercules, CA).

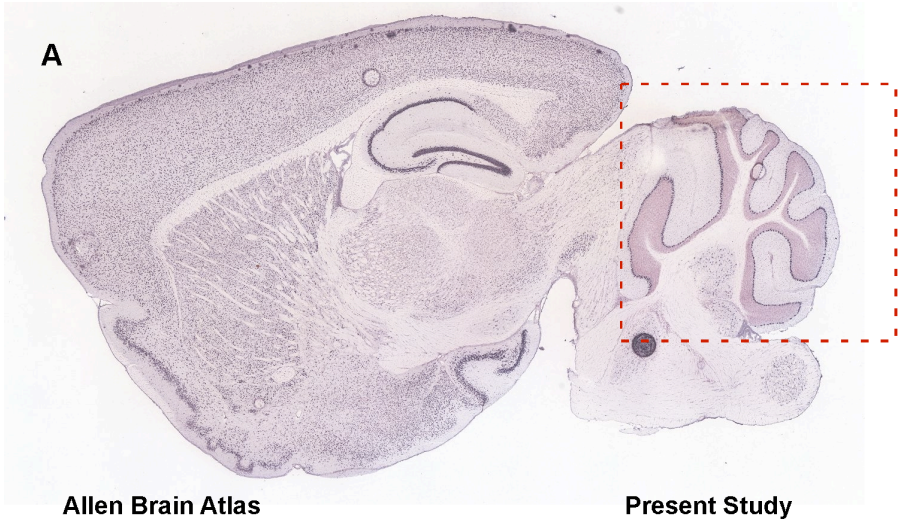

Allen Brain Atlas

Present Study

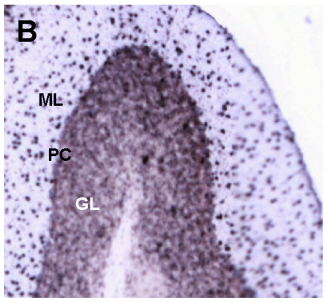

PSD-95
(Dlgh4)

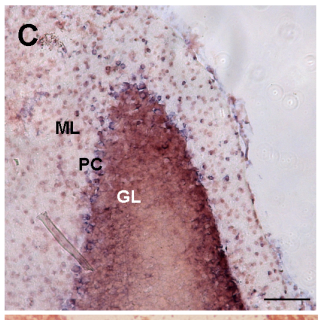

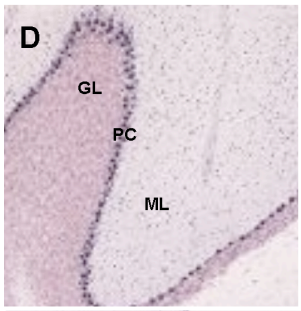

PSD-93
(Dlgh2)

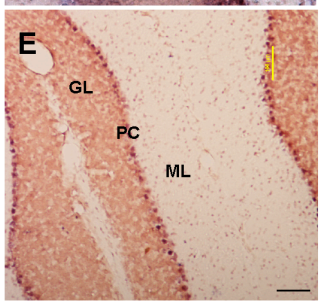

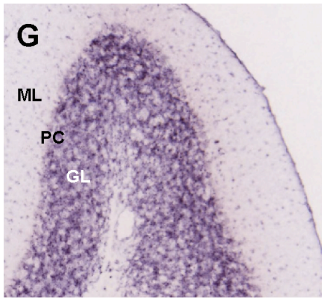

SAP97
(Dlgh1)

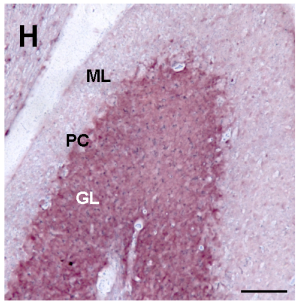

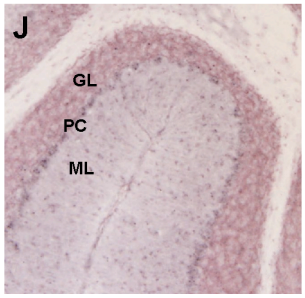

SAP102
(Dlgh3)

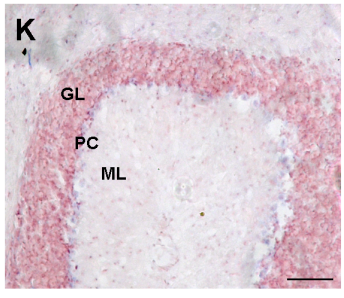

Supplemental Figure 2.2. The MAGUK riboprobes have layer/cell-type specific hybridization patterns in the adult mouse cerebellum.

All tissue sections shown are from adult mouse cerebellum either the Allen Brain Atlas (http://mouse.brain-map.org) (left column; A, B, D, F, H) or the present study (right column; C, E, G, I). The cerebellar layers are marked: molecular layer (ML), Purkinje cell layer (PC) and granule cell layer (GL).

Left column: In situ hybridization images of a whole sagittal brain section labeled with PSD-93 riboprobe (A) or enlarged images of the cerebellum labeled with PSD-95 (B), PSD-93 (D), SAP97 (F) or SAP102 (H) riboprobes. Hybridization signals were detected chromogenically.

Right column: In situ hybridization images are labeled with PSD-95 (C), PSD-93 (E), SAP97 (G) or SAP102 (I) riboprobes used in the present study. Hybridization signals were detected chromogenically (see Materials & Methods). Our four MAGUK riboprobes show layer and cell type specific expression comparable to that seen in the Allen Brain Atlas images as well as that published previously for in situ hybridization (Brenman et al., 1996; Chetkovich et al., 2002a; Muller et al., 1995). The PSD-95 riboprobes shows strong, diffuse labeling in the granule cell layer and strong cell-type expression in the molecular layer (B; cf., C) (Chetkovich et al., 2002a). PSD-93 riboprobes shows strong labeling in the Purkinje cells as well as diffuse labeling in granule cell layer (D; cf., E) (Brenman et al., 1996). SAP97 riboprobes does not label Purkinje cells but does strongly label the granule cell layer (F; cf., G) (Muller et al., 1995). Although more diffuse, the SAP102 riboprobes show most prominent labeling of the granule and Purkinje cell layers (H; cf., I). Scale bar, 100 μm.

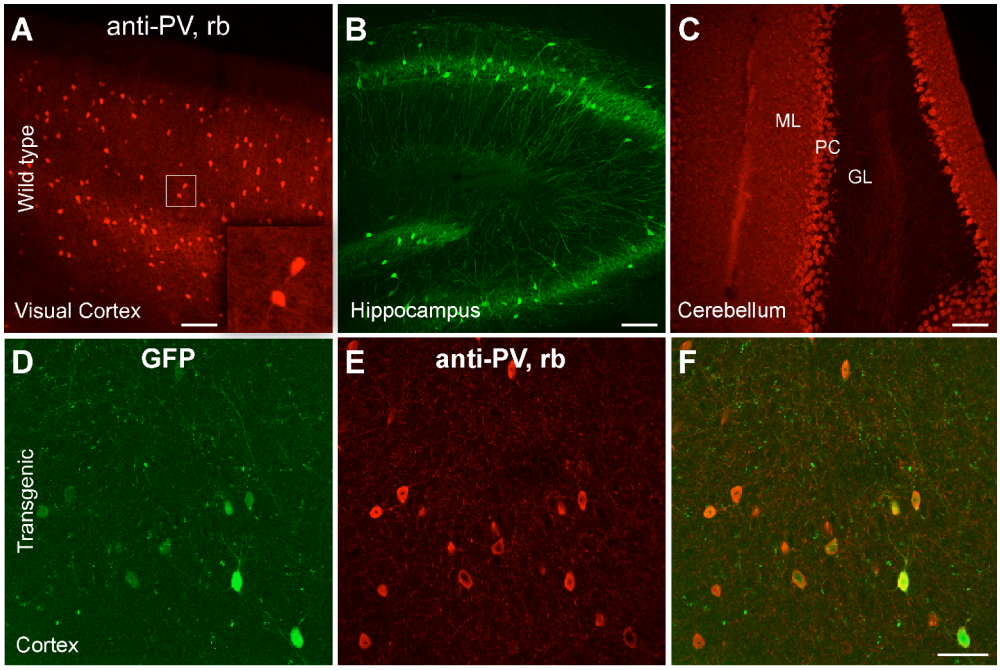

Supplemental Figure 2.3. Characterization of rabbit anti-PV on mouse tissue.
Cell-type specific staining of the cortex, hippocampus and cerebellum in wild type and transgenic mouse tissue is consistent with previous results.

Tissue sections were obtained from wild type (A-C) or transgenic (D-F) mouse brains and labeled with rabbit anti-PV. 50 µm floating sections were blocked with 10% normal serum at room temperature for 1 hour and probed with the primary antibody at room temperature overnight.

(A-C) Low magnification images show PV staining in the visual cortex (A), the hippocampus (B), and the cerebellum (C) (ML, molecular layer; PC, Purkinje cell layer; GL, granule cell layer). Immunofluorescent labeling is consistent with previous studies: In the cortex (Gonchar et al., 2007; Kawaguchi and Kubota, 1993), there is widespread labeling of interneurons; in the hippocampus (Dun et al., 1994), labeling is mainly restricted to the pyramidal layer as well as dentate gyrus; and in the cerebellum (Schneeberger et al., 1985), there is labeling of Purkinje and basket (ML) cells. Scale bar, 100 µm.

(D-F) The heterozygous transgenic mice (B13) express GFP in a subset of PV+ interneurons (Dumitriu et al., 2007). (D) Green cells in the transgenic mouse cortex are GFP expressing PV+ interneurons. (E) Red cells in the same tissue section are PV immunopositive neurons. The merge image (F) shows the overlap of GFP expression and antibody labeling. Consistent with previous results (Dumitriu et al., 2007), rabbit anti-PV stains every GFP expressing neuron and additional cells in the cortex (D-F) as well as in the hippocampus and cerebellum (data not shown).

We also found no labeling of any neurons/cells in the cortex of P10 animals (data not shown), consistent with the onset of parvalbumin expression, which is around P14, in the cortex (e.g., Gonchar et al., 2007). Scale bar, 50 µm.

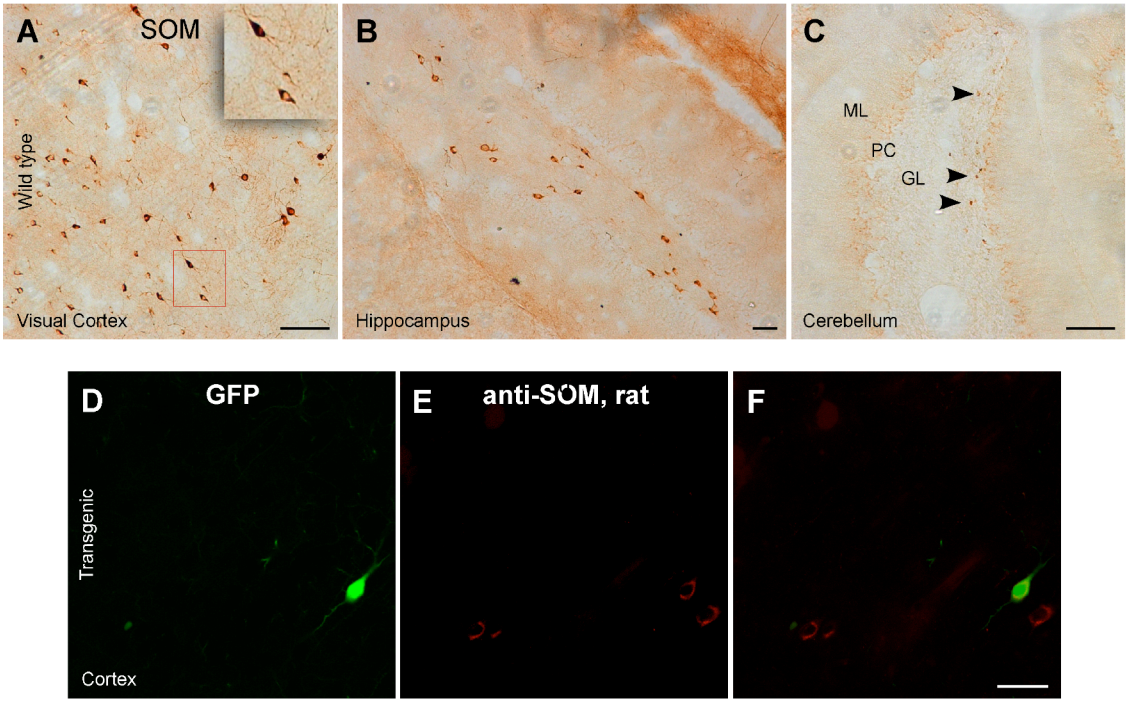

Supplemental Figure 2.4. Characterization of rat anti-SOM on mouse tissue.
Cell-type specific staining of the cortex, hippocampus and cerebellum in wild type and transgenic mouse tissue is consistent with previous results.
Tissue sections were obtained from wild type (A-C) or transgenic (D-F) mouse brains and labeled with rat anti-SOM.
(A-C) Brightfield images show SOM staining in the visual cortex (A), the hippocampus (B), and the cerebellum (C) (see Supplemental Figure 3 for additional details). Immunolabeling is consistent with previous results: In the mouse cortex (e.g., Kubota et al., 1994), there is widespread labeling of interneurons with known morphology (e.g., bitufted enlarged inset); in the hippocampus (Dun et al., 1994), there is dispersed labeling in the hilus; in the cerebellum (Geurts et al., 2001), only a few small cells are labeled in the granular layer (C).
(D-F) anti-SOM was tested on transgenic mouse tissue, in which a subset of SOM+ interneurons are expressing GFP (Oliva et al., 2000). Green cell on the confocal images of the section of transgenic mouse cortex is a GFP expressing SOM+ interneuron (D), and red cells on the same tissue section are SOM immunopositive neurons (E). Consistent with previous results (Oliva et al., 2000), rat anti-SOM stains every GFP expressing neuron and additional cells in the cortex (D-F) as well as in the hippocampus (data not shown). Scale bar, 50 µm.

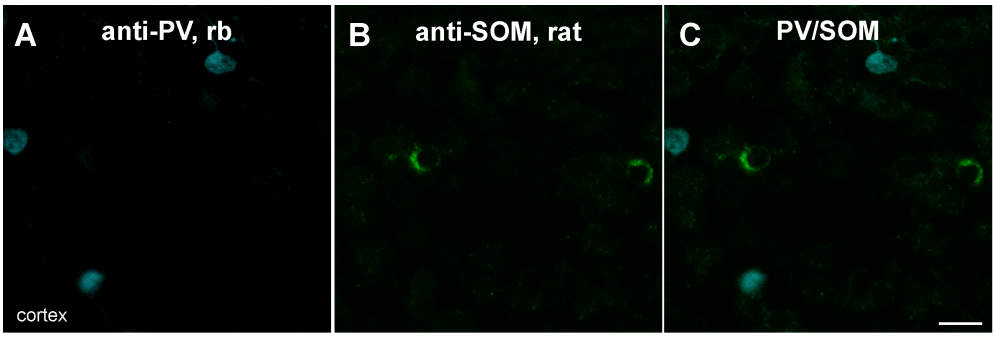

Supplemental Figure 2.5. Double labeling of the mouse cortex with rabbit anti-PV and rat anti-SOM.

No apparent overlap in the visual cortex between anti-PV and anti-SOM.

Tissue sections were obtained from wild type mouse cortex and double immunostained.

(A) Sections were labeled with rabbit anti-PV (blue). (B) The same sections were labeled with rat anti-SOM (green). As shown in the merged image (C), there is no obvious overlap between the two probes consistent with previously published data (Gonchar et al., 2007; Kubota et al., 1994). Images are magnified at 63X. Scale bar, 20 μm.

CHAPTER 3: SAP97 IS A MULTIFUNCTIONAL PROTEIN IN PV INTERNEURONS

ABSTRACT

SAP97 belongs to a family of proteins, MAGuKs, commonly found in the postsynaptic density of glutamatergic synapses. In neurons, it has been implicated in trafficking and positioning ionotropic glutamate receptors at the synaptic sites in pyramidal-to-pyramidal connections. Expression of SAP97 is differential and developmentally regulated in fast-spiking PV interneurons of the mouse visual cortex. Starting right after the eye opening through adulthood, we identified two subpopulations of PV interneurons based on SAP97 mRNA expression determined by single cell RT-PCR. In juvenile mice, the percentage of SAP97 expressing PV interneurons are higher than the ones in adult. By whole cell patch clamping, we investigated the differences in the glutamatergic input as well as the passive and the active membrane properties of juvenile and adult SAP97-expressing and –nonexpressing PV interneurons. In agreement with some of the previous reports, we found that SAP97-expressing PV interneurons receive glutamatergic input at a higher frequency, which can be due to the enhanced dendritic branching we observed in this subpopulation. Most probably as a homeostatic regulation to the increased input, we recorded a lower membrane resistance and a higher rheobase from these interneurons. In terms of active membrane properties, SAP97 expressing PV interneurons fired action potentials at a faster rate, in an irregular manner. Overexpression of SAP97 drove the membrane properties of the recorded interneurons towards the same direction as native SAP97 expressing PV interneurons. Our results propose of multifunctional role for SAP97 in cortical PV interneurons.

INTRODUCTION

Parvalbumin (PV) positive interneurons are the most prominent GABAergic interneuron subtype in the cortex (Gonchar et al., 2007). They contribute to the physiological excitation-inhibiton balance and are involved in oscillatory activity by synchronizing pyramidal cells (Cardin et al., 2009). Disruption of PV interneuron function results in behavioral abnormality and cognitive deficits and has pathological consequences such as epilepsy, schizophrenia and autism (Curley and Lewis, 2012; Marin, 2012).

PV interneurons target the perisomatic regions and have a strong control over the generation of action potentials in pyramidal neurons (Freund and Katona, 2007; Merchan-Perez et al., 2009). The inhibitory output of PV interneurons is controlled by the balance of excitatory and inhibitory input they receive as well as their intrinsic membrane properties. PV interneurons are characterized by fast-spiking firing pattern (Cauli et al., 1997; Miyoshi et al., 2007; Okaty et al., 2009). The excitatory synaptic input is the driving factor for the interneuron activity. The excitatory synaptic currents seen in these interneurons are brief due to the high levels of Ca^{2+} -permeable AMPARs (Angulo et al., 1997; Geiger et al., 1995; Goldberg et al., 2003b) and limited levels of NMDARs expressed in these interneurons (Standaert et al., 1996). The molecular mechanisms that regulate input-output properties of PV interneurons are not fully understood.

SAP97 is a member of the MAGuK (membrane-associated guanylate kinase) family of scaffolding proteins (Gardoni, 2008). SAP97 is associated with components of the postsynaptic density at glutamatergic synapses; however, its exact function in synaptic transmission remains unknown. SAP97 can interact with specific AMPA (Leonard et al., 1998; Regalado et al., 2006)

and NMDA (Cousins et al., 2008) receptor subunits, and it might be responsible for receptor clustering and trafficking to the membrane (Elias and Nicoll, 2007; Stephenson et al., 2008). SAP97 is also a mediator of transsynaptic communication, possibly through cell adhesion molecules (Regalado et al., 2006). Additionally, in cardiac myocytes, SAP97 has a role in regulating membrane excitability (El-Haou et al., 2009) via various interactions with K and Na channels. SAP97 regulates their expression and clustering at the membrane (Abi-Char et al., 2008; Goult et al., 2007; Mathur et al., 2006) and also affects the biophysical properties of these channels (Vikstrom et al., 2009). Although SAP97 and K channel interaction has been shown in neurons (Leonoudakis et al., 2004b; Leonoudakis et al., 2001; Tiffany et al., 2000), a role of SAP97 in regulating neuronal membrane properties is unknown.

SAP97 expression in cortical PV interneurons is developmentally regulated. In both juvenile and adult, it is expressed in a fraction of entire PV population. Although the fraction gets smaller with age, it still represents a significant group of adult PV interneurons (Akgul and Wollmuth, 2010). Given the important functional roles of SAP97 to membrane excitability, we wanted to address the functional consequences of SAP97 expression in PV interneurons. To do so, we used whole-cell patch clamp technique to monitor physiological properties of PV interneurons and assayed SAP97 expression using single cell RT-PCR. Our results showed that SAP97-expressing PV interneurons exhibit a distinct membrane phenotype of low excitability and faster action potential firing. Additionally, the glutamatergic synaptic currents of SAP97-expressing PV interneurons have significantly increased frequency than the currents of SAP97-nonexpressing subgroup. Overexpression of SAP97 in PV interneurons drives their membrane properties toward SAP97 expressing phenotype.

MATERIALS AND METHODS

Animals

Two transgenic mouse lines were used to identify PV interneurons in the visual cortex: PV-Cre and lox-STOP-lox-tdTomato (LSL-tdTomato). The PV-Cre line has expression of Cre recombinase driven by a PV promoter (an IRES-Cre-pA cassette inserted at the 3' end of the PV gene) (Hippenmeyer et al., 2005; Kuhlman and Huang, 2008). The LSL-tdTomato line (B6;129S6-Gt(ROSA)26Sor$_{tm9(CAG-tdTomato)Hze}$/J from Jackson Labs, donator: Allen Brain Institute) has lox-flanked STOP (LSL) cassette upstream of the tdTomato sequence inserted in their genome and is used as a conditional reporter line. When the PV-Cre line is crossed with the LSL-tdTomato line, Cre-mediated recombination excises the STOP cassette upstream of the tdTomato gene yielding tdTomato expression. The offspring of this breeding was used for the fluorescent visualization of PV interneurons. By adulthood, greater than 95% of PV expressing cells express tdTomato and all tdTomato cells express PV (Fig. 1B), consistent with previously published results for these mice (Hippenmeyer et al., 2005; Kuhlman and Huang, 2008).

Maintenance of all animal and the surgical procedures used were approved by the institutional animal care and usage committee at Stony Brook University and were in line with the guidelines established by the National Institutes of Health.

Electrophysiological Recording

Recording solutions. The artificial cerebral spinal fluid (ACSF) bath solution used for recordings consisted of (in mM): 125 NaCl, 2.5 KCl, 25 glucose, 25 $NaHCO_3$, 1.25 NaH_2PO_4, 2 $CaCl_2$, 1.2 $MgCl_2$, 1.3 Na-Ascorbate and 0.6 Na-Pyruvate, and was saturated with 95% O_2/ 5% CO_2 under all conditions. All pharmacological agents were added to the external solution without

substitution. Our standard internal solution was an ATP generating internal solution containing (in mM): 135 K-gluconate, 4.3 KCl, 2 NaCl, 10 HEPES, 20 phosphocreatine, 4 Mg-ATP and 0.3 GTP, pH 7.3 (KOH), and adjusted to 300 mOsm with sucrose. Biocytin (0.2%) was included in the internal solution for post-fixation neuronal labeling.

For RNase-sensitive experiments, we prepared the internal solution under RNase-free conditions, including using nuclease-free water and opening chemicals for the first time. The internal solution was filtered with a sterile filter (0.2 μm). Isolated mouse brain RNA was incubated overnight at 37^0C with a sample of the internal solution, nuclease-free water, or RNase A containing buffer separately, as controls. The RNA was run on agarose gel to confirm that the internal solution was RNase-free. Internal solutions passing this quality control were aliquoted and stored at -20^0C for future use.

All reagents including pharmacological compounds were obtained from either Sigma Aldrich Inc. (St. Louis, MO) or Tocris Cookson Inc. (Ellisville, MO) unless otherwise noted.

Acute slice preparation. Mice between postnatal day 15 (P15) and day 17 (P17) were anesthetized with isofluorane and then decapitated. Mice between postnatal day 56 - 65 (P56 - P65) were anesthetized with ketamine (0.12 cc/100 g) and xylazine (0.05 cc/100 g) and then transcardially perfused with ice-cold ACSF with Kynurenic acid (200 mg/ml) prior to decapitation. The brains of both ages were dissected out in the same solution. Coronal slices were collected from each blocked hemisphere using a vibratome (Leica). Slice collection began 1 mm rostral to the caudal cortical surface and totaled four 300 μm slices per hemisphere. Slices were placed into oxygenated ACSF at 32^0C for 15 minutes then left incubated at room.

Electrophysiology. Membrane potentials or currents were recorded at 32 - 34 ˚C using an EPC 10 USB amplifier with PatchMaster software (HEKA Elektronik, Lambrecht, Germany). Recordings were sampled at 20 kHz (action potentials) or 50 kHz (sEPSCs/mEPSCs), and low pass filtered using a 4-pole Bessel filter at 10 kHz. mEPSCs were digitally refiltered at 2 kHz. Pipettes had resistances of 2-4 MΩ when filled with internal solution and measured in the ACSF bath. External solutions were bath applied at a perfusion rate of approximately 3 mL/min. Membrane potentials were not corrected for liquid junction potentials.

Targeting neurons. We initially identified layers 2/3 in relation to the pial edge of the slice, and targeted the visual cortex using the lateral ventricle size and shape as a reference. We then visually identified interneurons by searching for tdTomato or EGFP (infected mice, see below) expression under magnification (Olympus BX50WI fitted with a x 40-W/0.80 NA objective, and cooled CCD camera Quantifire XI from Optronics).

Recording of passive and active membrane properties. Upon achieving the whole cell mode, resting membrane potentials (V_m) were measured in current clamp. The amplifier mode was changed to voltage clamp and the baseline holding potential set to –70 mV. We placed all cells at the same membrane potential so that voltage dependent channels would be at a similar starting state and rheobase current would be independent of Vm. Pipette series resistance, neuronal membrane resistance, and neuronal membrane capacitance (C_m) were monitored at the start and regularly throughout the experiment using the LOCKIN Sine+DC protocol from HEKA (Gillis 1995), with a 20 mV (–90 to –70 mV) sine wave of 1 kHz for 100 ms. The amplifier was then switched to current clamp mode and the current adjusted to bring the reported membrane potential to approximately –70 mV. Action potentials were evoked using a series of depolarizing pulses of 1 s duration each, with 5 s between each stimulus. Depolarizing currents varied with

cell type and membrane resistance but ranged from 10 pA to 1 nA. Rheobase (see below) was found by applying 10 pA increments of current. The amplifier was subsequently switched to voltage clamp mode with the holding potential set to –70 mV to record EPSCs.

sEPSC/mEPSC recording. Neurons were voltage clamped at –70 mV and recorded in 1-5 minute blocks. Spontaneous excitatory post-synaptic currents (sEPSCs) were recorded in the standard ACSF (containing Mg^{2+}) used to measure action potentials. Miniature EPSCs (mEPSCs) were recorded in the same solution as well as the Na_v blocker tetrodotoxin (TTX) (1 μM) to block APs and the $GABA_A$ competitive antagonist bicuculine (50 μM) or the non-competitive antagonist picrotoxin (50 μM) to block inhibitory synaptic responses. For selected recordings, 6-cyano-7-nitroquinoxaline-2,3-dione (CNQX) (10 μM) was applied to confirm that mEPSCs were mediated by AMPARs. In all instances tested, mEPSCs were completely blocked by CNQX (unpublished data; Helm et al., submitted).

Analysis of membrane properties

Passive/subthreshold membrane properties. Resting membrane potential (V_m) was measured in current clamp upon achieving the whole-cell mode. Series resistance and membrane capacitance (C_m) were analyzed in real-time using the PatchMaster LOCKIN online analysis software. Subsequent analysis was performed using IgorPro (WaveMetrics). Membrane resistance (R_m) is the slope of a line fit to subthreshold voltage responses to current input. Rheobase is the minimum current input over a one second stimulus that generates an action potential.

Active/action potential shape. The first action potential evoked by rheobase was used to characterize action potential (AP) shape. AP threshold was determined by the third derivative of the action potential found over the AP rising phase. Smoothing of the AP waveform was

performed after each derivative. AP peak and half-width were used to describe the rising and falling phases of the AP. Half-width was measured as the time from the rising phase to the falling phase of the AP at 1/2 the distance from threshold to peak. After hyper-polarization (AHP) was characterized by the AHP peak, latency, and area. AHP peak is the difference between threshold and maximum after-hyperpolarization. AHP latency is the time from AP peak to AHP peak. AHP area is the area under a line defined by the AP threshold membrane potential.

Active/firing pattern. The delay to onset of the 1st AP is measured from the start of a depolarizing stimulus pulse to the peak of the first AP evoked in response to rheobase. AP firing patterns, as outlined below, were analyzed in the trace which contained around 30 APs, e.g. fired APs at 30 Hz, the low range of the gamma frequency (Jagadeesh et al., 1992; Steriade et al., 1996). Interspike interval (ISI) was measured as the time between successive AP peaks. Spike frequency adaptation was measured as the last ISI divided by the first ISI. Maximum and minimum instantaneous ISI are the maximum and minimum instantaneous ISI detected in the 30 AP trace. Instantaneous frequency of AP_x is the inverse of the interspike interval (in seconds) AP_x to AP_{x+1}. The coefficient of variation (CV) of the firing rate (CV frequency) is the standard deviation of the frequency divided by the average frequency. Input-output response (I/F slope) was measured as the slope of a line fit to a plot of the number of evoked action potentials versus current input. Cells were included in analysis only if the neurons showed fast-spiking behavior, had resting membrane potentials < -57 mV, and had a stable baseline.

mEPSP analysis. mEPSCs were analyzed using the MiniAnalysis program (Synaptosoft). Event detection parameters averaged a 2 ms baseline 4 ms prior to a suprathreshold peak. Amplitude threshold levels were set at 5 pA and recordings with baseline noise root mean squared (RMS) greater than 5 pA were discarded. The area threshold was set at 1.5 times the amplitude

threshold. Five or more events separated by maximum intervals of 5 ms were labeled as bursts and removed. Segments with high levels of noise that obscured the baseline were omitted, and event detection resumed when the baseline leveled. mEPSC events from individual cells were measured for amplitude, 10-90% rise-time, half-width, area, and time to 50% decay and averaged. Average mEPSC frequency was measured as the total number of events recorded divided by the total time. Instantaneous frequency was the inverse of the time in seconds between $mEPSC_x$ and $mEPSC_{x+1}$. To determine significant difference between the synaptic inputs to subgroups, we used two approaches. First, 500 mEPSCs were randomly sampled from each cell and combined for each subgroup and the Komogorov-Smirnov (KS) test ($\alpha = 0.05$) was used to test for significance. The resulting p value was adjusted for multiple pairs using the Bonferroni correction. Second, mEPSC measurements were averaged for each cell and an ANOVA followed by Tukey test was performed for each parameter. Statistical analysis was performed in IgorPro (WaveMetrics).

Single Cell RT-PCR

Single-cell RT-PCR was performed according to published methods *(Toledo-Rodriguez and Markram, 2007)*. Briefly, following a recording session, cytoplasm of the recorded neuron was partially aspirated into the recording pipette. Then, by applying positive pressure, the pipette contents were released into a RNase-free microcentrifuge tube (8 µl) containing 3 µl nuclease-free water (Ambion), 2 µl RNase inhibitor (Invitrogen, 40U/µl) and 1 µl of random hexanucleotides (Gibco BRL, 3 mg/ml). The mixture was sonicated in icy water for 5 min and then heated to 70^0C for 10 min. After a brief incubation (1 - 2 min) on ice, 4 µl of 5X first-strand buffer (250 mM Tris-HCl 375 mM KCl, 15 mM MgCl), 0.5 µl DTT (0.1 M), 1 µl mixed deoxynucleotide triphosphates (dNTPs, Invitrogen, 10 mM) were added and the mixture was

incubated 10 min at room temperature before adding 1 µl of SuperScript II reverse transcriptase (RT-II, Gibco BRL, 2U/ml). The reverse transcription reaction was carried out at 42^0C for 60-90 min to synthesize cDNA. The reaction solution was incubated then at 95^0C for 5 min to deactivate RT-II and removed the RNA strand from the RNA-DNA hybrid. For PCR, the reaction mixtures contained 2.0 mM $MgCl_2$, 0.5 mM of each of the dNTPs (Invitrogen), 0.8-1.0 mM primers, 2.5 U Taq DNA polymerase (Invitrogen), 5 µl 10X Buffer, 2 µl cDNA template from the single cell RT reaction and primers for each GAD67, GAD65, Parvalbumin, SAP97 and VGluT1 (Table 1). Each reaction went through 35 cycles of the first round of PCR followed by additional 35 cycles of the second round of PCR with the nested primer pairs under the same conditions. The products were visualized by ethidium bromide staining after electrophoresis in 2% agarose gels. Primers were tested on the cDNA made with dilutions of RNA (2 pg-100 ng) isolated from mouse cortex (S. Fig. 3.2 and 3.3).

Virus Injection

Recombinant virus production.

In neuron, SAP97 is expressed in two spliced isoforms, α and β, that differ in their N-terminus (Table 3.2) (Schluter et al., 2006). They show differences in their subsynaptic localization and role in glutamatergic synaptic transmission. α-SAP97 is localized itself and clusters AMPARs at the synaptic site and causes an increase in the synaptic amplitudes. β-SAP97, on the other hand, keeps AMPARs and NMDARs at the extrasynaptic sites preventing their diffusion into the PSD (Li et al., 2011; Waites et al., 2009). We chose to overexpress α isoform because we observed an increase in the synaptic activity in the presence of endogenous SAP97, although the change was in the frequency not in the amplitude.

alpha-SAP97 (α-SAP97) (Schluter et al., 2006) with an enhanced green fluorescent protein (EGFP) gene at the C-terminus (Table 3.2) was cloned into a plasmid carrying a FLEX switch (Atasoy et al., 2008). The FLEX switch was constructed with two pairs of lox cassettes (loxP/lox2272) facing each other. The vector and the gene of interest were digested with SpeI restriction enzyme. Upon cloning into the FLEX switch vector, the orientation of the gene was verified with sequence analysis. The FLEX switch with α-SAP97-EGFP in reverse orientation was digested with BamH1/EcoRI (BamHI site in α-SAP97 was removed via site-directed mutagenesis) and ligated into a vector (supplied by ZJ Huang, CSHL) containing the CMV promoter, SV40 polyA sequence, and two inverted terminal repeats required for recombinant adeno-associated virus (AAV2/9) production (S. Fig. 4). To verify the fidelity of the construct, HEK 293 cells were transfected using Fugene HD (Roche Diagnostics) according to the manufacturer's instructions. α-SAP97-EGFP_AAV vectors were cotransfected with Cre in pcDNA3.1 vector (Invitrogen) or with empty pcDNA3.1. After 48 h, cells were imaged for EGFP fluorescence (S. Fig. 5). FLEX-rev-α-SAP97-EGFP_AAV was produced by the University of North Caroline Gene Therapy Program Vector Core.

Stereotaxic injections into mouse visual cortex. Mice were anesthetized with ketamine (100 µg/gram body weight) and xylazine (10 µg/gram body weight) and were placed into a stereotaxic apparatus (Steolting). The hair on the head was removed and the skin was wiped with 70% EtOH. The skull was exposed via a small incision, and a small hole was opened with a dental drill. The following stereotaxic coordinates were used for visual cortex: -1.0 mm anterior to lambda; 2.5-3.0 mm lateral from the midline; 0.5 mm down from the dural surface. A 1 µl Hamilton, flat-tip syringe was mounted and 0.5 µl AAV was injected at a rate of 0.25 µl/min into

the visual cortex. The syringe was withdrawn 5 min after the final injection. For injection, a-SAP97-EGFP_AAV titer was 1.8 X 10^{12} GC/ml.

Morphology

Biocytin labeling. The slices were fixed in 4% paraformaldehyde in PBS overnight. After they were permeabilized using 1% triton-X in PBS for 1 hour, the slices were stained with Texas Red Streptavidin or DyLight649 Streptavidin (1:2000) in 0.1% Triton-X in PBS for 3 hours at room temperature or overnight at 4ºC. Stained slices were washed three times for at least minutes each in PBS before mounting on a glass slide for microscopy. Labeled neurons were imaged using a confocal microscope and software (Olympus Fluoview).

Tracing. Confocal images of interneurons were traced in Imaris (Bitplane, South Windsor, CT). Imaris was used to measure the number of primary dendrites, branches, terminal points, and to perform Scholl analysis. ImageJ (Rasband, NIH, MD) was used to generate a projection image. The vertical and horizontal extent of soma and dendritic arbor and distance from soma to pia were measured in the projection image.

*Scholl analysis.*The number of intersections at concentric circles (20 μm apart) was counted for each cell with Scholl analysis component of Imaris (Sholl, 1953).

Immunohistochemistry

Tissue preparation. P15 - 17 (juvenile) or P56 - 65 (adult) mice were deeply anesthetized with intraperitoneal administration of ketamine (0.12 cc/100 g) and xylazine (0.05 cc/100 g) and then perfused transcardially with 0.1 M phosphate buffer (PB) and fixed with 4% paraformaldehyde. Brains were dissected out and postfixed in the same fixative for 3 hours at room temperature. A

postfixed brain was left in 30% sucrose solution for dehydration at 4^0C and was then cut longitudinally into two hemispheres. A hemisphere was then immersed in Shandon M-1 embedding matrix (Thermo Scientific, Rockford, IL) and cryosectioned at -20^0C (Leica LM1850; Leica Microsystems, Bannockburn, IL) at 20 lm thick. Sections were kept in cryobuffer (27% glycerol, 27% ethylene glycerol) at -20^0C.

Antibodies. The following primary antibodies were used: rabbit polyclonal anti-PV (Abcam, Cambridge, MA) and rat monoclonal anti-SOM (Chemicon, Temecula, CA). As secondaries, we used fluorescent Alexa 488-conjugated anti-rabbit and anti-rat IgG (Molecular Probes, Eugene, OR) (see Akgul & Wollmuth, 2010).

Staining. Tissue sections were washed with phosphate-buffered saline (PBS). Tissue was blocked for 30 minutes in blocking solution (100 mM Tris-Cl, pH 7.5, 150 mM NaCl, 0.5% Triton X-100, 2% normal sheep serum). Tissue sections were then incubated with primary antibody at room temperature overnight. Secondary antibody incubations were carried out at room temperature for 2 hrs. Tissue sections were washed with phosphate-buffered saline (PBS) between two steps. The sections were then mounted with Vectashield mounting medium (Vector Laboratories, Burlingame, CA). Images were taken and analyzed with an Olympus Fluoview FV1000 confocal microscope.

Statistical Analysis

Statistical analysis of experimental measures including curve fitting was performed in Igor Pro (WaveMetrics, Inc., Lake Oswego, OR) or Excel. Results are reported as mean ± S.E.M. The Student's t-test and an analysis of variance (ANOVA) were used to test for statistical differences with the Tukey test used for multiple comparisons. Significance was assumed if $p < 0.05$.

Table 3.1. Primer list for single cell RT-PCR

Marker	Genbank #	First PCR primers	Size (bp)	Second PCR primers	Size (bp)
GAD65	NM_08078.2	Sense, 99: CCAAAAGTTCACGGGCGG* A-sense, 454: TCCTCCAGATTTTGCGGTTG*	375	Sense, 219: CACCTGCGACCAAAAACCCT A-sense, 447: GATTTTGCGGTTGGTCTGCC	248
GAD67	NM_008077.4	Sense, 83: ATGATACTTGGTGTGGCGTAGC* A-sense, 314: GTTTGCTCCTCCCCGTTCTTAG*	253	Sense,159:CAATAGCCTGGAAGAGAAGAGTCG A-sense, 314: GTTTGCTCCTCCCCGTTCTTAG	177
PV	NM_013645.3	Sense, 67: GATAGGAGCCTTTGCTGCTG A-sense, 347: CAGCCACCAGAGTGGAGAAT	281	Sense, 124: GGGCCTGAAGAAAAAGAACC A-sense, same as the 1st PCR	224
SAP97	NM_007862.3	Sense, 481: AAGGCAAATCCTCCTCCAGT A-sense, 1445: ACCGATATGATGCGATCTCC	964	Sense, same as the 1st PCR A-sense, 719: TTTACCCGCAATCTTCCATC	239
3' UTR	NM_007862.3	Sense, GGTTTGGCCAGTGTATTAGCTC A-sense, GAGCTAATACACTGGCCAAACC		Sense, GTCCTCCACACTGACACAGATC A-sense, CAGAGCCGTAACCACAGTGTAC	380
VGlut1	NM_182993.2	Sense, 124: CCCTTAGAACGGAGTCGGCT** A-sense, 697: TATCCGACCACCAGCAGCAG**	593	Sense, 148: ACGACAGCCTTTTGCGGTTC** A-sense, 495: CAAAGTAGGCGGGCTGAGAG**	367

Note: Position 1, first base of the start codon.
A-sense, Antisense sequence.
*(Karagiannis et al., 2009)
**(Vullhorst et al., 2009)
***(Cauli et al., 1997)

Table 3.2. Domain structure and spliced forms of endogenous and overexpressed SAP97.

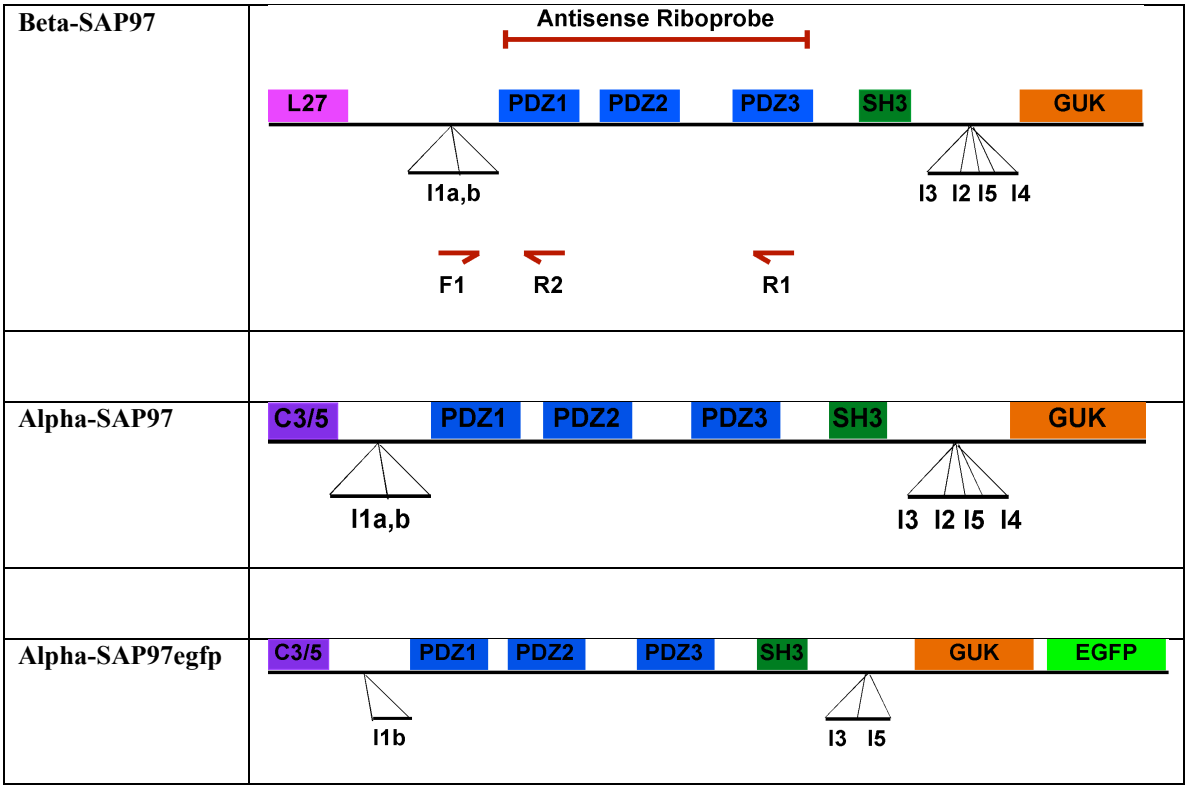

Two spliced isoforms of SAP97 characterized in the CNS are beta-SAP97 (β-SAP97) and alpha-SAP97 (α-SAP97) are differentiated with their N-terminus. Instead of L27 domain of β-SAP97, in α-SAP97 there are two cytosines (C3/5) that are myristoylated in the cell (Li et al., 2011; Schluter et al., 2006; Waites et al., 2009). I1-I5 are the other splicing sites found in different isoforms of SAP97 which are involved in tissue specific expression as well as in different functional roles (Godreau et al., 2003; Nikandrova et al., 2010). Antisense riboprobe desgined for in situ hybridization and PCR primers (F1, R1, R2) designed for single cell RT-PCR experiments are also indicated on β-SAP97. Overxpression construct was made with α-SAP97 with EGFP fused to the C-terminus (Waites et al., 2009).

RESULTS

Parvalbumin positive interneurons in layers 2/3 of the visual cortex from juvenile and adult PV-tdTomato mice

In our study, we took advantage of a transgenic line (PV-Cre) that expresses Cre recombinase under the control of the endogenous parvalbumin promoter (Hippenmeyer et al., 2005). We crossed PV-Cre mice with another line that carries tdTomato gene expressed conditionally in the presence of Cre recombinase (see Materials & Methods). As a result, their offspring, PV-tdTomato (PVdT) mice, express tdTomato in PV interneurons.

To confirm cell-type specific expression of tdTomato, we stained the visual cortex from juvenile and adult PVdT mice with PV antibody. Figure 3.1 shows confocal images of tissue sections, encompassing the visual cortex, from juvenile (P16; Fig. 3.1A_1-A_4) or adult (Fig. 3.1B_1-B_4) mice labeled with PV antibody (green, first column) and visualized for tdTomato expression (red, second column). The third and fourth columns show merged images. In juvenile mice, PV and tdTomato signals largely overlap (Fig. 3.1A_3-A_4). As seen in Fig. 3.1A_4, which is an enlarged image, a small number of PV+ cells lack the tdTomato signal. PV expression is turned on in the mouse visual cortex around P14 (Gonchar et al., 2007; Kawaguchi, 1995). Presumably, the difference between PV+ label and tdTomato signals in juvenile mice results from the time window between the activation of the PV promoter and the successful Cre/lox recombination and subsequent tdTomato expression. Consistent with this idea, in adults (Fig 3.1B_3-B_4), almost all (>95%) PV+ interneurons express tdTomato. To further verify the cell-type specificity of tdTomato expression, we stained the visual cortex of adult PVdT mice with SOM antibody, which labels SOM interneurons. These interneurons are the second largest interneuron population in the visual cortex and are non-overlapping with PV interneurons (Gonchar et al.,

2007; Kubota and Kawaguchi, 1994). Figure 3.1C_1-C_4 shows no overlap between SOM+ label and tdTomato signal, confirming the cell-type specificity of tdTomato expression in PV interneurons.

The expression of SAP97 in a subset of juvenile and adult is developmentally regulated.

To address the functional significance of SAP97 expression in PV interneurons in the visual cortex, we initially used single cell RT-PCR to determine the gene expression profiles of recorded neurons. PV interneurons in layers 2/3 of the visual cortex in acute slices were identified by tdTomato fluorescence, patched in the whole cell configuration, and stimulated to confirm fast-spiking firing patterns. We recorded the passive and active membrane properties as well as miniature excitatory postsynaptic currents (mEPSCs) from P15 to P17 (juvenile) and P56 to P65 (adult) PVdT mice. Once the recording protocol was completed, we harvested cell contents for single cell RT-PCR (see Materials and Methods).

We used gene specific primers (Table 3.1) to assay for expression of mouse parvalbumin (PV), SAP97, two isoforms of glutamate decarboxylase (GAD65, GAD67) and vesicular glutamate transporter (VGluT1). We first assayed for PV expression to verify the quality of mRNA and to insure that negative results for SAP97 were not false negative. We therefore included in subsequent analysis only those samples positive for PV. The expression of GAD67 and GAD65, which are expressed in all GABAergic interneurons (Cauli et al., 2000; Vullhorst et al., 2009), were used as positive controls. VGluT1, which is a pyramidal neuron marker (Fremeau et al., 2001), was also tested on each sample to rule out possible nonspecific RNA contamination.

In the juvenile visual cortex, SAP97 mRNA was detected in a majority of interneurons (12 out of 19 or 63% PV interneurons; e.g., Fig. 3.2A_1, A_2). In contrast, SAP97 mRNA was detected in a much smaller fraction of interneurons in the adult visual cortex (6 out of 21 or 29% PV interneurons; e.g., Fig. 3.2A_3, A_4). This developmental expression of SAP97, where it is expressed in a higher percentage of juvenile than adult PV interneurons, is consistent with previous results (Akgul and Wollmuth, 2010) (see also Discussion).

SAP97-expressing and nonexpressing PV interneurons show distinct membrane properties. For functional analysis, we generally sorted PV interneurons into subsets based on SAP97 mRNA expression, either SAP97-expressing (SAP97+) or SAP97-nonexpressing (SAP97-) (Fig. 3.2A_1-A_4). Figures 2B-D show representative recording traces for juvenile or adult PV interneurons either SAP97+ or SAP97-. The voltage traces (V_m) in Fig 3.2B show examples of firing patterns around 30 Hz, at the low end of gamma frequency, along with the associated current injections (I_m). The voltage traces in Fig. 2C show the first action potential (AP) in response to rheobase current. These APs are magnified in Fig. 3.2D.

In terms of membrane properties, PV interneurons in layers 2/3 undergo significant developmental changes (Goldberg et al. 2011; Lazarus and Huang 2011). We also observed a significant shift in membrane excitability and AP shape of PV interneurons between juvenile and adult PV interneurons (Fig. 3.2, Table 3.3). Most notable was a narrowing of AP half-width (juvenile, 0.54 ± 0.04 ms; adult, 0.44 ± 0.03 ms; $p < 0.05$), reduced AHPs (juvenile, -298 ± 42 V*s; adult, -213 ± 15 V*s; $p < 0.05$) and less sensitivity to current input (I/F slope: juvenile, 2.2 ± 0.3 pA/Hz; adult, 1.2 ± 0.1 pA/Hz; $p < 0.01$). In both juvenile and adult PVdT mice, membrane properties recorded from either SAP97+ or SAP97- PV interneurons show significant differences (Fig. 3.2, Table 3.4). Although there were developmental changes in membrane properties, these

changes occur with a similar pattern in both age groups.

In terms of firing patterns, PV interneurons expressing SAP97 typically fire with an irregular or stuttering pattern with clusters of APs fired at high frequency separated by quiet periods (Fig. 3.2B_1 & B_3). In contrast, SAP97-nonexpressing PV interneurons fire action potentials in a more regular manner (Fig. 3.2B_2 & B_4). The differences in firing patterns are best represented quantitatively by the ratio of maximum to minimum interspike intervals (Max/Min ISI) (Table 3.4). The Max/Min ISI ratio of SAP97+ interneurons (juvenile, 9.2 ± 2.6; adult, 20.2 ± 7.4) is significantly greater than that for SAP97- interneurons at the same age (juvenile, 2.8 ± 0.5; adult, 3.1 ± 0.8). Further, SAP97+ PV interneurons fire faster spikes manifested as a decrease in minimum interspike interval (Min ISI) (juvenile, 18.2 ± 1.5; adult, 15.5 ± 1.1) in comparison to SAP97- interneurons (juvenile, 23.0 ± 1.7; adult, 19.4 ± 1.7).

SAP97+ and SAP97- PV interneurons also show significant differences in terms of passive membrane properties and action potential shape (Fig. 3.2C-D, Table 3.4). For example, SAP97+ PV interneurons have a lower input resistance (Rm) (juvenile, 88 ± 9.4 MΩ; adult, 118 ± 13 MΩ) (Fig. 3.2C_1 & C_3) than SAP97- interneurons (juvenile, 130 ± 13 MΩ; adult, 173 ± 14 MΩ) (Fig. 3.2C_2 & C_4). Similarly, the rheobase current is higher for SAP97+ PV interneurons (juvenile, 450 ± 66 pA; adult, 270 ± 10 pA) than that for SAP97- interneurons (juvenile, 290 ± 40 pA; adult, 215 ± 20 pA). In terms of AP shape, SAP97+ PV interneurons have significantly smaller after hyperpolarization (AHP) (juvenile, -210 ± 20 V*s; adult, 140 ± 10 V*s) (Fig. 3.2C_1 & C_3) and a narrower AP half-width (juvenile, 0.48 ± 0.02 ms; adult, 0.37 ± 0.02 ms) (Fig. 3.2D_1 & D_3) than those of SAP97- interneurons (AHP: juvenile, -420 ± 70 V*s; adult, -240 ± 10 V*s; Fig. 3.2C_2 & C_4. AP half-width: juvenile, 0.63 ± 0.08 ms; adult, 0.46 ± 0.04 ms; Fig. 3.2D_2 & D_4).

In summary, the endogenous expression of SAP97 in PV interneurons is correlated with two general membrane properties: less excitability and firing action potentials at a faster rate with long pauses.

PV interneurons expressing SAP97 show a higher frequency of excitatory input.

To address whether SAP97 affects excitatory input to PV interneurons, we initially monitored AMPAR-mediated miniature excitatory postsynaptic currents (mEPSCs). Figure 3.3 illustrates 10 s and 100 ms current traces from representative juvenile or adult interneurons either expressing or not expressing SAP97 (Fig. 3A-B), cumulative histograms of mEPSC frequency and amplitude (Fig. 3.3C), and mean values for mEPSC frequency, amplitude, half-width, and decay (Fig. 3.3D) (see Materials and Methods).

In both juvenile and adult mice, the mEPSCs of interneurons expressing SAP97 (juvenile, 33.5 ± 5.4 Hz; adult, 40 ± 6.5 Hz; Fig. 3.3C_1, C_3 & D_1) were significantly more frequent than those not expressing SAP97 (juvenile, 20 ± 2.7 Hz; adult, 20.1 ± 2.0 Hz; Fig. 3.3C_1, C_4 & D_4). Interestingly, the overall frequency of mEPSCs does not change with development (juvenile, 28.3 ± 4.0 Hz; adult, 26.4 ± 3.2 Hz). Adult SAP97+ PV interneurons showed a modest but significant shift toward smaller mEPSC amplitudes compared to SAP97- interneurons (Fig. 3.3C_3) whereas there is no difference in juvenile interneurons (Fig. 3.3C_2) ($p < 0.01$, Kolmogorov-Smirnov test). The amplitudes of mEPSCs decrease overall by age (amplitude: juvenile, 23.2 ± 1.6 pA; adult, 17.5 ± 1.0 pA. area: juvenile, 28.6 ± 1.9 pA*ms; adult, 18.2 ± 1.4 pA*ms). On the other hand, the amplitudes of the synaptic events on average are not significantly different in SAP97+ and SAP97- interneurons at either age (Fig. 3.3D_2).

In either age, the individual mEPSC events are more rapid (cf., B_1 & B_2 and B_3 & B_4). The half-width of the synaptic events on average is narrower in the interneurons expressing SAP97 (Fig. 3.3D_3) due to faster decay kinetics (Fig. 3.3D_4) whereas there is a significant decrease in area of synaptic events in juvenile PV interneurons expressing SAP97 compared to interneurons nonexpressing SAP97.

Overexpression of SAP97 drives membrane properties of adult PV interneurons towards those of interneurons expressing endogenous SAP97.

The experiments presented so far demonstrate that SAP97 expression in PV interneurons is correlated with reduced membrane excitability, firing APs at higher rates and more excitatory input. To address if these phenotypes are causally related with SAP97 expression, we overexpressed SAP97 in adult PV interneurons. We delivered AAV vectors carrying the reverse oriented SAP97 tagged with EGFP (SAP97egfp) into PV-Cre mouse brain with stereotexic injections (see Materials and Methods). The expression of SAP97egfp was dependent on Cre/lox recombination upon the activation of the endogenous PV promoter.

Figure 4 shows confocal images of layers 2/3 of PVdT visual cortex injected with AAV. All PV interneurons (red, Fig. 3.4A_1) show EGFP fluorescence (green, Fig. 3.4A_2, A_3). EGFP signal is localized in the soma and dendrites. Magnified image (Fig. 3.4A_4) highlights the punctate EGFP signal at dendrites and the periphery of soma.

We identified SAP97egfp overexpressing PV interneurons (PV97egfp) in acute slices of adult PV-Cre mice with EGFP signal for our recording protocol. For recorded neurons, we also assayed endogenous SAP97 expression with primers targeting its 3'UTR (Fig. 3.5A). Most recorded PV97egfp interneurons did not express SAP97 (7 out of 8).

Like endogenous SAP97-expressing interneurons, PV97egfp interneurons showed stuttering firing pattern (Fig. 3.5B) with increased Max/Min ISI ratio (97egfp, 17 ± 3.6; 97-, 3.1 ± 0.8; $P < 0.01$). These SAP97egfp overexpressing PV interneuons also fired at high frequency reflected with a significantly lower Min ISI (97egfp, 12.3 ± 1.3 ms; 97-, 19.4 ± 1.7 ms; $P < 0.01$). Additionally, their membrane is less excitable (Fig. 3.5C) with decreased Rm (97egfp, 110 ± 15 MΩ; 97-, 173 ± 14 MΩ; $P < 0.01$) and increased rheobase (97egfp, 346 ± 62 pA; 97-, 215 ± 20 pA; $P < 0.05$). AP half-width is narrower (97egfp, 0.32 ± 0.01 ms; 97-, 0.46 ± 0.04 ms; $P < 0.05$) and AHP area is much smaller (97egfp, 137 ± 10 V*s; 97-, 238± 15 V*s; $P < 0.001$) than that of SAP97-nonexpressing PV interneurons and in the same range with that of SAP97-expressing PV interneurons (Fig. 3.5D). These results confirmed that overexpression of SAP97 is sufficient to create the membrane properties associated with endogenous expression of SAP97.

SAP97 overexpression enhances the frequency of the glutamatergic synaptic input onto adult PV interneurons.

SAP97egfp overexpression resulted a similar shift in the synaptic activity of PV interneurons. Figure 3.6 shows representative current traces recorded from PV97egfp interneurons and associated plots. MEPSC frequency increased in SAP97egfp overexpressing cells (97egfp, 52 ± 6 Hz; 97-, 20 ± 2 Hz; $P < 0.01$) (Fig. 3.6A, B & C_1). The distribution of mEPSC amplitudes shows a modest but significant change (Fig. 3.6A, B & C_2). mEPSC half-width and decay kinetics also changed in the same direction as SAP97 expressing PV interneurons (Fig. 3.6B, C_3 & C_4).

SAP97 enhances dendritic branching in adult PV interneurons.

SAP97 is known to regulate dendritic branching, which provides additional synaptic

harborizations in spinal motoneurons (Zhou et al., 2008). We used 3D reconstructions of biocytin-filled PV interneurons confocal images of acute slices to investigate the role of SAP97 in dendritic branching. Figure 3.7 shows confocal images and traces of SAP97-nonexpressing (Fig. 3.7A_1 & A_2) and SAP97egfp expressing (Fig. 3.7B_1 & B_2) adult PV interneurons. We assayed the complexity of dendritic tree by Scholl analysis (Sholl, 1953). The number of dendritic intersections across concentric rings at 20 - 40 μm away from soma is increased in adult PV interneurons expressing SAP97 and SAP97egfp than that in SAP97- interneurons (Fig. 3.7C).

DISCUSSION

In this chapter, we describe the functional role of a MAGuK, SAP97, in PV interneurons in mouse visual cortex. Consistent with previous work, we find that the percentage of PV interneurons expressing SAP97 decreases with age. (Fig. 3.2A_1-A_2). Nevertheless, a significant fraction of adult PV interneurons, at minimum around 30%, continue to express SAP97. Using patch clamp electrophysiology, we show that the membrane properties and synaptic inputs to PV interneurons expressing SAP97 is distinct to those not expressing SAP97. In particular, SAP97-expressing interneurons display less excitable membrane properties including areduced Rm and increased rheobase, but also fire at higher frequency with APs having narrower half-width and smaller AHP (Fig. 3.2B-D, Table 3.4). Additionally, they also receive a higher frequency of mEPSCs (Fig. 3.3). We confirmed the causal relationship between SAP97 expression and membrane and synaptic properties by overexpressing SAP97 in adult PV interneurons.

Developmental expression of SAP97 in PV interneurons

The percentage of SAP97 expressing PV interneurons in mouse visual cortex decreases from juvenile to adulthood (Akgul and Wollmuth, 2010)(present study). Based on in situ hybridization, we found higher percentages of SAP97 expressing PV interneurons in both juvenile (around 90%) and adult (40%) visual cortex compared to the present study, around 60% (juvenile) and 30% (adult) based on single cell RT-PCR. We believe that the difference for juvenile visual cortex reflects that in the present study we tended to sample slightly more mature 'juvenile' PV interneurons. Specifically, there appears to be a lag between the turning on of the PV promoter and subsequent expression of PV and expression of tdTomato (Fig. 3.1A), which requires an intervening Cre/lox recombination. Hence, for the single cell RT-PCR sampling, we patched only cells expressing tdTomato, whereas for in situ hybridization we sampled PV

expression. If correct, this suggests that the development transition from SAP97-expressing to SAP97-nonexpressing PV interneurons occur around eye opening. Still the specific time course of SAP97 expression and the factors that regulate its expression will require specific experiments to address.

For adult PV interneurons in the visual cortex, the quantitative difference between in situ hybridization (around 40%) and single cell RT-PCR (around 30%) presumably reflects a sampling issue where a much large population of PV interneurons was sampled using in situ hybridization. Nevertheless, both approaches highlight that a significant fraction of adult PV interneurons, around 30-40%, express SAP97.

Developmental regulation of neuronal excitability

Visual cortex goes through a dramatic change around eye opening and later in development. in relation to that, the intrinsic membrane properties of cortical PV interneurons show developmental changes. Membranes of PV interneruons show less excitability and action potential shape changes with narrower half width and smaller after hyperpolarization. (Kuhlman et al., 2010; Lazarus and Huang, 2011; Okaty et al., 2009). Consistent with previous reports, in PV interneurons, we observed a drastic shift in membrane excitability and AP shape monitored as a reduction in Rm, increase in rheobase and narrowing of AP half-width, smaller AHP at older age (P56 - 65) (Table 3.3). Interestingly, most of these changes occur in both SAP97-expressing and SAP97-nonexpressing PV interneurons (Table 3.4) in the same direction. For example, input resistance decreases in SAP97+ PV interneurons with age as well as in SAP97- interneurons, and so do the rheobase, AP half-width and AHP suggesting that both PV interneurons subsets described in this study are going thorough similar developmental changes.

The role of SAP97 in membrane excitability and firing pattern

In the same age group (either juvenile or adult), SAP97 expression is accompanied with reduced Rm and I/F ratio and increased rheobase suggesting less membrane excitability of PV interneurons expressing SAP97 in comparison to SAP97-nonexpressing subset (Figure 3.2B-C, Table 3.4). In cardiac myocytes, the role of SAP97 in regulating cardiac membrane excitability has been evident (Vikstrom et al., 2009). It has not been known whether SAP97 has a similar role in neurons but previous reports about SAP97 and K channel interactions (Abi-Char et al., 2008; Petitprez et al., 2011; Tiffany et al., 2000) suggest that SAP97 might be regulating the number of ion channels expressed and their positioning and clustering at the neuronal membrane. Additionally, SAP97 can harbor kinases mediating ion channel phosphorylations and therefore can influence ion channel conductance (Vikstrom et al., 2009). The details of the mechanism for the phenotype we observed due to SAP97 expression will require additional experimantation. Another distinct property of PV interneurons expressing SAP97 is the drastic increase in their action potential firing rate in comparison to that of SAP97- interneurons. Although average interspike interval (ISI average) is comparable between SAP97+ and SAP97- PV interneurons at both ages, minimum interspike interval is significantly decreased in the former subset (Table 3.4). Dramatic decrease in AP half-width and AHP give clues about the enhanced firing rate of endogenous SAP97 expressing and SAP97egfp overexpressing PV interneurons. However, exact mechanism has remained to be elucidated with further experiments. PV interneurons exhibit fast-spiking firing pattern, which is associated with generation of gamma frequency oscillations in brain (Cardin et al., 2009; Carlen et al., 2011; Sohal et al., 2009). It would also be very intriguing to see how SAP97 + and SAP97- PV interneurons behave in neuronal networks and different activity states.

The role of SAP97 in synaptic transmission

SAP97 has been implicated with GluR trafficking and regulation of excitatory synaptic transmission in pyramidal neurons. Although there are conflicting reports about it exact role, SAP97 is believed to have a transsynaptic effect and might be regulating both presynaptic activity levels and postsynaptic receptor content (Regalado et al., 2006; Rumbaugh et al., 2003; Waites et al., 2009). Our results indicate that mEPSC frequency is at least 2-fold higher in PV interneurons expressing SAP97 in comparison to SAP97-nonexpressing interneurons independent of age (Fig. 3.3). SAP97egfp overexpressing PV interneurons receive excitatory input at much higher frequency than both native interneuron subsets (Fig. 3.6). This suggests that SAP97 is regulating either the number of synapses or /and presynaptic activity. While enhanced dendritic branching in SAP97egfp expressing PV interneurons (Fig. 3.7) supports the former idea, possible changes of presynaptic activity in parallel to SAP97 expression should be tested with paired-recordings. Additionally, the slight difference in mEPSC amplitudes of SAP97-expressing, SAP97-nonexpressing and SAP97egfp overexpressing PV interneurons indicate also a trafficking role for SAP97.

TABLES AND FIGURES

Table 3.3. Passive and active membrane properties of juvenile and adult PV interneurons

	Juvenile	Adult
Firing pattern		
Delay 1st AP (ms)	462 ± 57	395 ± 79
ISI average (ms)	25.9 ± 1.2	24.2 ± 1.4
Frequency adapt.	1.03 ± 0.12	1.30* ± 0.09
Max. inst. ISI (ms)	109 ± 23	120 ± 40
Min. inst. ISI (ms)	20.3 ± 1.3	18.4 ± 1.3
Max/Min ISI ratio	6.4 ± 1.7	7.6 ± 2.6
CV frequency	0.20 ± 0.02	0.20 ± 0.03
I/F slope	2.2 ± 0.3	1.2*** ± 0.1
Passive		
V_m (mV)	-86 ± 1.4	-87 ± 1.2
R_m (MW)	106 ± 10	159*** ± 12
rheobase (pA)	384 ± 46	228** ± 16
AP shape		
AP threshold (mV)	-46.3 ± 1.5	-49.6* ± 1.0
AP half-width (ms)	0.54 ± 0.04	0.44* ± 0.03
AHP peak (mV)	-24.7 ± 0.6	-23.8 ± 1.0
AHP latency (ms)	2.2 ± 0.4	1.4* ± 0.2
AHP area (V*s)	-298 ± 42	-213* ± 15
# of interneurons	14	20

Juvenile (P15 - P17) or adult (P56 – P65) PV interneurons are characterized by firing pattern, passive membrane properties, and action potential shape (see Materials and Methods). Max/Min ISI ratio is the ratio of maximum to minimum interspike intervals. Values shown as mean ± SEM. A *t*-test was used to determine whether the value for juvenile was significantly different from that for adult (* indicates $p < 0.05$, ** indicates $p < 0.01$, and *** indicates $p < 0.001$).

Table 3.4. Passive and active membrane properties of juvenile and adult PV interneurons either expressing or not expressing SAP97.

	Juvenile		Adult	
	SAP97+	SAP97-	SAP97+	SAP97-
Firing pattern				
Delay 1st AP (ms)	440 ± 80	500 ± 80	510 ± 170	360 ± 90
ISI average (ms)	28.9 ± 1.2	29.5 ± 1.5	26.9 ± 2.6	27.1 ± 2.2
Frequency adapt.	0.96 ± 0.20	1.12 ± 0.12	1.42 ± 0.23	1.27 ± 0.11
Max. inst. ISI (ms)	144* ± 35	62 ± 10	308* ± 118	53 ± 9
Min. inst. ISI (ms)	18.2* ± 1.5	23.0 ± 1.7	15.5* ± 1.1	19.4 ± 1.7
Max/Min ISI ratio	9.2* ± 2.6	2.8 ± 0.5	20.2* ± 7.4	3.1 ± 0.8
CV frequency	0.22 ± 0.04	0.17 ± 0.03	0.24 ± 0.03	0.20 ± 0.04
I/F slope	1.8* ± 0.3	2.6 ± 0.4	$0.9^{*\$}$ ± 0.05	$1.2^{\$}$ ± 0.15
Passive				
V_m (mV)	-85* ± 1.8	-90 ± 1.7	-85 ± 1.7	-88 ± 1.5
R_m (MW)	88** ± 9.7	130 ± 13	$118^{**\$}$ ± 13	$173^{\$}$ ± 14
rheobase (pA)	450* ± 66	290 ± 40	$270^{*\$}$ ± 10	215 ± 20
AP shape				
AP threshold (mV)	-45.6 ± 2.5	-47.3 ± 1.2	-49.3 ± 1.6	-49.7 ± 1.5
AP half-width (ms)	0.48* ± 0.02	0.63 ± 0.08	$0.37^{*\$}$ ± 0.02	$0.46^{\$}$ ± 0.04
AHP peak (mV)	-25.3 ± 0.6	-23.9 ± 1.0	-24.5 ± 1.5	-23.6 ± 1.0
AHP latency (ms)	1.7 ± 0.1	3.0 ± 0.9	$1.1^{*\$}$ ± 0.1	1.5 ± 0.2
AHP area (V*s)	-210** ± 20	-420 ± 70	$-140^{***\$}$ ± 10	$-240^{\$}$ ± 10
# of interneurons	8	6	5	15

Juvenile (P15 - P17) or adult (P56 – P65) PV interneurons are characterized by firing pattern, passive membrane properties, and action potential shape (see Materials and Methods). Max/Min ISI ratio is the ratio of maximum to minimum interspike intervals. Values shown as mean ± SEM. A *t*-test was used to determine whether the value for SAP97+ was significantly different from that for SAP97- within the same age (* indicates $p < 0.05$, ** indicates $p < 0.01$, and *** indicates $p < 0.001$) or between different ages within SAP97- or SAP97+ ($^{\$}$ indicates $p < 0.05$).

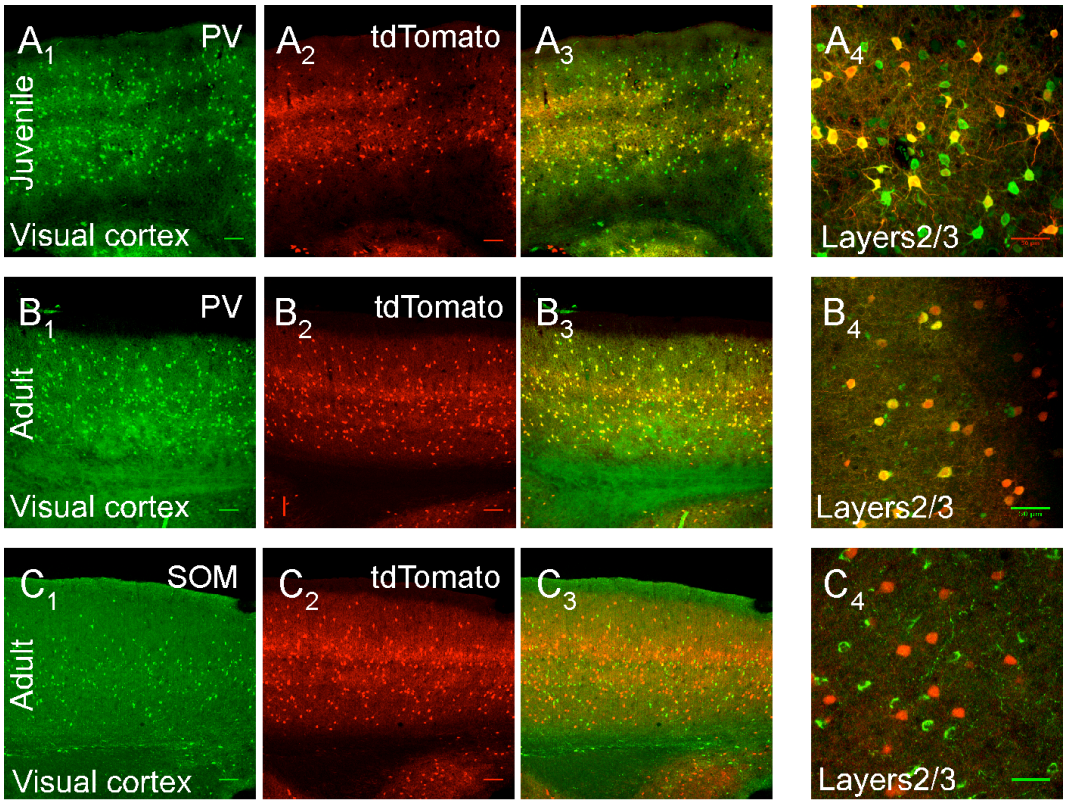

Figure 3.1. In PVdT mice, tdTomato colocalizes with parvalbumin (PV).
Confocal images of the visual cortex from juvenile (A_1-A_4) or adult (B_1-B_4 & C_1-C_4) PVdT mice. Tissue sections were labeled with either rabbit anti-PV (A_1 & B_1) or rat anti-SOM (C_1) and visualized for either PV (green; A_1 & B_1) or SOM (green; C_1) and tdTomato (red; A_2, B_2 & C_2) signals. Merged images are shown in A_3-A_4 & B_3-B_4 & C_3-C_4. The images are at either 10X (A_1-A_3, B_1-B_3 & C_1-C_3) or 63X (A_4, B_4 & C_4). Scale bars, 100 µm for 10X and 50 µm for 63X images. The higher magnified images (A_4, B_4 & C_4) show a smaller region in layers 2/3 of the merged images in A_3, B_3 and C_3. The specificity of the PV and SOM antibodies has been verified (Akgul and Wollmuth, 2010). Merged images show either colocalization of PV and tdTomato (A_3-A_4 & B_3-B_4) or lack of overlap between SOM and tdTomato (C_3-C_4).

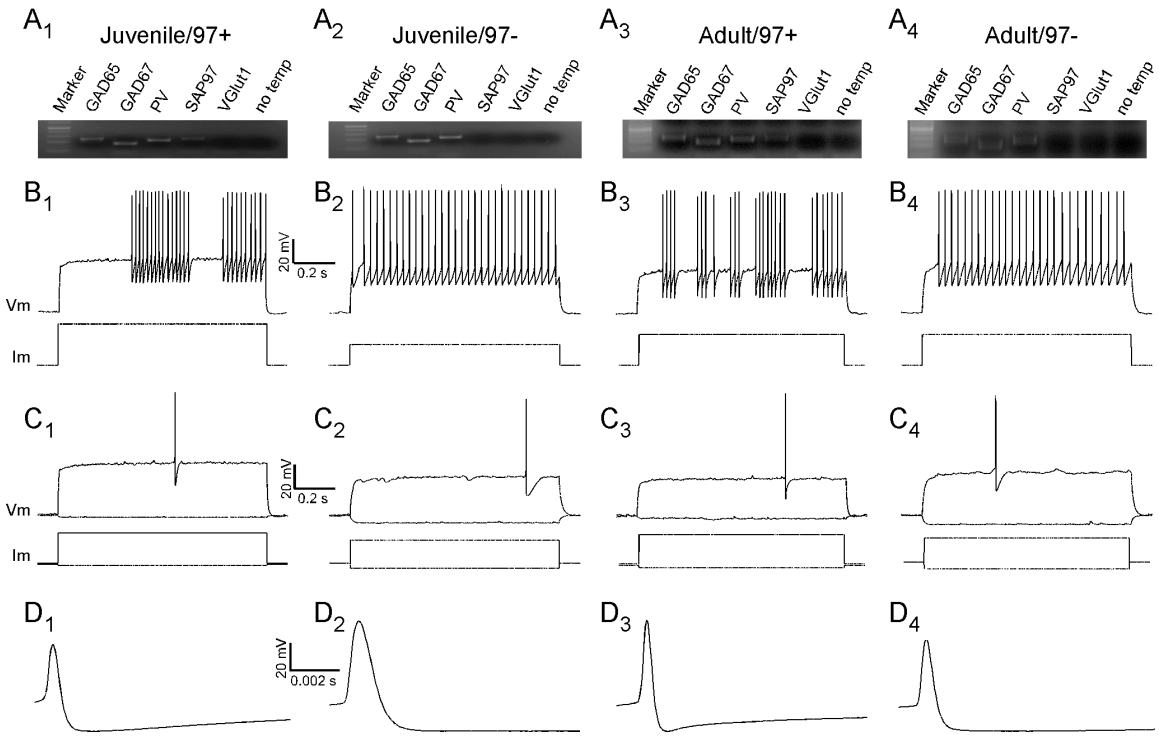

Figure 3.2. Membrane properties of SAP97-expressing and SAP97-nonexpressing PV interneurons.

Analysis of membrane properties in juvenile PV interneurons either expressing (first column, Juvenile/97+) or not expressing (second column, Juvenile/97-) SAP97 or adult PV interneurons either expressing (third column, Adult/97+) or not expressing (last column, Adult/97-) SAP97. Each column represents the results from the same interneuron.

A_1-A_4. Gene expression profiles of individual interneurons. GAD67 and GAD65 are GABAergic interneuron markers and PV is PV interneuron marker. GAD67 and GAD65 are used as positive controls. VGluT1 and no template lanes are negative controls.

B_1-B_4. Voltage traces (V_m) of individual interneurons firing at approximately 30 Hz. The depolarizing currents (I_m) to elicit 30 Hz firing are 790, 310, 340 and 200 pA, respectively.

C_1-C_4. Voltage traces (V_m) for the hyperpolarized membrane potential and the first action potential (AP) in response to rheobase current are shown along with the injected current traces. Rheobase currents are 720, 190, 200 and 150 pA, respectively.

D_1-D_4. The rheobase APs are expanded (10 ms total time) to highlight differences in AP shape.

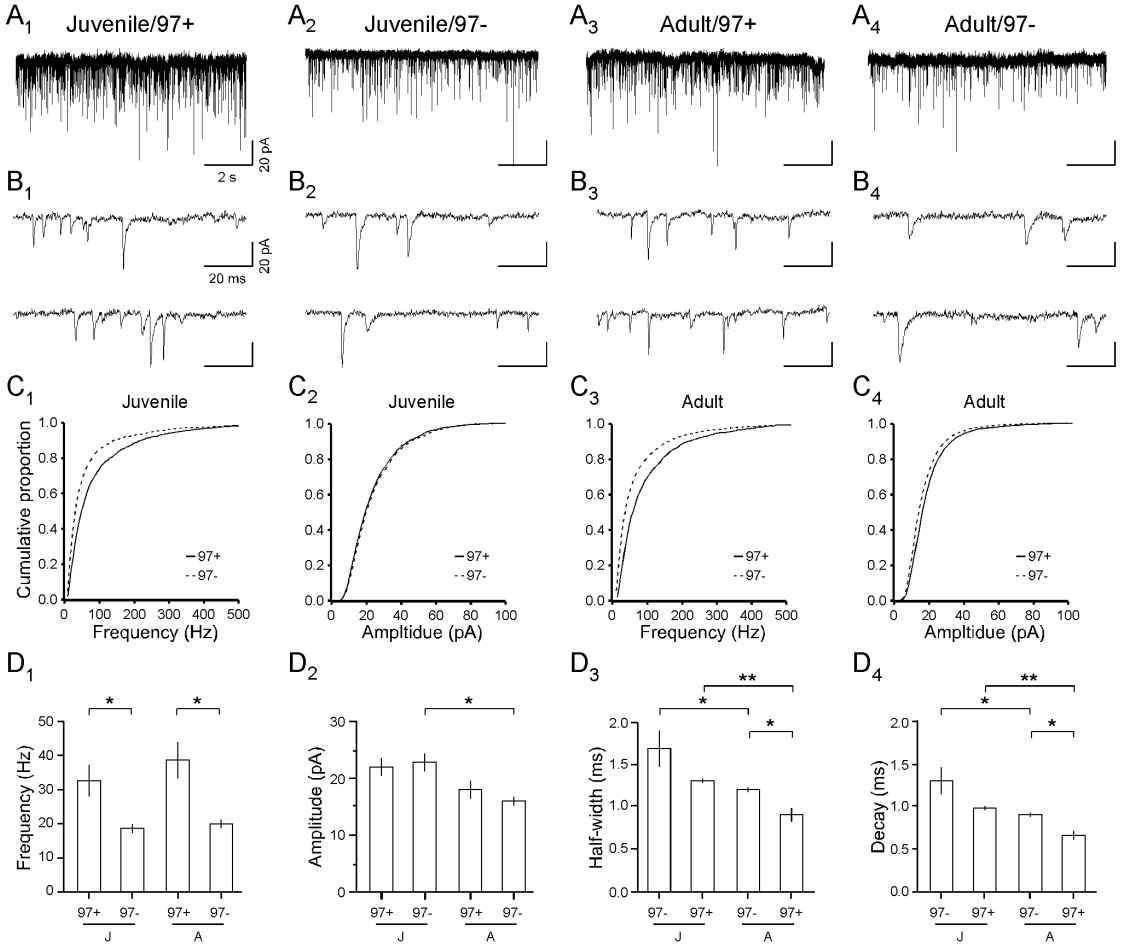

Figure 3.3. SAP97-expressing and SAP97-nonexpressing PV interneurons receive different excitatory input.

Analysis of mEPSCs in juvenile PV interneurons either expressing (first column, Juvenile/97+) or not expressing (second column, Juvenile/97-) SAP97 or adult PV interneurons either expressing (third column, Adult/97+) or not expressing (last column, Adult/97-) SAP97. Each column represents the results from the same interneuron.

A_1-A_4. Representative current traces (10 s) from individual interneurons recorded in whole cell voltage clamp (V_h= –70 mV) in the presence of Mg^{2+}, TTX, and bicuculine.

B_1-B_4. Segments of the same current traces expanded to show 100 ms of recording.

C_1-C_4. Cumulative histograms of mEPSC frequency (C_1 & C_3) and amplitude (C_2 & C_4). Continuous lines indicate SAP97+ and dashed lines indicate SAP97- interneurons. mEPSC frequency distributions in both juvenile and adult SAP97+ interneurons are significantly different from those in SAP97- interneurons. mEPSC amplitude distributions are significantly different between SAP97+ and SAP97- interneurons only in adult ($p < 0.01$, Kolmogorov-Smirnov test).

D_1-D_2. Bar graphs of mEPSC frequency (D_1), amplitude (D_2), half-width (D_3) and decay (D_4). Values shown are mean ± SEM. * indicates $p < 0.05$ and ** indicates $p < 0.01$; Student's t-test. V_h, V_{hold}; 97-, SAP97-; 97+, SAP97+; J, Juvenile and A, Adult.

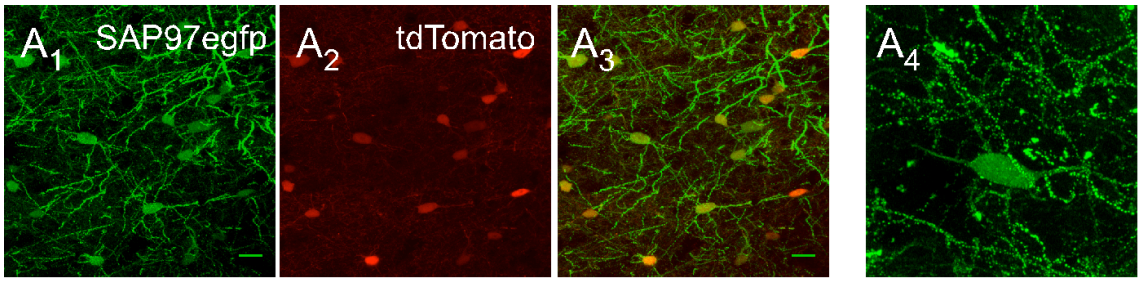

Figure 3.4. Overexpression of SAP97egfp in PV interneurons.
Confocal images of the visual cortex from adult (A_1-A_4) PVdT mice. FLEX-rev-a-SAP97-EGFP_AAV was stereotaxically injected into the visual cortex. Tissue sections were visualized for either EGFP (green; A_1, A_4) or tdTomato (red; A_2) signals. Merged image is shown in A_3. The images are at either 10X (A_1-A_3) or 63X (A_4). Scale bars, 100 µm for 10X and 50 µm for 63X images. The higher magnified image (A_4) show a smaller region in layers 2/3 of A_1. Merged image shows colocalization of EGFP and tdTomato and the magnified image shows somatodendritic localization of punctuate EGFP signal.

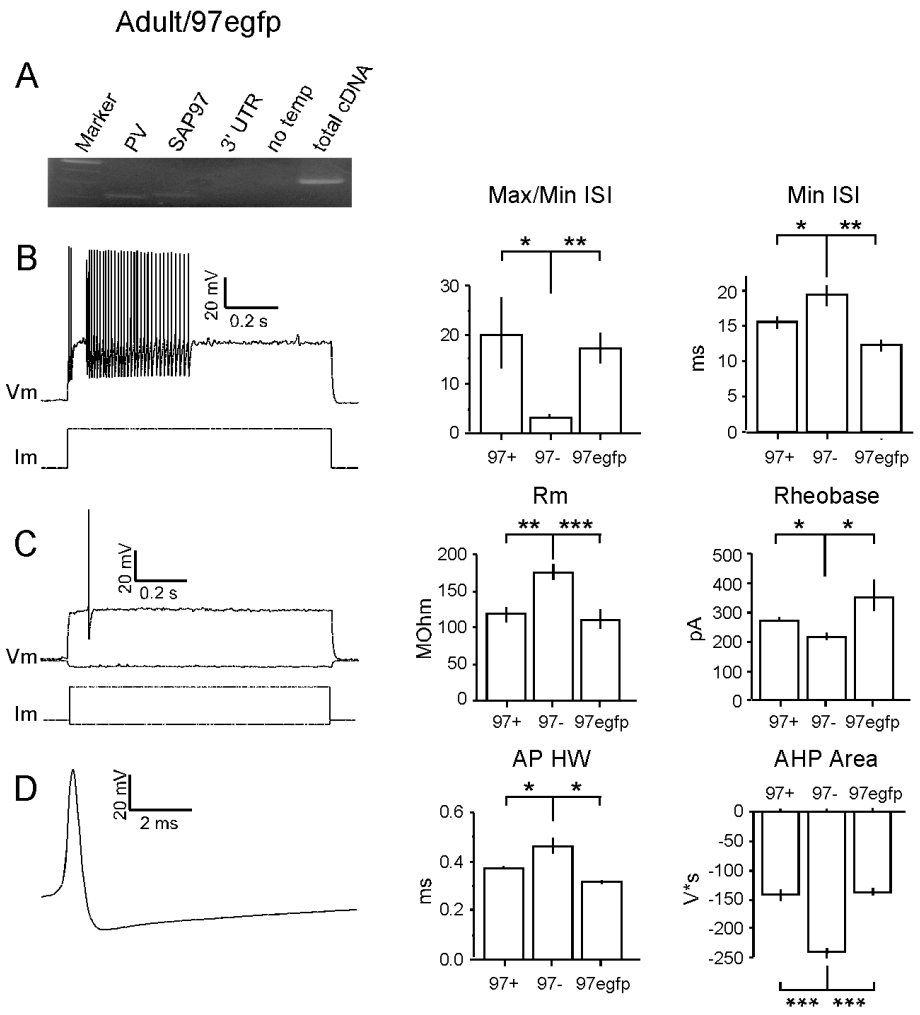

Figure 3.5. Membrane properties of adult PV interneurons overexpressing SAP97egfp.
A. Gene expression profile of an individual adult PV interneuron overexpressing SAP97egfp (Adult/97egfp). PV and SAP97 primers target parvalbumin and SAP97 open reading frame; and 3'UTR primers target the 3'UTR region of SAP97 to detect endogenous SAP97. No template is negative control. 3'UTR primers were also used on cDNA preparation of total isolated cortical RNA as a positive control.
B. Voltage trace (V_m) of an individual interneuron firing at approximately 30 Hz. The depolarizing current (I_m) to elicit 30 Hz firing is 420 pA. Bar graphs show Max/Min interspike interval (Max/Min ISI) and current/frequency (I/F) ratios for SAP97-expressing (97+), SAP97-nonexpressing (97-) and SAP97egfp (97egfp) overexpressing adult PV interneurons.
C. The membrane potential in response to hyperpolarizing current (-40 pA) and the first action potential (AP) firing in response to rheobase current (280 pA). Bar graphs show R_m and rheobase.
D. The rheobase AP is expanded (10 ms total time). Bar graphs show AP half-width (HW) and AHP area.
Values shown in bar graphs are mean ± SEM. All values are compared to SAP97- group. * indicates $p < 0.05$, ** indicates $p < 0.01$ and *** indicates $p < 0.001$; Student's t-test.

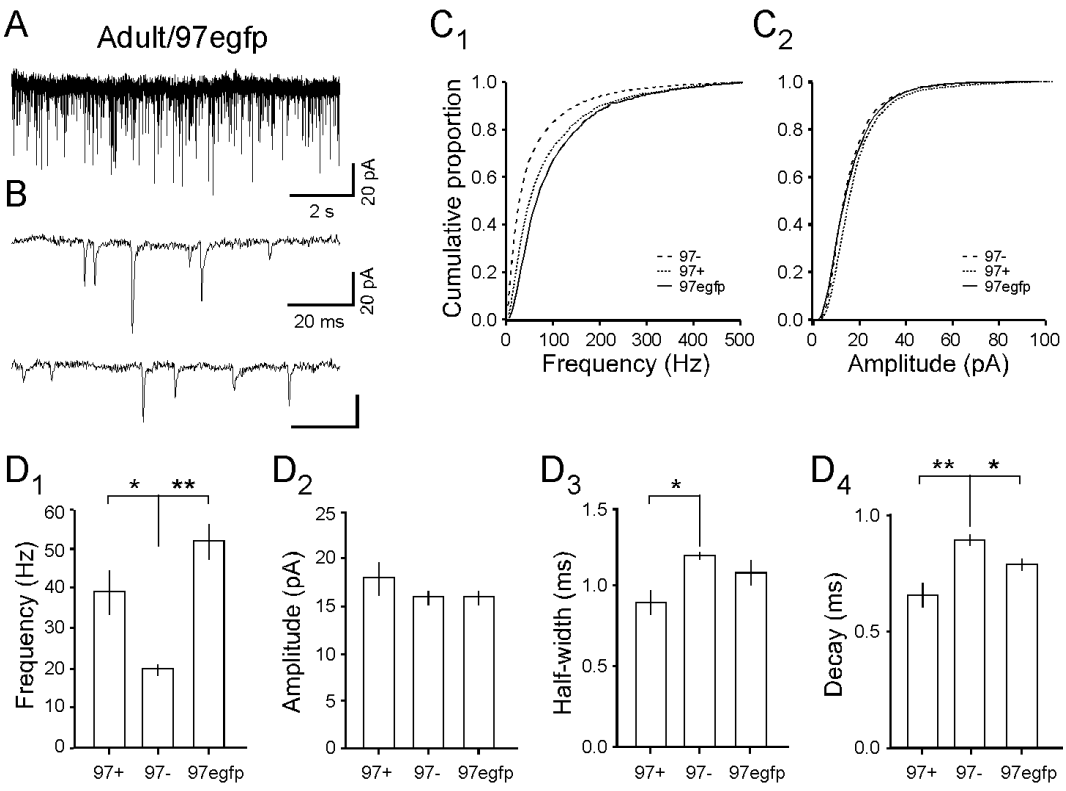

Figure 3.6. PV interneurons overexpressing SAP97egfp show higher levels of excitatory activity.

Analysis of mEPSCs in adult PV interneurons overexpressing SAP97egfp in comparison to SAP97- and SAP97+ adult interneurons.

A. Representative current trace (10 s) from an individual interneuron recorded in whole cell voltage clamp (V_h= –70 mV) in the presence of Mg^{2+}, TTX, and bicuculine.

B. Segments of the same current trace are expanded to show 100 ms recording.

C_1-C_2. Cumulative histograms of mEPSC frequency (C_1) and amplitude (C_2). Dashed line indicates SAP97-; dotted line, SAP97+ and solid line, SAP97egfp. Both frequency and amplitude distributions for SAP97+ and SAP97egfp interneurons are significantly than those for SAP97- ($p < 0.01$, Kolmogorov-Smirnov test)

D_1-D_2. Bar graphs of mEPSC frequency (D_1), amplitude (D_2), half-width (D_3) and decay (D_4). Values shown in bar graphs are mean ± SEM. * indicates $p < 0.05$ and ** indicates $p < 0.01$. 97-, SAP97; 97+, SAP97+; 97egfp, SAP97egfp; V_h: V_{hold}.

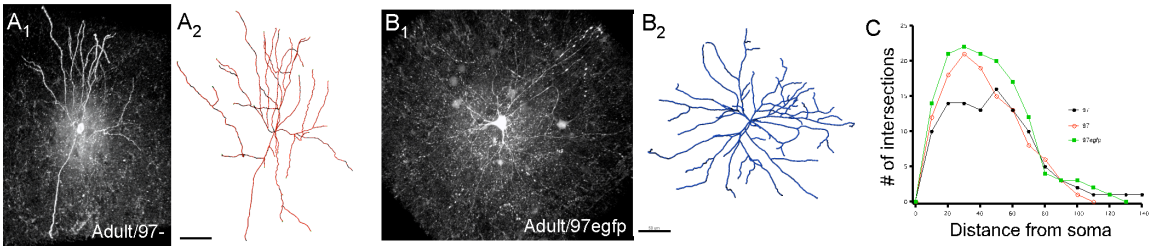

Figure 3.7. Dendritic branching of SAP97- and SAP97egfp PV interneurons
A-B. Representative micrographs (A_1 & B_1) and Imaris traces (A_2 & B_2) of biocytin-filled SAP97- and SAP97egfp PV interneurons. Scale bar, 50 µm.
C. Scholl analysis in SAP97-, SAP97+ and SAP97egfp expressing interneurons.

SUPPLEMENTAL INFORMATION

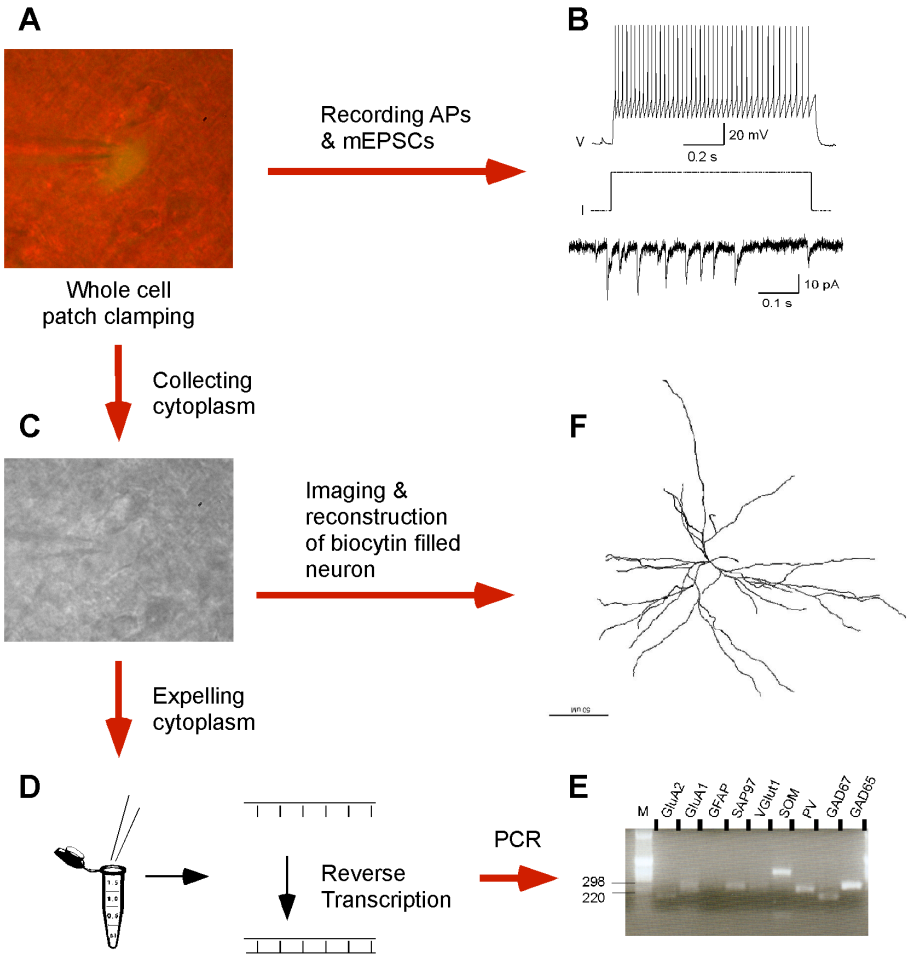

Supplemental Figure 3.1. Single cell reverse transcription polymerase chain reaction protocol.
A) Whole patch clamp recording from fluorescently identified interneuron in acute mouse brain slices. **B)** Membrane properties including action potential shape and firing pattern are measured by injecting current. **C)** After the recording, cytoplasm of the interneuron is harvested. **D)** mRNAs of the cell are reverse transcribed with oligodT primers by Superscript RT-II using oligodT primers. **E)** Gene expression profile of the neuron is shown the agarose gel with PCR is run with gene specific primers (Table S1) to show gene expression profile of the neuron. PCR amplicons are run and monitored on an agarose gel. **F)** During recording, the cell is filled with biocytin to label with anti-biocytin and visualize its morphology. Adapted from Toledo-Rodriguez and Markram, 2007.

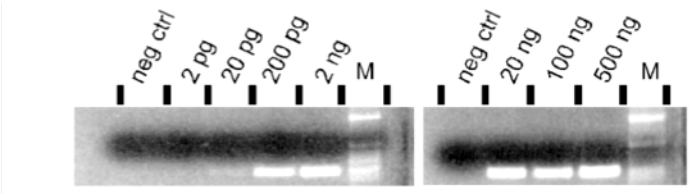

Supplemental Figure 3.2. Parvalbumin primers tested for single cell RT-PCR.
The template cDNA was synthesized with the isolated and serially diluted [500 ng/µl – 2 pg/µl] mouse brain RNA. The amplified product could be detected with the dilution of RNA at pg level. M, DNA Marker; neg ctrl, Negative control (no template).

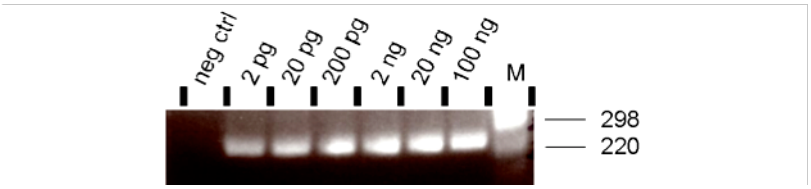

Supplemental Figure 3.3. SAP97 primers tested for single cell RT-PCR.
The template cDNA was synthesized with the isolated and serially diluted [500 ng/µl – 2 pg/µl] mouse brain RNA. The amplified product could be detected with the dilution of RNA at pg level. M, DNA Marker; neg ctrl, Negative control (no template).

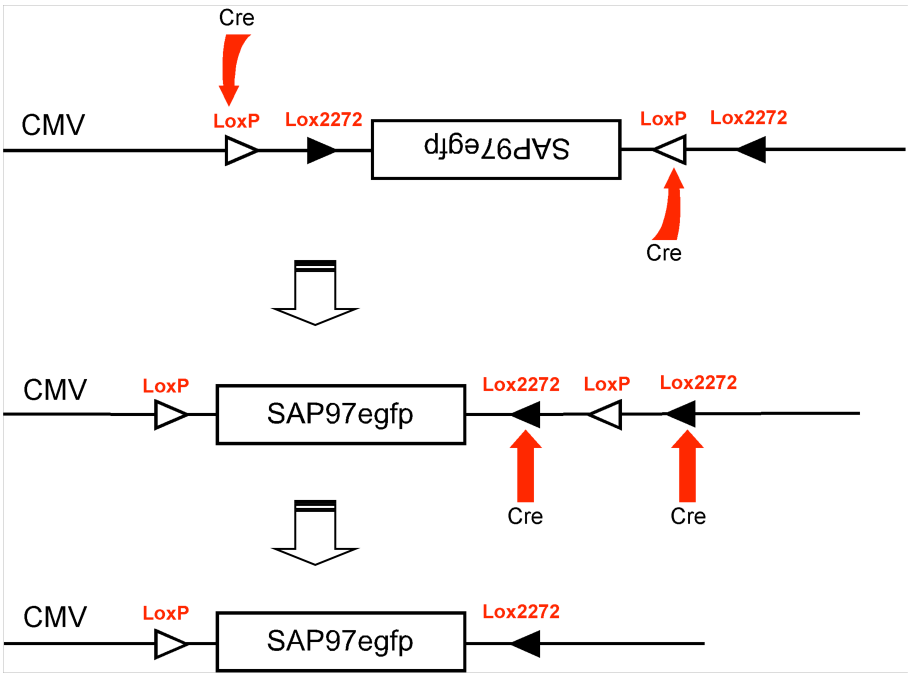

Supplemental Figure 3.4. Schematic representation of the reverse oriented viral construct and Cre/lox recombination.
SAP97 cDNA is in reverse orientation and flanked with two incompatible lox cassettes (LoxP and Lox2272) facing each other to favor inversion. Cre recombinase inverts the gene of interest to forward orientation in the first round or recombination. Then, it excises out one of each pair of lox cassettes leaving a pair of incompatible lox cassettes. CMV promoter drives the expression of the gene of interest.

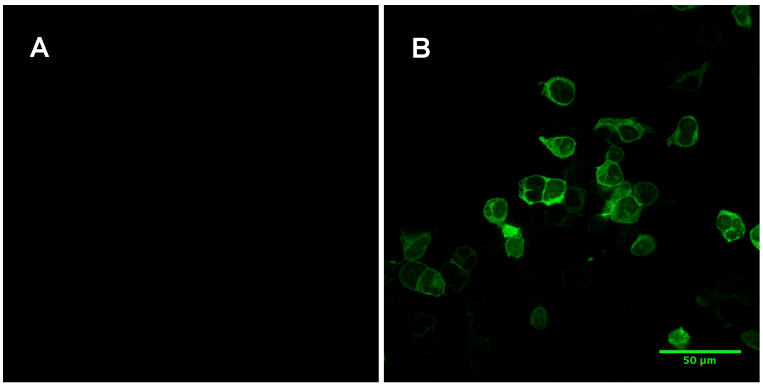

Supplemental Figure 3.5. Reverse oriented viral construct tested in HEK293 cells.
HEK293 cells were transfected with rev-a-SAP97egfp_AAV either alone (A) or with pCMV-Cre (B). No green fluorescence could be detected when the viral construct was transfected alone (A) whereas cotransfection with pCMV-Cre turns on the fluorescence indicating that the expression of SAP97egfp. Scale bar is 50 µm.

Supplemental Table 3.1. Passive and active membrane properties of juvenile and adult PV interneurons either SAP97- or SAP97+ or SAP97egfp.

	SAP97-	SAP97+	SAP97egfp
Firing pattern			
Delay 1st AP (ms)	360 ± 90	510 ± 170	276 ± 125
ISI average (ms)	27.1 ± 2.2	26.9 ± 2.6	26.1 ± 3.0
Frequency adapt.	1.27 ± 0.11	1.42 ± 0.23	0.72 ± 0.24
Max. inst. ISI (ms)	53 ± 9	308* ± 118	208** ± 46
Min. inst. ISI (ms)	19.4 ± 1.7	15.5* ± 1.1	12.3** ± 1.3
Max/Min ISI ratio	3.1 ± 0.8	20.2* ± 7.4	17.4** ± 3.6
CV frequency	0.20 ± 0.04	0.24 ± 0.03	0.28* ± 0.02
I/F slope	1.2 ± 0.15	0.9* ± 0.05	1.01 ± 0.14
Passive			
V_m (mV)	-88 ± 1.5	-85 ± 1.7	-86 ± 2.0
R_m (MW)	173 ± 14	118** ± 13	110** ± 15
rheobase (pA)	215 ± 20	270* ± 10	346* ± 62
AP shape			
AP threshold (mV)	-49.7 ± 1.5	-49.3 ± 1.6	-53.4 ± 2.1
AP half-width (ms)	0.46 ± 0.04	0.37* ± 0.02	0.32*** ± 0.01
AHP peak (mV)	-23.6 ± 1.0	-24.5 ± 1.5	-23.6 ± 1.5
AHP latency (ms)	1.5 ± 0.2	1.1* ± 0.1	0.8** ± 0.04
AHP area (V*s)	-240 ± 10	-140*** ± 10	-137*** ± 10
# of interneurons	15	5	8

Adult (P56 – P65) PV interneurons are characterized by firing pattern, passive membrane properties, and action potential shape (see Materials and Methods). Values shown as mean ± SEM. A *t*-test was used to determine whether the value for SAP97+ or SAP97egfp were significantly different from that for SAP97- (* indicates $p < 0.05$, ** indicates $p < 0.01$, and *** indicates $p < 0.001$).

CHAPTER 4: DISCUSSIONS AND CONCLUSIONS

The physiological and anatomical properties of neurons define how they function in a network. Combination of various molecular complexes and mechanisms create the distinct phenotype for each neuron type for normal brain functions as well as their disconcerted activity can lead to abnormal brain functions and diseases. Scaffolding proteins harbor macromolecular complexes that exert concerted effects in cellular physiology. Here, I described the expression profile of all four members, PSD-95, PSD-93, SAP97 and SAP102, of the MAGuK family of scaffolding proteins in the two major subgroups of GABAergic interneurons, PV and SOM, of juvenile and adult mouse visual cortex. I also investigated the functional significance of SAP97 in physiological and anatomical properties of PV interneurons. I showed that among all MAGuK members, SAP97 expression shows a distinct pattern that changes over development and identifies two subsets in cortical PV interneurons. SAP97 is involved in at least two mechanisms in PV interneuons: regulating their membrane properties and frequency of excitatory input. However, there are still questions remained to be answered in future studies.

Does the mRNA expression pattern of MAGuKs reflect its protein expression? In our study, we assayed MAGuK mRNA rather than protein expression. The reason we tended to target mRNA was the lack of high quality MAGuK specific antibodies at the moment. We assumed that the protein expression will be similar to mRNA expression of MAGuKs but it still needs to be confirmed with double immunolabeling experiments.

Is the developmental change in SAP97 expression in PV and SOM interneurons similar in all GABAergic interneurons? We do not know whether other GABAergic interneuron subgroups

(e.g., VIP, CR) show MAGuK expression pattern similar to the pattern seen in PV and SOM interneurons. A similar study with more global GABAergic and larger number of interneuron specific labeling in several brain regions would give us a better understanding of SAP97 expression in GABAergic interneurons.

How is SAP97 expression changing over development from precursor cells to mature neurons? Since a similar SAP97 expression pattern is observed in both PV and SOM interneurons, we can speculate that it has a global developmental role in all GABAergic interneurons rather than an interneuron specific role. At the moment, there is no implication for the developmental role of SAP97 in neurons mostly due to the lethal effect of SAP97 knock out (Caruana and Bernstein, 2001). However, hormone or promoter dependent transgenic Cre lines allow temporal and spatial deletion of SAP97 (Taniguchi et al., 2011). Using conditional knock-outs and imaging and recording techniques, the developmental role of SAP97 in the cortical interneurons or other systems could be investigated.

Is SAP97 expression changing in an activity dependent manner? Eye opening at P13-14 in mice initiates activity dependent changes in intrinsic and synaptic properties of neurons in the visual cortex (Lazarus and Huang, 2011; Maffei and Turrigiano, 2008). The developmental expression pattern we observed for SAP97 mRNA in PV and SOM interneurons might be a part of the activity dependent adaptation of the visual cortex. To test whether SAP97 expression pattern in the visual cortex changes with different sensory stimulation and activity level, visual stimuli coming from one or both eyes could be blocked with either eye suture or TTX injections into eyes and assay SAP97 expression in the interneurons.

What is the subcellular localization of SAP97 in aspiny PV and spiny SOM interneurons? MAGuKs are known to be PSD proteins with functional roles in GluR trafficking and positioning at PSD of glutamatergic synapses (Elias and Nicoll, 2007). However, there are reports showing that they might also be localized in axonal regions of neurons (Muller et al., 1995). We also know that dendritic and synaptic morphology vary among cell types. Given the structural differences between the dendrites of PV and of SOM interneurons, it would be very interesting to study the subcellular localization of SAP97 in PV and SOM interneurons with electron microscopy.

How does SAP97 regulate membrane excitability and firing rate of action potentials in PV interneuron? Multiple mechanisms regulate membrane excitability, firing pattern and shape of action potentials in neurons such as the composition of K and Na channels, their localization at the membrane and biochemical modifications. SAP97 is involved in trafficking and positioning of preferential subunits of ion channels at the membrane in neurons and cardiac myocytes (Abi-Char et al., 2008; Leonoudakis et al., 2004a; Leonoudakis et al., 2004b; Petitprez et al., 2011; Vikstrom et al., 2009) and in regulating unitary conductance of ion channels in cardiac myocytes (Ikematsu et al., 2011; Vikstrom et al., 2009). Future work should focus initially on discovering the correlations between SAP97 ion channel expressions in PV interneurons by microarray analysis.

What are the presynaptic and postsynaptic partners of SAP97-expressing and SAP97-nonexpressing interneurons? To understand the functional role of the interneurons in neuronal circuits, it is essential to know their presynaptic and postsynaptic partners. We do not know whether PV interneurons expressing SAP97 have same synaptically connecting partners as SAP97- interneurons. To address this question, paired recordings from a presynaptic pyramidal

neuron and a postsynaptic interneuron as well as the reverse orientation would be applied. In addition to this crude electrophysiological approach, several alternative genetic and optical tools would be advantageous and more efficient to analyze connecting neurons in circuits. For example, recombinant Rabies virus that spreads transsynaptically is a very powerful tool to study synaptically connecting neurons (Osakada et al., 2011; Wall et al., 2010). This virus can deliver reporter genes to visualize the presynaptic and postsynaptic neuron pairs, Ca^{2+} indicator to monitor neuronal activity in response to various sensory stimuli and behavioral states, ChR2 to photoactivate the neurons, and various other genes and small interfering RNA sequences to manipulate gene expression in targeted neurons (Atasoy et al., 2008; Zhao et al., 2011). By using optogenetic tools in particular, the activity of neurons of interest is easily manipulated and the consequences in network dynamics can be investigated to understand the function of the neuron in neuronal circuitry.

What is the functional role of SAP97 in juvenile and adult SOM interneurons? Similar to PV interneurons, SOM interneurons express SAP97 in a relatively smaller fraction of cells in adult mice (Akgul and Wollmuth, 2010). The typical membrane properties of SOM interneurons are very different from the ones of PV interneurons. For example, SOM interneurons have high input resistance, low rheobase and more depolarized resting membrane potential that keeps them in a more excitable state than PV interneurons. In addition to that, SOM interneurons fire action potentials at a relatively slower rate. (Fanselow et al., 2008; Kawaguchi and Kubota, 1996; Lazarus and Huang, 2011). Whether SAP97 regulates membrane excitability, AP firing rate as well as glutamatergic synaptic transmission in SOM interneurons similar to PV interneurons, could be inferred by conducting similar experiments explained in this study or proposed further.

In conclusion, our study presents new insights on the role of SAP97 in neuronal activity and consequently in network dynamics. However, a persistent pursuit of more experimental results and answers by using a combination of new experimental tools and approaches are required to understand various aspects of these mechanisms to explain normal and abnormal brain functions.

REFERENCES

Abi-Char, J., El-Haou, S., Balse, E., Neyroud, N., Vranckx, R., Coulombe, A., and Hatem, S.N. (2008). The anchoring protein SAP97 retains Kv1.5 channels in the plasma membrane of cardiac myocytes. Am J Physiol Heart Circ Physiol *294*, H1851-1861.

Akgul, G., and Wollmuth, L.P. (2010). Expression pattern of membrane-associated guanylate kinases in interneurons of the visual cortex. J Comp Neurol *518*, 4842-4854.

Angulo, M.C., Lambolez, B., Audinat, E., Hestrin, S., and Rossier, J. (1997). Subunit composition, kinetic, and permeation properties of AMPA receptors in single neocortical nonpyramidal cells. J Neurosci *17*, 6685-6696.

Angulo, M.C., Rossier, J., and Audinat, E. (1999). Postsynaptic glutamate receptors and integrative properties of fast-spiking interneurons in the rat neocortex. J Neurophysiol *82*, 1295-1302.

Aoki, C., Miko, I., Oviedo, H., Mikeladze-Dvali, T., Alexandre, L., Sweeney, N., and Bredt, D.S. (2001). Electron microscopic immunocytochemical detection of PSD-95, PSD-93, SAP-102, and SAP-97 at postsynaptic, presynaptic, and nonsynaptic sites of adult and neonatal rat visual cortex. Synapse *40*, 239-257.

Ascoli, G.A., Alonso-Nanclares, L., Anderson, S.A., Barrionuevo, G., Benavides-Piccione, R., Burkhalter, A., Buzsaki, G., Cauli, B., Defelipe, J., Fairen, A.*, et al.* (2008). Petilla terminology: nomenclature of features of GABAergic interneurons of the cerebral cortex. Nat Rev Neurosci *9*, 557-568.

Atasoy, D., Aponte, Y., Su, H.H., and Sternson, S.M. (2008). A FLEX switch targets Channelrhodopsin-2 to multiple cell types for imaging and long-range circuit mapping. J Neurosci *28*, 7025-7030.

Batista-Brito, R., and Fishell, G. (2009). The developmental integration of cortical interneurons into a functional network. Curr Top Dev Biol *87*, 81-118.

Bats, C., Groc, L., and Choquet, D. (2007). The interaction between Stargazin and PSD-95 regulates AMPA receptor surface trafficking. Neuron *53*, 719-734.

Bekenstein, J.W., and Lothman, E.W. (1993). Dormancy of inhibitory interneurons in a model of temporal lobe epilepsy. Science *259*, 97-100.

Belforte, J.E., Zsiros, V., Sklar, E.R., Jiang, Z., Yu, G., Li, Y., Quinlan, E.M., and Nakazawa, K. (2010). Postnatal NMDA receptor ablation in corticolimbic interneurons confers schizophrenia-like phenotypes. Nat Neurosci *13*, 76-83.

Bender, K.J., and Trussell, L.O. (2012). The physiology of the axon initial segment. Annu Rev Neurosci *35*, 249-265.

Benes, F.M., McSparren, J., Bird, E.D., SanGiovanni, J.P., and Vincent, S.L. (1991). Deficits in small interneurons in prefrontal and cingulate cortices of schizophrenic and schizoaffective patients. Arch Gen Psychiatry *48*, 996-1001.

Betley, J.N., and Sternson, S.M. (2011). Adeno-associated viral vectors for mapping, monitoring, and manipulating neural circuits. Hum Gene Ther *22*, 669-677.

Bingol, B., and Schuman, E.M. (2005). Synaptic protein degradation by the ubiquitin proteasome system. Curr Opin Neurobiol *15*, 536-541.

Bozzi, Y., Casarosa, S., and Caleo, M. (2012). Epilepsy as a neurodevelopmental disorder. Front Psychiatry *3*, 19.

Breininger, J.F., and Baskin, D.G. (2000). Fluorescence in situ hybridization of scarce leptin receptor mRNA using the enzyme-labeled fluorescent substrate method and tyramide signal amplification. J Histochem Cytochem *48*, 1593-1599.

Brenman, J.E., Christopherson, K.S., Craven, S.E., McGee, A.W., and Bredt, D.S. (1996). Cloning and characterization of postsynaptic density 93, a nitric oxide synthase interacting protein. J Neurosci *16*, 7407-7415.

Burkhalter, A. (2008). Many specialists for suppressing cortical excitation. Front Neurosci *2*, 155-167.

Buzsaki, G., and Draguhn, A. (2004). Neuronal oscillations in cortical networks. Science *304*, 1926-1929.

Cai, C., Coleman, S.K., Niemi, K., and Keinanen, K. (2002). Selective binding of synapse-associated protein 97 to GluR-A alpha-amino-5-hydroxy-3-methyl-4-isoxazole propionate receptor subunit is determined by a novel sequence motif. J Biol Chem *277*, 31484-31490.

Callaway, E.M. (2004). Feedforward, feedback and inhibitory connections in primate visual cortex. Neural Netw *17*, 625-632.

Caputi, A., Rozov, A., Blatow, M., and Monyer, H. (2009). Two calretinin-positive GABAergic cell types in layer 2/3 of the mouse neocortex provide different forms of inhibition. Cereb Cortex *19*, 1345-1359.

Cardin, J.A., Carlen, M., Meletis, K., Knoblich, U., Zhang, F., Deisseroth, K., Tsai, L.H., and Moore, C.I. (2009). Driving fast-spiking cells induces gamma rhythm and controls sensory responses. Nature *459*, 663-667.

Carlen, M., Meletis, K., Siegle, J.H., Cardin, J.A., Futai, K., Vierling-Claassen, D., Ruhlmann, C., Jones, S.R., Deisseroth, K., Sheng, M.*, et al.* (2011). A critical role for NMDA receptors in parvalbumin interneurons for gamma rhythm induction and behavior. Mol Psychiatry *17*, 537-548.

Carlisle, H.J., Fink, A.E., Grant, S.G., and O'Dell, T.J. (2008). Opposing effects of PSD-93 and PSD-95 on long-term potentiation and spike timing-dependent plasticity. J Physiol *586*, 5885-5900.

Caruana, G., and Bernstein, A. (2001). Craniofacial dysmorphogenesis including cleft palate in mice with an insertional mutation in the discs large gene. Mol Cell Biol *21*, 1475-1483.

Cauli, B., Audinat, E., Lambolez, B., Angulo, M.C., Ropert, N., Tsuzuki, K., Hestrin, S., and Rossier, J. (1997). Molecular and physiological diversity of cortical nonpyramidal cells. J Neurosci *17*, 3894-3906.

Chen, L., Chetkovich, D.M., Petralia, R.S., Sweeney, N.T., Kawasaki, Y., Wenthold, R.J., Bredt, D.S., and Nicoll, R.A. (2000). Stargazin regulates synaptic targeting of AMPA receptors by two distinct mechanisms. Nature *408*, 936-943.

Chetkovich, D.M., Bunn, R.C., Kuo, S.H., Kawasaki, Y., Kohwi, M., and Bredt, D.S. (2002a). Postsynaptic targeting of alternative postsynaptic density-95 isoforms by distinct mechanisms. J Neurosci *22*, 6415-6425.

Chetkovich, D.M., Chen, L., Stocker, T.J., Nicoll, R.A., and Bredt, D.S. (2002b). Phosphorylation of the postsynaptic density-95 (PSD-95)/discs large/zona occludens-1 binding site of stargazin regulates binding to PSD-95 and synaptic targeting of AMPA receptors. J Neurosci *22*, 5791-5796.

Choquet, D. (2010). Fast AMPAR trafficking for a high-frequency synaptic transmission. Eur J Neurosci *32*, 250-260.

Cobb, S.R., Buhl, E.H., Halasy, K., Paulsen, O., and Somogyi, P. (1995). Synchronization of neuronal activity in hippocampus by individual GABAergic interneurons. Nature *378*, 75-78.

Connors, B.W., and Gutnick, M.J. (1990). Intrinsic firing patterns of diverse neocortical neurons. Trends Neurosci *13*, 99-104.

Cousins, S.L., Papadakis, M., Rutter, A.R., and Stephenson, F.A. (2008). Differential interaction of NMDA receptor subtypes with the post-synaptic density-95 family of membrane associated guanylate kinase proteins. Journal of neurochemistry *104*, 903-913.

Curley, A.A., and Lewis, D.A. (2012). Cortical basket cell dysfunction in schizophrenia. J Physiol *590*, 715-724.

DeFelipe, J. (1993). Neocortical neuronal diversity: chemical heterogeneity revealed by colocalization studies of classic neurotransmitters, neuropeptides, calcium-binding proteins, and cell surface molecules. Cereb Cortex *3*, 273-289.

DeFelipe, J. (1999). Chandelier cells and epilepsy. Brain *122 (Pt 10)*, 1807-1822.

DeFelipe, J., Alonso-Nanclares, L., and Arellano, J.I. (2002). Microstructure of the neocortex: comparative aspects. J Neurocytol *31*, 299-316.

DeFelipe, J., Hendry, S.H., and Jones, E.G. (1989). Visualization of chandelier cell axons by parvalbumin immunoreactivity in monkey cerebral cortex. Proc Natl Acad Sci U S A *86*, 2093-2097.

Di Cristo, G. (2007). Development of cortical GABAergic circuits and its implications for neurodevelopmental disorders. Clin Genet *72*, 1-8.

Di Cristo, G., Wu, C., Chattopadhyaya, B., Ango, F., Knott, G., Welker, E., Svoboda, K., and Huang, Z.J. (2004). Subcellular domain-restricted GABAergic innervation in primary visual cortex in the absence of sensory and thalamic inputs. Nat Neurosci *7*, 1184-1186.

Dichter, M.A., and Ayala, G.F. (1987). Cellular mechanisms of epilepsy: a status report. Science *237*, 157-164.

Dumitriu, D., Rosa, C., Huang, J., and Yuste, R. (2007). Correlation between axonal morphologies and synaptic input kinetics of interneurons from mouse visual cortex. Cerebral Cortex *17*.

Dun, N.J., Dun, S.L., Wong, R.K., and Forstermann, U. (1994). Colocalization of nitric oxide synthase and somatostatin immunoreactivity in rat dentate hilar neurons. Proc Natl Acad Sci U S A *91*, 2955-2959.

El-Haou, S., Balse, E., Neyroud, N., Dilanian, G., Gavillet, B., Abriel, H., Coulombe, A., Jeromin, A., and Hatem, S.N. (2009). Kv4 potassium channels form a tripartite complex with the anchoring protein SAP97 and CaMKII in cardiac myocytes. Circ Res *104*, 758-769.

Elias, G.M., Elias, L.A., Apostolides, P.F., Kriegstein, A.R., and Nicoll, R.A. (2008). Differential trafficking of AMPA and NMDA receptors by SAP102 and PSD-95 underlies synapse development. Proc Natl Acad Sci U S A *105*, 20953-20958.

Elias, G.M., Funke, L., Stein, V., Grant, S.G., Bredt, D.S., and Nicoll, R.A. (2006). Synapse-specific and developmentally regulated targeting of AMPA receptors by a family of MAGUK scaffolding proteins. Neuron *52*, 307-320.

Elias, G.M., and Nicoll, R.A. (2007). Synaptic trafficking of glutamate receptors by MAGUK scaffolding proteins. Trends Cell Biol *17*, 343-352.

Fan, M.M., and Raymond, L.A. (2007). N-methyl-D-aspartate (NMDA) receptor function and excitotoxicity in Huntington's disease. Prog Neurobiol *81*, 272-293.

Fanselow, E.E., Richardson, K.A., and Connors, B.W. (2008). Selective, state-dependent activation of somatostatin-expressing inhibitory interneurons in mouse neocortex. J Neurophysiol *100*, 2640-2652.

Fishell, G., and Rudy, B. (2011). Mechanisms of inhibition within the telencephalon: "where the wild things are". Annu Rev Neurosci *34*, 535-567.

Freund, T.F. (2003). Interneuron Diversity series: Rhythm and mood in perisomatic inhibition. Trends Neurosci *26*, 489-495.

Freund, T.F., and Katona, I. (2007). Perisomatic inhibition. Neuron *56*, 33-42.

Fukaya, M., Ueda, H., Yamauchi, K., Inoue, Y., and Watanabe, M. (1999). Distinct spatiotemporal expression of mRNAs for the PSD-95/SAP90 protein family in the mouse brain. Neurosci Res *33*, 111-118.

Fukaya, M., and Watanabe, M. (2000). Improved immunohistochemical detection of postsynaptically located PSD-95/SAP90 protein family by protease section pretreatment: a study in the adult mouse brain. J Comp Neurol *426*, 572-586.

Fukuda, T., and Kosaka, T. (2000). The dual network of GABAergic interneurons linked by both chemical and electrical synapses: a possible infrastructure of the cerebral cortex. Neurosci Res *38*, 123-130.

Funke, L., Dakoji, S., and Bredt, D.S. (2005). Membrane-associated guanylate kinases regulate adhesion and plasticity at cell junctions. Annu Rev Biochem *74*, 219-245.

Futai, K., Kim, M.J., Hashikawa, T., Scheiffele, P., Sheng, M., and Hayashi, Y. (2007). Retrograde modulation of presynaptic release probability through signaling mediated by PSD-95-neuroligin. Nat Neurosci *10*, 186-195.

Galarreta, M., and Hestrin, S. (1999). A network of fast-spiking cells in the neocortex connected by electrical synapses. Nature *402*, 72-75.

Gardoni, F. (2008). MAGUK proteins: new targets for pharmacological intervention in the glutamatergic synapse. Eur J Pharmacol *585*, 147-152.

Gardoni, F., Marcello, E., and Di Luca, M. (2009). Postsynaptic density-membrane associated guanylate kinase proteins (PSD-MAGUKs) and their role in CNS disorders. Neuroscience *158*, 324-333.

Geiger, J.R., Melcher, T., Koh, D.S., Sakmann, B., Seeburg, P.H., Jonas, P., and Monyer, H. (1995). Relative abundance of subunit mRNAs determines gating and Ca2+ permeability of AMPA receptors in principal neurons and interneurons in rat CNS. Neuron *15*, 193-204.

Gelman, D.M., and Marin, O. (2010). Generation of interneuron diversity in the mouse cerebral cortex. Eur J Neurosci *31*, 2136-2141.

Geurts, F.J., Timmermans, J., Shigemoto, R., and De Schutter, E. (2001). Morphological and neurochemical differentiation of large granular layer interneurons in the adult rat cerebellum. Neuroscience *104*, 499-512.

Gibson, J.R., Beierlein, M., and Connors, B.W. (1999). Two networks of electrically coupled inhibitory neurons in neocortex. Nature *402*, 75-79.

Godreau, D., Vranckx, R., Maguy, A., Goyenvalle, C., and Hatem, S.N. (2003). Different isoforms of synapse-associated protein, SAP97, are expressed in the heart and have distinct effects on the voltage-gated K+ channel Kv1.5. J Biol Chem *278*, 47046-47052.

Goldberg, J.H., Tamas, G., Aronov, D., and Yuste, R. (2003a). Calcium microdomains in aspiny dendrites. Neuron *40*, 807-821.

Goldberg, J.H., and Yuste, R. (2005). Space matters: local and global dendritic Ca2+ compartmentalization in cortical interneurons. Trends Neurosci *28*, 158-167.

Goldberg, J.H., Yuste, R., and Tamas, G. (2003b). Ca2+ imaging of mouse neocortical interneurone dendrites: contribution of Ca2+-permeable AMPA and NMDA receptors to subthreshold Ca2+dynamics. J Physiol *551*, 67-78.

Gonchar, Y., and Burkhalter, A. (1999). Connectivity of GABAergic calretinin-immunoreactive neurons in rat primary visual cortex. Cereb Cortex *9*, 683-696.

Gonchar, Y., Turney, S., Price, J.L., and Burkhalter, A. (2002). Axo-axonic synapses formed by somatostatin-expressing GABAergic neurons in rat and monkey visual cortex. J Comp Neurol *443*, 1-14.

Gonchar, Y., Wang, Q., and Burkhalter, A. (2007). Multiple distinct subtypes of GABAergic neurons in mouse visual cortex identified by triple immunostaining. Front Neuroanat *1*, 3.

Goult, B.T., Rapley, J.D., Dart, C., Kitmitto, A., Grossmann, J.G., Leyland, M.L., and Lian, L.Y. (2007). Small-angle X-ray scattering and NMR studies of the conformation of the PDZ region of SAP97 and its interactions with Kir2.1. Biochemistry *46*, 14117-14128.

Gupta, A., Wang, Y., and Markram, H. (2000). Organizing principles for a diversity of GABAergic interneurons and synapses in the neocortex. Science *287*, 273-278.

Hashimoto, T., Volk, D.W., Eggan, S.M., Mirnics, K., Pierri, J.N., Sun, Z., Sampson, A.R., and Lewis, D.A. (2003). Gene expression deficits in a subclass of GABA neurons in the prefrontal cortex of subjects with schizophrenia. J Neurosci *23*, 6315-6326.

Hennou, S., Khalilov, I., Diabira, D., Ben-Ari, Y., and Gozlan, H. (2002). Early sequential formation of functional GABA(A) and glutamatergic synapses on CA1 interneurons of the rat foetal hippocampus. Eur J Neurosci *16*, 197-208.

Hippenmeyer, S., Vrieseling, E., Sigrist, M., Portmann, T., Laengle, C., Ladle, D.R., and Arber, S. (2005). A developmental switch in the response of DRG neurons to ETS transcription factor signaling. PLoS biology *3*, e159.

Hirling, H. (2009). Endosomal trafficking of AMPA-type glutamate receptors. Neuroscience *158*, 36-44.

Hou, Q., Gilbert, J., and Man, H.Y. (2011). Homeostatic regulation of AMPA receptor trafficking and degradation by light-controlled single-synaptic activation. Neuron *72*, 806-818.

Hume, R.I., Dingledine, R., and Heinemann, S.F. (1991). Identification of a site in glutamate receptor subunits that controls calcium permeability. Science *253*, 1028-1031.

Hunt, D.L., and Castillo, P.E. (2012). Synaptic plasticity of NMDA receptors: mechanisms and functional implications. Curr Opin Neurobiol *22*, 496-508.

Ikematsu, N., Dallas, M.L., Ross, F.A., Lewis, R.W., Rafferty, J.N., David, J.A., Suman, R., Peers, C., Hardie, D.G., and Evans, A.M. (2011). Phosphorylation of the voltage-gated potassium channel Kv2.1 by AMP-activated protein kinase regulates membrane excitability. Proc Natl Acad Sci U S A *108*, 18132-18137.

Jagadeesh, B., Gray, C.M., and Ferster, D. (1992). Visually evoked oscillations of membrane potential in cells of cat visual cortex. Science (New York, NY *257*, 552-554.

Jeyifous, O., Waites, C.L., Specht, C.G., Fujisawa, S., Schubert, M., Lin, E.I., Marshall, J., Aoki, C., de Silva, T., Montgomery, J.M*., et al.* (2009). SAP97 and CASK mediate sorting of NMDA receptors through a previously unknown secretory pathway. Nat Neurosci *12*, 1011-1019.

Jonas, P., Bischofberger, J., Fricker, D., and Miles, R. (2004). Interneuron Diversity series: Fast in, fast out - temporal and spatial signal processing in hippocampal interneurons. Trends in Neurosciences *27*, 30-40.

Jonas, P., Racca, C., Sakmann, B., Seeburg, P.H., and Monyer, H. (1994). Differences in Ca2+ permeability of AMPA-type glutamate receptor channels in neocortical neurons caused by differential GluR-B subunit expression. Neuron *12*, 1281-1289.

Jones, E.G. (2000). Microcolumns in the cerebral cortex. Proc Natl Acad Sci U S A *97*, 5019-5021.

Karagiannis, A., Gallopin, T., David, C., Battaglia, D., Geoffroy, H., Rossier, J., Hillman, E.M., Staiger, J.F., and Cauli, B. (2009). Classification of NPY-expressing neocortical interneurons. J Neurosci *29*, 3642-3659.

Kawaguchi, Y. (1995). Physiological subgroups of nonpyramidal cells with specific morphological characteristics in layer II/III of rat frontal cortex. J Neurosci *15*, 2638-2655.

Kawaguchi, Y., and Kubota, Y. (1993). Correlation of physiological subgroupings of nonpyramidal cells with parvalbumin- and calbindinD28k-immunoreactive neurons in layer V of rat frontal cortex. J Neurophysiol *70*, 387-396.

Kawaguchi, Y., and Kubota, Y. (1996). Physiological and morphological identification of somatostatin- or vasoactive intestinal polypeptide-containing cells among GABAergic cell subtypes in rat frontal cortex. J Neurosci *16*, 2701-2715.

Kerlin, A.M., Andermann, M.L., Berezovskii, V.K., and Reid, R.C. (2010). Broadly tuned response properties of diverse inhibitory neuron subtypes in mouse visual cortex. Neuron *67*, 858-871.

Kessels, H.W., and Malinow, R. (2009). Synaptic AMPA receptor plasticity and behavior. Neuron *61*, 340-350.

Kim, E., and Sheng, M. (1996). Differential K+ channel clustering activity of PSD-95 and SAP97, two related membrane-associated putative guanylate kinases. Neuropharmacology *35*, 993-1000.

Kim, E., and Sheng, M. (2004). PDZ domain proteins of synapses. Nat Rev Neurosci *5*, 771-781.

Klocker, N., Bunn, R.C., Schnell, E., Caruana, G., Bernstein, A., Nicoll, R.A., and Bredt, D.S. (2002). Synaptic glutamate receptor clustering in mice lacking the SH3 and GK domains of SAP97. Eur J Neurosci *16*, 1517-1522.

Kornau, H.C., Schenker, L.T., Kennedy, M.B., and Seeburg, P.H. (1995). Domain interaction between NMDA receptor subunits and the postsynaptic density protein PSD-95. Science *269*, 1737-1740.

Korotkova, T., Fuchs, E.C., Ponomarenko, A., von Engelhardt, J., and Monyer, H. (2010). NMDA receptor ablation on parvalbumin-positive interneurons impairs hippocampal synchrony, spatial representations, and working memory. Neuron *68*, 557-569.

Kristiansen, L.V., Huerta, I., Beneyto, M., and Meador-Woodruff, J.H. (2007). NMDA receptors and schizophrenia. Curr Opin Pharmacol *7*, 48-55.

Kubota, Y., Hattori, R., and Yui, Y. (1994). Three distinct subpopulations of GABAergic neurons in rat frontal agranular cortex. Brain research *649*, 159-173.

Kubota, Y., and Kawaguchi, Y. (1994). Three classes of GABAergic interneurons in neocortex and neostriatum. Jpn J Physiol *44 Suppl 2*, S145-148.

Kuhlman, S.J., and Huang, Z.J. (2008). High-resolution labeling and functional manipulation of specific neuron types in mouse brain by Cre-activated viral gene expression. PloS one *3*, e2005.

Kuhlman, S.J., Lu, J., Lazarus, M.S., and Huang, Z.J. (2010). Maturation of GABAergic inhibition promotes strengthening of temporally coherent inputs among convergent pathways. PLoS computational biology *6*, e1000797.

Kullmann, D.M., and Lamsa, K.P. (2007). Long-term synaptic plasticity in hippocampal interneurons. Nat Rev Neurosci *8*, 687-699.

Kuriu, T., Inoue, A., Bito, H., Sobue, K., and Okabe, S. (2006). Differential control of postsynaptic density scaffolds via actin-dependent and -independent mechanisms. J Neurosci *26*, 7693-7706.

Lawrence, J.J., and McBain, C.J. (2003). Interneuron diversity series: containing the detonation--feedforward inhibition in the CA3 hippocampus. Trends Neurosci *26*, 631-640.

Lazarus, M.S., and Huang, Z.J. (2011). Distinct maturation profiles of perisomatic and dendritic targeting GABAergic interneurons in the mouse primary visual cortex during the critical period of ocular dominance plasticity. J Neurophysiol *106*, 775-787.

Leonard, A.S., Davare, M.A., Horne, M.C., Garner, C.C., and Hell, J.W. (1998). SAP97 is associated with the alpha-amino-3-hydroxy-5-methylisoxazole-4-propionic acid receptor GluR1 subunit. J Biol Chem *273*, 19518-19524.

Leonoudakis, D., Conti, L.R., Anderson, S., Radeke, C.M., McGuire, L.M., Adams, M.E., Froehner, S.C., Yates, J.R., 3rd, and Vandenberg, C.A. (2004a). Protein trafficking and anchoring complexes revealed by proteomic analysis of inward rectifier potassium channel (Kir2.x)-associated proteins. J Biol Chem *279*, 22331-22346.

Leonoudakis, D., Conti, L.R., Radeke, C.M., McGuire, L.M., and Vandenberg, C.A. (2004b). A multiprotein trafficking complex composed of SAP97, CASK, Veli, and Mint1 is associated with inward rectifier Kir2 potassium channels. J Biol Chem *279*, 19051-19063.

Leonoudakis, D., Mailliard, W., Wingerd, K., Clegg, D., and Vandenberg, C. (2001). Inward rectifier potassium channel Kir2.2 is associated with synapse-associated protein SAP97. J Cell Sci *114*, 987-998.

Li, D., Specht, C.G., Waites, C.L., Butler-Munro, C., Leal-Ortiz, S., Foote, J.W., Genoux, D., Garner, C.C., and Montgomery, J.M. (2011). SAP97 directs NMDA receptor spine targeting and synaptic plasticity. J Physiol *589*, 4491-4510.

Lisman, J.E., Coyle, J.T., Green, R.W., Javitt, D.C., Benes, F.M., Heckers, S., and Grace, A.A. (2008). Circuit-based framework for understanding neurotransmitter and risk gene interactions in schizophrenia. Trends Neurosci *31*, 234-242.

MacDermott, A.B., Mayer, M.L., Westbrook, G.L., Smith, S.J., and Barker, J.L. (1986). NMDA-receptor activation increases cytoplasmic calcium concentration in cultured spinal cord neurones. Nature *321*, 519-522.

Maffei, A., and Turrigiano, G. (2008). The age of plasticity: developmental regulation of synaptic plasticity in neocortical microcircuits. Prog Brain Res *169*, 211-223.

Marin, O. (2012). Interneuron dysfunction in psychiatric disorders. Nat Rev Neurosci *13*, 107-120.

Markram, H., Toledo-Rodriguez, M., Wang, Y., Gupta, A., Silberberg, G., and Wu, C. (2004). Interneurons of the neocortical inhibitory system. Nat Rev Neurosci *5*, 793-807.

Martina, M., Krasteniakov, N.V., and Bergeron, R. (2003). D-Serine differently modulates NMDA receptor function in rat CA1 hippocampal pyramidal cells and interneurons. J Physiol *548*, 411-423.

Mathur, R., Choi, W.S., Eldstrom, J., Wang, Z., Kim, J., Steele, D.F., and Fedida, D. (2006). A specific N-terminal residue in Kv1.5 is required for upregulation of the channel by SAP97. Biochemical and biophysical research communications *342*, 1-8.

Merchan-Perez, A., Rodriguez, J.R., Ribak, C.E., and DeFelipe, J. (2009). Proximity of excitatory and inhibitory axon terminals adjacent to pyramidal cell bodies provides a putative basis for nonsynaptic interactions. Proc Natl Acad Sci U S A *106*, 9878-9883.

Miller, M.W. (1986). Maturation of rat visual cortex. III. Postnatal morphogenesis and synaptogenesis of local circuit neurons. Brain Res *390*, 271-285.

Miyoshi, G., Butt, S.J., Takebayashi, H., and Fishell, G. (2007). Physiologically distinct temporal cohorts of cortical interneurons arise from telencephalic Olig2-expressing precursors. J Neurosci *27*, 7786-7798.

Moga, D., Hof, P.R., Vissavajjhala, P., Moran, T.M., and Morrison, J.H. (2002). Parvalbumin-containing interneurons in rat hippocampus have an AMPA receptor profile suggestive of vulnerability to excitotoxicity. J Chem Neuroanat *23*, 249-253.

Montgomery, J.M., Zamorano, P.L., and Garner, C.C. (2004). MAGUKs in synapse assembly and function: an emerging view. Cell Mol Life Sci *61*, 911-929.

Monyer, H., Burnashev, N., Laurie, D.J., Sakmann, B., and Seeburg, P.H. (1994). Developmental and regional expression in the rat brain and functional properties of four NMDA receptors. Neuron *12*, 529-540.

Muller, B.M., Kistner, U., Kindler, S., Chung, W.J., Kuhlendahl, S., Fenster, S.D., Lau, L.F., Veh, R.W., Huganir, R.L., Gundelfinger, E.D*., et al.* (1996). SAP102, a novel postsynaptic protein that interacts with NMDA receptor complexes in vivo. Neuron *17*, 255-265.

Muller, B.M., Kistner, U., Veh, R.W., Cases-Langhoff, C., Becker, B., Gundelfinger, E.D., and Garner, C.C. (1995). Molecular characterization and spatial distribution of SAP97, a novel presynaptic protein homologous to SAP90 and the Drosophila discs-large tumor suppressor protein. J Neurosci *15*, 2354-2366.

Murayama, M., Perez-Garci, E., Nevian, T., Bock, T., Senn, W., and Larkum, M.E. (2009). Dendritic encoding of sensory stimuli controlled by deep cortical interneurons. Nature *457*, 1137-1141.

Nam, C.I., and Chen, L. (2005). Postsynaptic assembly induced by neurexin-neuroligin interaction and neurotransmitter. Proc Natl Acad Sci U S A *102*, 6137-6142.

Newpher, T.M., and Ehlers, M.D. (2008). Glutamate receptor dynamics in dendritic microdomains. Neuron *58*, 472-497.

Nikandrova, Y.A., Jiao, Y., Baucum, A.J., Tavalin, S.J., and Colbran, R.J. (2010). Ca2+/calmodulin-dependent protein kinase II binds to and phosphorylates a specific SAP97 splice variant to disrupt association with AKAP79/150 and modulate alpha-amino-3-hydroxy-5-methyl-4-isoxazolepropionic acid-type glutamate receptor (AMPAR) activity. J Biol Chem *285*, 923-934.

Nissen, W., Szabo, A., Somogyi, J., Somogyi, P., and Lamsa, K.P. (2010). Cell type-specific long-term plasticity at glutamatergic synapses onto hippocampal interneurons expressing either parvalbumin or CB1 cannabinoid receptor. J Neurosci *30*, 1337-1347.

Nyiri, G., Stephenson, F.A., Freund, T.F., and Somogyi, P. (2003). Large variability in synaptic N-methyl-D-aspartate receptor density on interneurons and a comparison with pyramidal-cell spines in the rat hippocampus. Neuroscience *119*, 347-363.

Okaty, B.W., Miller, M.N., Sugino, K., Hempel, C.M., and Nelson, S.B. (2009). Transcriptional and electrophysiological maturation of neocortical fast-spiking GABAergic interneurons. J Neurosci *29*, 7040-7052.

Oliva, A.J., Jiang, M., Lam, T., Smith, K., and Swann, J. (2000). Novel hippocampal interneuronal subtypes identified using transgenic mice that express green fluorescent protein in GABAergic interneurons. J Neurosci *20*.

Osakada, F., Mori, T., Cetin, A.H., Marshel, J.H., Virgen, B., and Callaway, E.M. (2011). New rabies virus variants for monitoring and manipulating activity and gene expression in defined neural circuits. Neuron *71*, 617-631.

Palmer, L., Murayama, M., and Larkum, M. (2012). Inhibitory Regulation of Dendritic Activity in vivo. Front Neural Circuits *6*, 26.

Papale, A., Cerovic, M., and Brambilla, R. (2009). Viral vector approaches to modify gene expression in the brain. J Neurosci Methods *185*, 1-14.

Peters, A., and Harriman, K.M. (1990). Different kinds of axon terminals forming symmetric synapses with the cell bodies and initial axon segments of layer II/III pyramidal cells. I. Morphometric analysis. J Neurocytol *19*, 154-174.

Peters, A., Sethares, C., and Harriman, K.M. (1990). Different kinds of axon terminals forming symmetric synapses with the cell bodies and initial axon segments of layer II/III pyramidal cells. II. Synaptic junctions. J Neurocytol *19*, 584-600.

Peterson, D.A. (1999). Quantitative histology using confocal microscopy: implementation of unbiased stereology procedures. Methods *18*, 493-507.

Petitprez, S., Zmoos, A.F., Ogrodnik, J., Balse, E., Raad, N., El-Haou, S., Albesa, M., Bittihn, P., Luther, S., Lehnart, S.E*., et al.* (2011). SAP97 and dystrophin macromolecular complexes determine two pools of cardiac sodium channels Nav1.5 in cardiomyocytes. Circ Res *108*, 294-304.

Picconi, B., Gardoni, F., Centonze, D., Mauceri, D., Cenci, M.A., Bernardi, G., Calabresi, P., and Di Luca, M. (2004). Abnormal Ca2+-calmodulin-dependent protein kinase II function mediates synaptic and motor deficits in experimental parkinsonism. J Neurosci *24*, 5283-5291.

Porter, J.T., Johnson, C.K., and Agmon, A. (2001). Diverse types of interneurons generate thalamus-evoked feedforward inhibition in the mouse barrel cortex. J Neurosci *21*, 2699-2710.

Rakic, P. (2007). The radial edifice of cortical architecture: from neuronal silhouettes to genetic engineering. Brain Res Rev *55*, 204-219.

Regalado, M.P., Terry-Lorenzo, R.T., Waites, C.L., Garner, C.C., and Malenka, R.C. (2006). Transsynaptic signaling by postsynaptic synapse-associated protein 97. J Neurosci *26*, 2343-2357.

Rial Verde, E.M., Lee-Osbourne, J., Worley, P.F., Malinow, R., and Cline, H.T. (2006). Increased expression of the immediate-early gene arc/arg3.1 reduces AMPA receptor-mediated synaptic transmission. Neuron *52*, 461-474.

Robertson, H.R., Gibson, E.S., Benke, T.A., and Dell'Acqua, M.L. (2009). Regulation of postsynaptic structure and function by an A-kinase anchoring protein-membrane-associated guanylate kinase scaffolding complex. J Neurosci *29*, 7929-7943.

Rotaru, D.C., Yoshino, H., Lewis, D.A., Ermentrout, G.B., and Gonzalez-Burgos, G. (2011). Glutamate receptor subtypes mediating synaptic activation of prefrontal cortex neurons: relevance for schizophrenia. J Neurosci *31*, 142-156.

Rumbaugh, G., Sia, G.M., Garner, C.C., and Huganir, R.L. (2003). Synapse-associated protein-97 isoform-specific regulation of surface AMPA receptors and synaptic function in cultured neurons. J Neurosci *23*, 4567-4576.

Runyan, C.A., Schummers, J., Van Wart, A., Kuhlman, S.J., Wilson, N.R., Huang, Z.J., and Sur, M. (2010). Response features of parvalbumin-expressing interneurons suggest precise roles for subtypes of inhibition in visual cortex. Neuron *67*, 847-857.

Sans, N., Prybylowski, K., Petralia, R.S., Chang, K., Wang, Y.X., Racca, C., Vicini, S., and Wenthold, R.J. (2003). NMDA receptor trafficking through an interaction between PDZ proteins and the exocyst complex. Nat Cell Biol *5*, 520-530.

Sans, N., Racca, C., Petralia, R.S., Wang, Y.X., McCallum, J., and Wenthold, R.J. (2001). Synapse-associated protein 97 selectively associates with a subset of AMPA receptors early in their biosynthetic pathway. J Neurosci *21*, 7506-7516.

Schiller, J., Schiller, Y., Stuart, G., and Sakmann, B. (1997). Calcium action potentials restricted to distal apical dendrites of rat neocortical pyramidal neurons. J Physiol *505 (Pt 3)*, 605-616.

Schluter, O.M., Xu, W., and Malenka, R.C. (2006). Alternative N-terminal domains of PSD-95 and SAP97 govern activity-dependent regulation of synaptic AMPA receptor function. Neuron *51*, 99-111.

Schmid, A., Hallermann, S., Kittel, R.J., Khorramshahi, O., Frolich, A.M., Quentin, C., Rasse, T.M., Mertel, S., Heckmann, M., and Sigrist, S.J. (2008). Activity-dependent site-specific changes of glutamate receptor composition in vivo. Nat Neurosci *11*, 659-666.

Schneeberger, P.R., Norman, A.W., and Heizmann, C.W. (1985). Parvalbumin and vitamin D-dependent calcium-binding protein (Mr 28,000): comparison of their localization in the cerebellum of normal and rachitic rats. Neurosci Lett *59*, 97-103.

Schnell, E., Sizemore, M., Karimzadegan, S., Chen, L., Bredt, D.S., and Nicoll, R.A. (2002). Direct interactions between PSD-95 and stargazin control synaptic AMPA receptor number. Proc Natl Acad Sci U S A *99*, 13902-13907.

Sheng, M., and Hoogenraad, C.C. (2007). The postsynaptic architecture of excitatory synapses: a more quantitative view. Annu Rev Biochem *76*, 823-847.

Sholl, D.A. (1953). Dendritic organization in the neurons of the visual and motor cortices of the cat. Journal of anatomy *87*, 387-406.

Silberberg, G., Grillner, S., LeBeau, F.E., Maex, R., and Markram, H. (2005). Synaptic pathways in neural microcircuits. Trends Neurosci *28*, 541-551.

Sohal, V.S. (2012). Insights into cortical oscillations arising from optogenetic studies. Biol Psychiatry *71*, 1039-1045.

Sohal, V.S., Zhang, F., Yizhar, O., and Deisseroth, K. (2009). Parvalbumin neurons and gamma rhythms enhance cortical circuit performance. Nature *459*, 698-702.

Song, J.Y., Ichtchenko, K., Sudhof, T.C., and Brose, N. (1999). Neuroligin 1 is a postsynaptic cell-adhesion molecule of excitatory synapses. Proc Natl Acad Sci U S A *96*, 1100-1105.

Spruston, N. (2008). Pyramidal neurons: dendritic structure and synaptic integration. Nat Rev Neurosci *9*, 206-221.

Standaert, D.G., Landwehrmeyer, G.B., Kerner, J.A., Penney, J.B., Jr., and Young, A.B. (1996). Expression of NMDAR2D glutamate receptor subunit mRNA in neurochemically identified interneurons in the rat neostriatum, neocortex and hippocampus. Brain Res Mol Brain Res *42*, 89-102.

Standley, S., Roche, K.W., McCallum, J., Sans, N., and Wenthold, R.J. (2000). PDZ domain suppression of an ER retention signal in NMDA receptor NR1 splice variants. Neuron *28*, 887-898.

Stephenson, F.A., Cousins, S.L., and Kenny, A.V. (2008). Assembly and forward trafficking of NMDA receptors (Review). Molecular membrane biology *25*, 311-320.

Steriade, M., Amzica, F., and Contreras, D. (1996). Synchronization of fast (30-40 Hz) spontaneous cortical rhythms during brain activation. J Neurosci *16*, 392-417.

Stiffler, M.A., Chen, J.R., Grantcharova, V.P., Lei, Y., Fuchs, D., Allen, J.E., Zaslavskaia, L.A., and MacBeath, G. (2007). PDZ domain binding selectivity is optimized across the mouse proteome. Science *317*, 364-369.

Sun, Q., and Turrigiano, G.G. (2011). PSD-95 and PSD-93 play critical but distinct roles in synaptic scaling up and down. J Neurosci *31*, 6800-6808.

Szinyei, C., Heinbockel, T., Montagne, J., and Pape, H.C. (2000). Putative cortical and thalamic inputs elicit convergent excitation in a population of GABAergic interneurons of the lateral amygdala. J Neurosci *20*, 8909-8915.

Taniguchi, H., He, M., Wu, P., Kim, S., Paik, R., Sugino, K., Kvitsiani, D., Fu, Y., Lu, J., Lin, Y.*, et al.* (2011). A resource of Cre driver lines for genetic targeting of GABAergic neurons in cerebral cortex. Neuron *71*, 995-1013.

Thomson, A.M., and Bannister, A.P. (2003). Interlaminar connections in the neocortex. Cereb Cortex *13*, 5-14.

Tiffany, A.M., Manganas, L.N., Kim, E., Hsueh, Y.P., Sheng, M., and Trimmer, J.S. (2000). PSD-95 and SAP97 exhibit distinct mechanisms for regulating K(+) channel surface expression and clustering. J Cell Biol *148*, 147-158.

Toledo-Rodriguez, M., and Markram, H. (2007). Single-cell RT-PCR, a technique to decipher the electrical, anatomical, and genetic determinants of neuronal diversity. Methods Mol Biol *403*, 123-139.

Traynelis, S.F., Wollmuth, L.P., McBain, C.J., Menniti, F.S., Vance, K.M., Ogden, K.K., Hansen, K.B., Yuan, H., Myers, S.J., and Dingledine, R. (2010). Glutamate receptor ion channels: structure, regulation, and function. Pharmacol Rev *62*, 405-496.

Tricoire, L., Pelkey, K.A., Daw, M.I., Sousa, V.H., Miyoshi, G., Jeffries, B., Cauli, B., Fishell, G., and McBain, C.J. (2010). Common origins of hippocampal Ivy and nitric oxide synthase expressing neurogliaform cells. J Neurosci *30*, 2165-2176.

Turrigiano, G.G. (2008). The self-tuning neuron: synaptic scaling of excitatory synapses. Cell *135*, 422-435.

Vikstrom, K.L., Vaidyanathan, R., Levinsohn, S., O'Connell, R.P., Qian, Y., Crye, M., Mills, J.H., and Anumonwo, J.M. (2009). SAP97 regulates Kir2.3 channels by multiple mechanisms. Am J Physiol Heart Circ Physiol *297*, H1387-1397.

Vullhorst, D., Neddens, J., Karavanova, I., Tricoire, L., Petralia, R.S., McBain, C.J., and Buonanno, A. (2009). Selective expression of ErbB4 in interneurons, but not pyramidal cells, of the rodent hippocampus. J Neurosci *29*, 12255-12264.

Waites, C.L., Specht, C.G., Hartel, K., Leal-Ortiz, S., Genoux, D., Li, D., Drisdel, R.C., Jeyifous, O., Cheyne, J.E., Green, W.N.*, et al.* (2009). Synaptic SAP97 isoforms regulate AMPA receptor dynamics and access to presynaptic glutamate. J Neurosci *29*, 4332-4345.

Wakabayashi, K., Narisawa-Saito, M., Iwakura, Y., Arai, T., Ikeda, K., Takahashi, H., and Nawa, H. (1999). Phenotypic down-regulation of glutamate receptor subunit GluR1 in Alzheimer's disease. Neurobiol Aging *20*, 287-295.

Wall, N.R., Wickersham, I.R., Cetin, A., De La Parra, M., and Callaway, E.M. (2010). Monosynaptic circuit tracing in vivo through Cre-dependent targeting and complementation of modified rabies virus. Proc Natl Acad Sci U S A *107*, 21848-21853.

Wang, H.X., and Gao, W.J. (2010). Development of calcium-permeable AMPA receptors and their correlation with NMDA receptors in fast-spiking interneurons of rat prefrontal cortex. J Physiol *588*, 2823-2838.

Wenner, P. (2011). Mechanisms of GABAergic homeostatic plasticity. Neural plasticity *2011*, 489470.

Whittington, M.A., Traub, R.D., and Jefferys, J.G. (1995). Synchronized oscillations in interneuron networks driven by metabotropic glutamate receptor activation. Nature *373*, 612-615.

Williams, S.R., and Stuart, G.J. (2003). Role of dendritic synapse location in the control of action potential output. Trends Neurosci *26*, 147-154.

Yamanaka, T., and Ohno, S. (2008). Role of Lgl/Dlg/Scribble in the regulation of epithelial junction, polarity and growth. Front Biosci *13*, 6693-6707.

Zhao, S., Ting, J.T., Atallah, H.E., Qiu, L., Tan, J., Gloss, B., Augustine, G.J., Deisseroth, K., Luo, M., Graybiel, A.M.*, et al.* (2011). Cell type-specific channelrhodopsin-2 transgenic mice for optogenetic dissection of neural circuitry function. Nature methods *8*, 745-752.

Zheng, C.Y., Petralia, R.S., Wang, Y.X., Kachar, B., and Wenthold, R.J. (2010). SAP102 is a highly mobile MAGUK in spines. J Neurosci *30*, 4757-4766.

Zhou, W., Zhang, L., Guoxiang, X., Mojsilovic-Petrovic, J., Takamaya, K., Sattler, R., Huganir, R., and Kalb, R. (2008). GluR1 controls dendrite growth through its binding partner, SAP97. J Neurosci *28*, 10220-10233.